

POLITECNICO DI TORINO

Master's Degree in Aerospace Engineering



Master's Degree Thesis

Development of a Control Augmentation System for a Tilt-Rotor Aircraft

Supervisors

Prof. Giorgio GUGLIERI

Prof. Pierluigi CAPONE

Candidate

Alessandro BRIAMONTE

2021/2022

A mia madre, per l'amore
A mio padre, per la passione
A mia nonna, per la saggezza

Summary

The aim of this work is the development and implementation of a Control Augmentation System (CAS) for an existing real-time flight simulator model of the Bell XV-15 tilt-rotor research aircraft. The model was developed in MATLAB/Simulink environment and integrated with the Research and Didactic Simulator (ReDSim), a research and development flight simulator belonging to the Centre of Aviation (ZAV) at the Zurich University for Applied Sciences (ZHAW), in Winterthur, Switzerland. The work focuses on the design and parameter evaluation (PID and LEAD-LAG control algorithms) for a CAS to achieve a reasonable flight handling quality, preceded by an extensive review of the existing Stability Augmentation System (SAS). The control system implementation relies on gain scheduling technique. The first step is to compute the family of constant operating points and linearize the system at several equilibrium points. The second step is to design a family of linear controllers at each operating point that performs satisfactorily when the system is operating near the respective operating points. Last, sampled-data and nonlinear gain scheduling is performed. Offline and online simulation results (on ReDSim, as well as on FlightGear) will show if satisfactory performances are obtained throughout the vehicle flight envelope. The design method we used gave a framework for CAS design. Thus, this approach can be used for tilt-rotor control augmentation system design, as well as for any kind of aircraft category.

Table of Contents

List of Tables	VIII
List of Figures	IX
Acronyms	XIV
1 Introduction	1
1.1 Background	1
1.2 A Short History of VTOL Aircrafts	2
1.2.1 Most common VTOL concept	4
1.2.2 The XV-15 tilt-rotor	5
1.3 Starting Position and Problem Statement	11
1.4 Project Objective	11
2 Automatic Flight Control Summary	12
2.1 Introduction and Theory Recapitulation	12
2.1.1 Basic flight control concepts	12
2.1.2 Flight dynamics recap	13
2.1.3 Control Theory Recap: frequency domain and diagrams . . .	14
2.1.4 Control Theory Recap: system properties	15
2.2 Adjusting System Properties	17
2.2.1 Important system parameters	17
2.2.2 Controllers - time domain	21
2.2.3 Compensators - frequency domain	23
2.3 System Performance Specifications	24
2.3.1 Requirements on handling qualities	25
2.3.2 Parameters subject to requirements	26
2.4 Control Augmentation System (CAS)	29
2.4.1 Basic longitudinal control augmentation system	29
2.4.2 Basic lateral control augmentation system	31
2.5 Dynamic Compensation	33

2.5.1	PID regulators	33
2.5.2	Lead and lag compensators	36
3	Control Augmentation System Development and Implementation	39
3.1	XV-15 Simulink Model	39
3.1.1	Model overview	39
3.1.2	Pilot interface	40
3.1.3	Flight control computer	40
3.1.4	Actuation system	42
3.1.5	Aircraft dynamics	42
3.1.6	Sensor dynamics	42
3.1.7	Sign convention	42
3.1.8	Linearization	43
3.2	Basic Development and Review on SAS	43
3.2.1	Model linearization	44
3.2.2	Stability augmentation system re-design	45
3.2.3	Results	49
3.3	Control Augmentation System Implementation	50
3.3.1	Longitudinal motion controller	50
3.3.2	Lateral-Directional motion controller	52
3.4	Gain Evaluation	55
3.4.1	PID Controller	55
3.4.2	LEAD-LAG compensator - Case study	62
3.5	Gain Scheduling	71
3.5.1	Linear system	73
3.5.2	Sampled-data system	74
3.5.3	Nonlinear system	84
4	Results	87
4.1	Gain Evaluation	87
4.1.1	Gain Scheduling - Longitudinal CAS	88
4.1.2	Gain Scheduling - Lateral CAS	93
4.1.3	Gain Scheduling - Directional CAS	97
4.2	Scheduling Test	102
4.2.1	Helicopter mode	103
4.2.2	Airplane mode	109
4.2.3	CAS off test	115
4.2.4	Discussion	121
4.3	Pilot-in-the-loop Tests	123
5	FlightGear Simulation Environment	126

6	Conclusions and Remarks	130
A	Simulink models	132
B	Compensator	136
	References	139

List of Tables

2.1	$\zeta - M_p$ relationship	24
2.2	Steady state error e_{ss} table	35
2.3	Effect of increasing a parameter independently	36
3.1	Inputs range	43
3.2	Scaled gains	47
3.3	Sample points for CAS gain evaluation	73
4.1	K_{p_q} evaluated gain	88
4.2	K_{I_q} evaluated gain	89
4.3	K_{FF_q} evaluated gain	90
4.4	K'_{p_q} evaluated gain	91
4.5	K_{p_θ} evaluated gain	92
4.6	K_{p_p} evaluated gain	93
4.7	K_{I_p} evaluated gain	94
4.8	K_{FF_p} evaluated gain	95
4.9	K_{p_ϕ} evaluated gain	96
4.10	$K_{p_{n_y}}$ evaluated gain	97
4.11	$K_{I_{n_y}}$ evaluated gain	98
4.12	$K_{FF_{n_y}}$ evaluated gain	99
4.13	K_{p_r} evaluated gain	100
4.14	K_{I_r} evaluated gain	101

List of Figures

1.1	V-22 Osprey [23]	2
1.2	Lilium Jet [www.lilium.com]	4
1.3	Tailsitter [https://wingtra.com]	5
1.4	Bell XV-15 [https://nara.getarchive.net]	6
1.5	Overview about Pitching and Thrust Controls of the XV-15	8
1.6	Overview about Rolling and Yawing Controls of the XV-15	9
1.7	Conversion corridor	10
2.1	An overview of the pitch attitude holding system	30
2.2	An overview of the roll angle holding system	32
2.3	PID compensator	34
2.4	Lead-lag compensator	36
2.5	Effect of ratio z/p	37
2.6	Frequency analysis of the LAG compensator	38
2.7	Frequency analysis of the LEAD compensator	38
3.1	Model Overview	40
3.2	Block diagram for open loop system	44
3.3	Block diagram for closed loop system	45
3.4	Pitch rate response to -0.1 in input	46
3.5	Pitch rate response - comparison	47
3.6	Latest SAS linearized model	48
3.7	Yaw damper gains	48
3.8	Pitch rate response to a step input	49
3.9	Roll rate response to a step input	49
3.10	Yaw rate response to a step input	50
3.11	Pitch rate hold control system	51
3.12	Pitch hold control system	52
3.13	Roll rate hold control system	53
3.14	Roll hold control system	53
3.15	Yaw rate hold control system	54

3.16	Turn coordinator control system	55
3.17	Pitch rate control system implementation	56
3.18	Pitch rate response	57
3.19	Pitch control system implementation	57
3.20	Pitch response	58
3.21	Roll rate control system implementation	58
3.22	Roll rate response	59
3.23	Roll control system implementation	59
3.24	Roll response	60
3.25	Turn hold control system implementation	60
3.26	Lateral acceleration response	61
3.27	Yaw rate control system implementation	61
3.28	Yaw rate response	62
3.29	Inner Loop	63
3.30	Block diagram for inner loop system with constant gain	64
3.31	Inner loop step response	65
3.32	Block diagram for closed loop system	65
3.33	Step response	66
3.34	Bode plot for the lag compensator with the pole in -0.15 and the zero in -3	67
3.35	Bode plot of open loop transfer function G_0	68
3.36	Step response with lag compensator included	68
3.37	Bode plot of the open loop transfer function G_0 - action to speed up the response	69
3.38	Bode plot with the both compensator included	70
3.39	Closed loop step response with both compensators included	70
3.40	Closed loop step response (refinement)	71
3.41	s- and z-plane	74
3.42	Sampled-data system	75
3.43	Longitudinal motion controller	76
3.44	Stick/Pedal step input	78
3.45	Pitch rate response	78
3.46	Pitch response	79
3.47	Lateral-Directional motion controller (airplane mode)	79
3.48	Pedal step input	80
3.49	Roll rate response to a lateral step input XLT	80
3.50	Lateral acceleration response to a lateral step input XLT	81
3.51	Lateral acceleration response to a pedal step input XPD	81
3.52	Lateral-Directional motion controller (helicopter mode)	82
3.53	Roll rate response	83
3.54	Roll response	83

3.55	Yaw rate response	84
4.1	K_{p_q} evaluated gain throughout XV-15 flight envelope	88
4.2	K_{I_q} evaluated gain throughout XV-15 flight envelope	89
4.3	K_{FF_q} evaluated gain throughout XV-15 flight envelope	90
4.4	K'_{p_q} evaluated gain throughout XV-15 flight envelope	91
4.5	K_{p_θ} evaluated gain throughout XV-15 flight envelope	92
4.6	K_{p_p} evaluated gain throughout XV-15 flight envelope	93
4.7	K_{I_p} evaluated gain throughout XV-15 flight envelope	94
4.8	K_{FF_p} evaluated gain throughout XV-15 flight envelope	95
4.9	K_{p_ϕ} evaluated gain throughout XV-15 flight envelope	96
4.10	$K_{p_{n_y}}$ evaluated gain throughout XV-15 flight envelope	97
4.11	$K_{I_{n_y}}$ evaluated gain throughout XV-15 flight envelope	98
4.12	$K_{FF_{n_y}}$ evaluated gain throughout XV-15 flight envelope	99
4.13	K_{p_r} evaluated gain throughout XV-15 flight envelope	100
4.14	K_{I_r} evaluated gain throughout XV-15 flight envelope	101
4.15	XV-15 model response to a longitudinal step input	103
4.16	XV-15 model response to a lateral step input	104
4.17	XV-15 model response to a pedal step input	105
4.18	XV-15 model response to a longitudinal step input	106
4.19	XV-15 model response to a lateral step input	107
4.20	XV-15 model response to a pedal step input	108
4.21	XV-15 model response to a longitudinal step input	109
4.22	XV-15 model response to a lateral step input	110
4.23	XV-15 model response to a pedal step input	111
4.24	XV-15 model response to a longitudinal step input	112
4.25	XV-15 model response to a lateral step input	113
4.26	XV-15 model response to a pedal step input	114
4.27	XV-15 model response to a longitudinal step input	115
4.28	XV-15 model response to a lateral step input	116
4.29	XV-15 model response to a pedal step input	117
4.30	XV-15 model response to a longitudinal step input	118
4.31	XV-15 model response to a lateral step input	119
4.32	XV-15 model response to a pedal step input	120
4.33	ReDSim (Courtesy of ZAV)	122
4.34	Cooper-Harper Handling Qualities Rating Scale	123
5.1	FlightGear screenshot	126
5.2	Flight stick	127
5.3	Longitudinal stick input - comparison	128
5.4	FlightGear screenshot	129

A.1	Longitudinal motion controller	133
A.2	Lateral motion controller	134
A.3	Directional motion controller	135
B.1	Unit circle	137

Acronyms

VTOL

Vertical Take-Off and Landing

FCS

Flight Control System

SAS

Stability Augmentation System

CAS

Control Augmentation System

SISO

Single Input Single Output

MIMO

Multi Input Multi Output

GM

Gain Margin

PM

Phase Margin

PID

Proportional Integral Derivative

TF

Transfer Function

A/C

Aircraft

ACT

Actuator

SnS

Sensor

NAC

Nacelle

AoS

Angle of Sideslip

XLN

Stick Longitudinal Input

XLT

Stick Lateral Input

XPD

Pedal Input

PSAS

Pitch SAS

RSAS

Roll SAS

YSAS

Yaw SAS

ReDSim

Research and Didactic Simulator

Chapter 1

Introduction

This chapter introduces the present thesis work. First, a general background of the topic is presented, followed by an overview of the Bell XV-15 and its relevant systems. In the last two sections the problem statement and the goals of the project are explained. Overall, this chapter is intended to provide a general context for the work carried out.

1.1 Background

Helicopters (also referred to as rotorcraft) have been used in urban areas for decades and are a familiar sight to all of us. Helicopter Emergency Medical Services (HEMS) for example are a vital way of transport to quickly airlift seriously injured people. Instead, considering a military point of view, the sole purpose of helicopters is quick and easy transport of troops to the battlefield either from the base location or aircraft carriers.

The limitation in speed, range and transport capabilities led to the development of vertical take-off and landing (VTOL) aircraft with extensive attack capabilities to provide air support. VTOL aircrafts ability to take off and land vertically, as well as hover, fly slowly and land in small spaces, distinguishes them from the conventional vehicles.

Nowadays, Europe is getting ready to embrace Urban Air Mobility (UAM) as a new air transport system and EASA has received a number of requests for the type certification of vertical take-off and landing aircraft, also referred to as Air Taxis, with the ambition to enable Urban Air Mobility or create new solutions for Regional Air Mobility. Although both VTOL and conventional rotorcraft make use of propulsion to lift into the air, new VTOLs concepts intend to use more

than two propulsion units, referred to as distributed propulsion. If implemented properly, distributed propulsion can increase aircraft safety by sharing critical functions among several components. In conjunction with electric or other types of innovative propulsion, VTOLs also have the potential to reduce aviation's environmental footprint in terms of emissions and noise. However, in order to ensure that this objective is met, the full life cycle of the product (from design to operations) needs to be taken into account, including the energy sources.

1.2 A Short History of VTOL Aircrafts

The idea of vertical flight was first seen thousands of years ago in Leonardo da Vinci's sketchbook. He drafted an image of what would become the helicopter. The prototype for the first helicopter took flight in 1907 but was not perfected until after World War II.

In addition to the helicopter, other VTOL aircrafts approaches were attempted between 1920 and 1930. Between 1922 and 1925, Henry Berliner experimented with a horizontal rotor fixed-wing aircraft. In 1928 and 1930, Nikola Tesla and George Lehberger received patents for somewhat impractical VTOL fixed-wing aircraft with tilting engines. Leslie Everett Baynes received a patent in the late 1930s for the Baynes Heliplane, another tilt-rotor aircraft.



Figure 1.1: V-22 Osprey [23]

From the 1940s until today, over forty VTOL aircrafts have been tested, but only a few have actually made it to production. The four successes include: the British Harrier "jump jet" and its descendants, the Soviet An-72/74 transport aircraft, the Soviet Yak-38 naval fighter and the Bell/Boeing V-22 Osprey (figure 1.1). The V-22 Osprey is considered the world's first production tilt-rotor aircraft.

Throughout the 1960s, attempts were made to build a commercial passenger aircraft with VTOL abilities, but none successfully made it to production. All prototypes were dismissed as too heavy and expensive to operate.

Between 1964 and 1972, Canadair manufactured a VTOL turbine tilt-wing monoplane (an airplane with only one wing) called the CL-84. Three updated versions were ordered by the Canadian government for military evaluation. These planes were named CL-84-1. Between 1972 and 1974, the CL-84-1 was shown to and evaluated by the U.S. aboard the aircraft carriers USS Guam and USS Guadalcanal as well as other locations. Unfortunately, two of the CL-84s experienced mechanical failures and crashed during testing and production contracts were never granted.

In the 1960s and early 1970s, Germany also planned to produce three VTOL aircrafts. Two models were built, but the project was cancelled due to high costs and political problems.

Today, as a response to the rapid acceleration of action and investment in VTOLs, many traditional and new aerospace companies have started working to build capable new aircrafts. A number of these companies predict fully automated flight in the future. However, they also recognize that a human pilot is still necessary either in the craft or at a control center until the automated systems are stronger.

In 2014, testing began on the BlackFly VTOL aircraft, a lightweight, electric, personal aerial vehicle from the company Opener. BlackFly was first displayed at the 2018 EAA AirVenture Convention in Oshkosh, Wisconsin. It is the first fixed-wing eVTOL aircraft in the world. BlackFly introduces the reality of a new era of three dimensional personal transportation.

Lilium, a Munich-based aviation startup, hopes to offer an on demand flying taxi service, claiming it will be five times faster than driving. The prototype (figure 1.2) they have developed has two seats and is shaped like a conventional airplane but uses a VTOL system.

The uberAir project, from multinational transportation network company Uber, has pledged to launch its first flying taxis using VTOL in 2023.



Figure 1.2: Lilium Jet [www.lilium.com]

While the future looks bright for VTOL, there are still huge amounts of technical challenges on both the aircraft and infrastructure side as well as regulatory hurdles for the design and operations of the aircraft. Recently, in the absence of suitable certification specifications for the type certification of VTOLs, EASA developed a complete set of dedicated technical specifications in the form of a Special Condition for VTOL aircrafts. The Special Condition addresses the unique characteristics of these products and prescribes airworthiness standards for the issuance of a type certificate to ensure that VTOLs are following necessary safety requirements. The Special Condition, published in July 2019, launched the framework for manufacturers to develop innovative VTOL.

1.2.1 Most common VTOL concept

There are currently two different types of VTOL technology: rotary wing aircraft and powered-lift.

A rotary wing aircraft (or rotorcraft) uses lift created by rotor blades spinning around a central mast. Some examples of rotorcrafts are:

- Helicopter – The helicopter’s spinning rotors create thrust like a large propeller that is directed vertically, enabling it to liftoff. While in flight, a slight tilt in the desired direction pushes some of the aircraft’s thrust and sends the craft forward.
- Gyrodyne - The gyrodyne is also known as a compound helicopter because it has the powered rotor of a helicopter, but a separate forward thrust system.

- Cyclogyro - On the cyclogyro, the rotary wing's axis and surfaces remain sideways across the airflow, similar to a conventional wing.

Powered-lift aircraft takeoff and land vertically but behave differently than rotorcrafts while in flight. They often have a fixed-wing design. Some examples of powered-lift aircraft are:

- Convertiplane - The convertiplane relies on the rotor for lift when taking-off, but then switches to a fixed-wing lift while in flight.
- Tiltrotor - The tiltrotor, also known as a proprotor, moves its propellers or rotors vertical to achieve VTOL and then tilts them forwards while flying for horizontal wing-borne flight. The main wing remains fixed in place.
- Tailsitter - The tailsitter aircraft sits vertically for takeoff and landing, but, once in the air, the whole craft tilts forward to achieve horizontal flight. (figure 1.3)

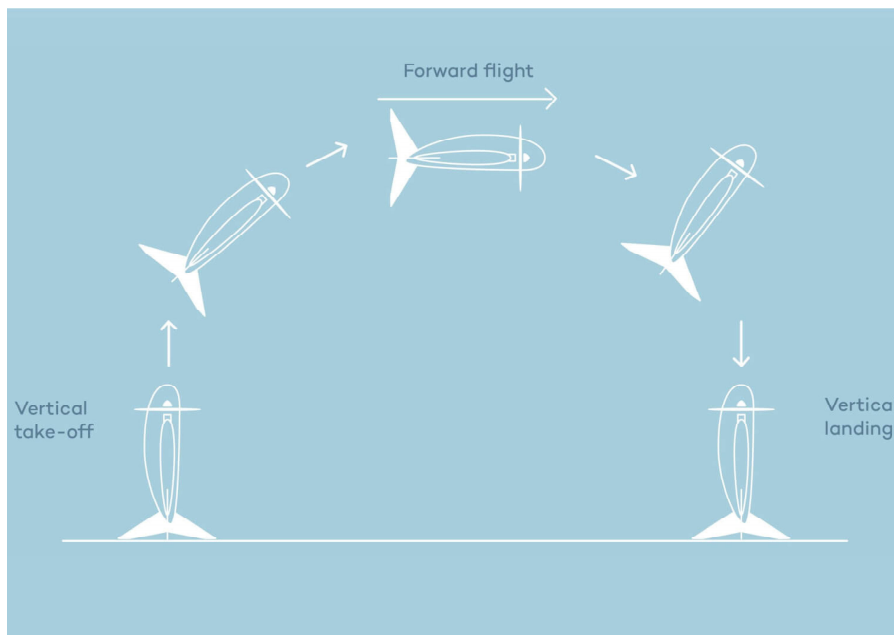


Figure 1.3: Tailsitter [<https://wingtra.com>]

1.2.2 The XV-15 tilt-rotor

In 1973, Bell Helicopter was chosen as prime contractor on a joint NASA/US Army Air Mobility Research and Development Laboratory research programme to

prove the concept of tilt-rotor technology. The purpose of this research programme was to explore the benefits that might be derived from vehicles that combined both helicopter and aeroplane characteristics. With the experience gained with its Model 200/ XV-3, the Bell team designed and proposed the Model 301 to meet this requirement. Complementary US Navy funding was provided in 1979 and 1980, and two prototypes were eventually ordered.

Designated XV-15, the Model 301 (figure 1.4) looked like a high-wing monoplane with two wingtip-mounted 1.550shp Avco Lycoming LTC1K-4K turboshafts, each fitted with 25ft diameter three-blade propeller-rotors able to be tilted from vertical take-off configuration to high-speed forward flight mode. Limiting rotor speed in forward flight was 458rpm and in hovering flight 565rpm. Transition took 12 seconds and the vehicle was designed to accelerate from hover to 450km/h in less than 30 seconds. Driveshafts were interconnected to permit single-engined operation in case of a failure.



Figure 1.4: Bell XV-15 [<https://nara.getarchive.net>]

In 1972, NASA and the U.S.Army Air Mobility Research and Development Laboratory jointly started the Tiltrotor Research Aircraft Program. Two phases were planned, a Proof-of-Concept phase and a Mission Suitability phase. The objectives of the Proof-of-Concept phase were to verify the rotor/pylon/wing dynamic stability, explore the limits of the operational flight envelope, establish safe operating limits, assess handling qualities, investigate gust sensitivity, and examine the effects of

disc loading and tip speed on downwash, noise, and hover operation. The objective of the mission suitability phase was to assess the application of tilt rotor technology to satisfy military and civil transport needs.

Since the Tiltrotor Research Aircraft Program was to be strictly a research program and would not lead to the production of an operational aircraft, costs were to be kept under control by not making weight minimization a major factor and encouraging the use of off the shelf components. Advanced technologies like fly-by-wire and composite structures were to be avoided. Weight growth and performance shortfalls would be tolerated in order to minimize cost and schedule impacts. Even the number of aircraft to be built was a factor. The two aircraft option was selected because of the high accident rate experienced by most other VTOL research programs.

Despite the successful early test flights in 1977, the XV-15 program did not fly again for almost two years. This was because of NASA's insistence on full-scale wind tunnel tests. Bell's position was that these tests were appropriate for investigating some potential problems, but that such testing would not guarantee discovering all potential problems. Bell was confident that problems with the rotor/wing/pylon stability, which plagued the XV-3 throughout its career, had been eliminated in the XV-15 design.

In October 1991, a first incident happened where one of the two prototypes crashed. The aircraft started to roll extensively in hover a few meters above the ground. Although the pilots gave a maximum correcting roll control input, the aircraft was not controllable anymore. Shortly after the crash NASA Ames Research Center ended the XV-15 program. The last existing XV-15 was then transferred to Bell which continued the research on the XV-15.

Flight modes and controls

The XV-15 cockpit has dual controls and resembles a helicopter cockpit, including a collective stick. The flight controls are designed to permit single pilot operation from either seat. The pilot inputs during the helicopter mode (nacelle angle at 90°) are identical to the ones of a conventional helicopter. In hover mode, the stick functions as a cyclic pitch controller. A lateral stick deflection generates a differential collective pitch of the rotors and the aircraft starts rolling in the commanded direction. This means that one of the rotors is generating more thrust than the other one and due to that a rolling effect is achieved. A forward or backward movement of the aircraft is achieved with a cyclic pitch input simultaneously on both of the rotors. This control input is given with a longitudinal input on the stick. A yawing movement can be achieved by a differential cyclic input which is done on the pedals.

In airplane mode (nacelle angle at 0°), the control columns and rudder pedals work conventionally too. Pitching the aircraft is done with the elevators at the tail. The elevators can be deflected with a longitudinal stick input. Rolling the aircraft is achieved by a lateral stick input which deflects the flaperons. The tail rudders controlled by the rudder pedals are used to initiate a yawing movement. The mechanical mixing unit does everything needed to convert the controls from the helicopter mode to the fixed wing mode. Control authority between helicopter and airplane mode is phased in as a function of the nacelle tilt angle. This includes changing the rotors from cyclic pitch control in vertical flight to constant speed control for fixed wing flight. In airplane mode, the collective lever can still be used as a power lever. Moving the collective lever causes the throttles on the center console to move.

Figure 1.5 and Figure 1.6 give a simplified overview of the controls of the XV-15 for the helicopter and airplane mode, which have been explained above. This helps to understand the different movements around the lateral, longitudinal and directional axis. Special attention must be paid to the differences between the control surfaces for the helicopter and airplane mode.

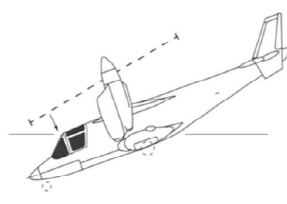
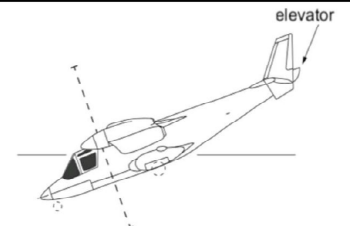
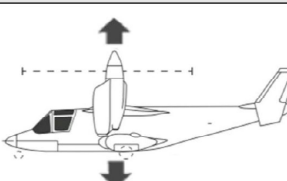
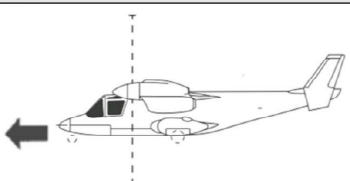
Helicopter Mode	Airplane Mode
Pitching Movement	
	
Generating Thrust	
	

Figure 1.5: Overview about Pitching and Thrust Controls of the XV-15

Two switches, mounted on the collective lever and operated by the pilot's thumb, control the nacelle tilt angle. One pivots the nacelles from end to end in about 12 seconds and allows them to be stopped at any position. The other switch moves the nacelles between pre-selected angles of 0, 60, 75, and 90 degrees (relative to horizontal). To rotate the nacelles, electrical valves activate hydraulic motors. In

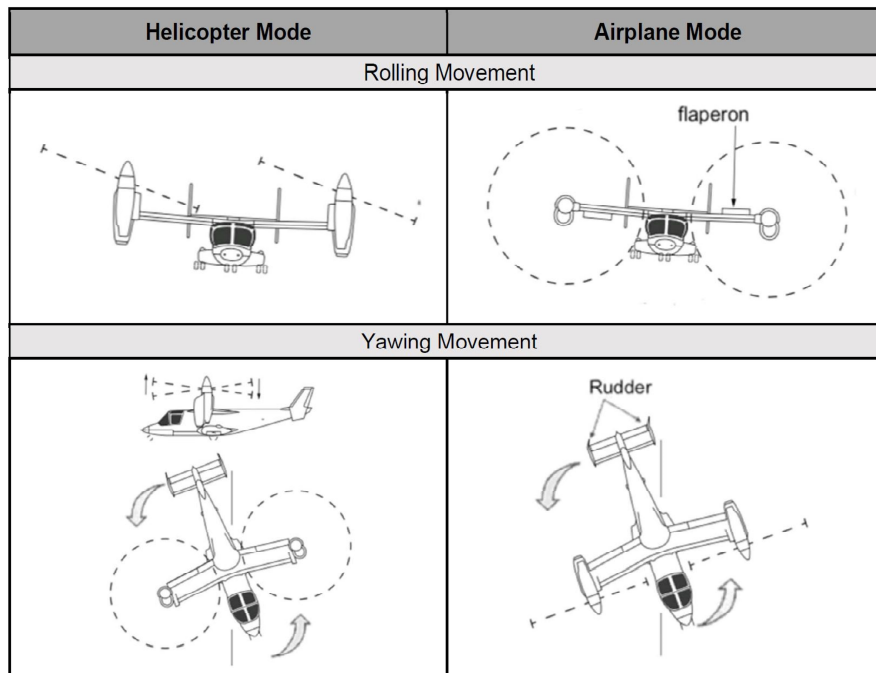


Figure 1.6: Overview about Rolling and Yawing Controls of the XV-15

the event of a complete electrical system failure, the pilot can manually open the valves. This will drive the nacelles to the helicopter position.

Vertical liftoff is very easy, even on a new pilot's first attempt. Whereas helicopters tend to liftoff and promptly bank and pitch up or down slightly, the XV-15 holds attitude on liftoff. Lateral movement is accomplished by banking slightly so that the thrust now has a small side component.

For touchdowns, the surface can have an uphill or downhill slant of as much as 15° , which is well above the limit of most helicopters. Single engine performance is relatively poor. Single engine hover is possible under only a very few conditions.

During transition from hovering to conventional flight (in figure 1.7 the conversion corridor is shown), there is a tendency to lose lift and sink, requiring the pilot to add power. But this is normal on VTOL aircraft. In summary, it can be said that through careful design of an extremely complex aircraft, flying the XV-15 and managing of all systems is straightforward. The safe airspeeds for various nacelle angles can be looked up too in the conversion corridor of the XV-15.

With the nose up and full aft stick, level stalls in the clean configuration give a slight vibration at 205km/h. The aircraft will begin to sink, but there is no wing

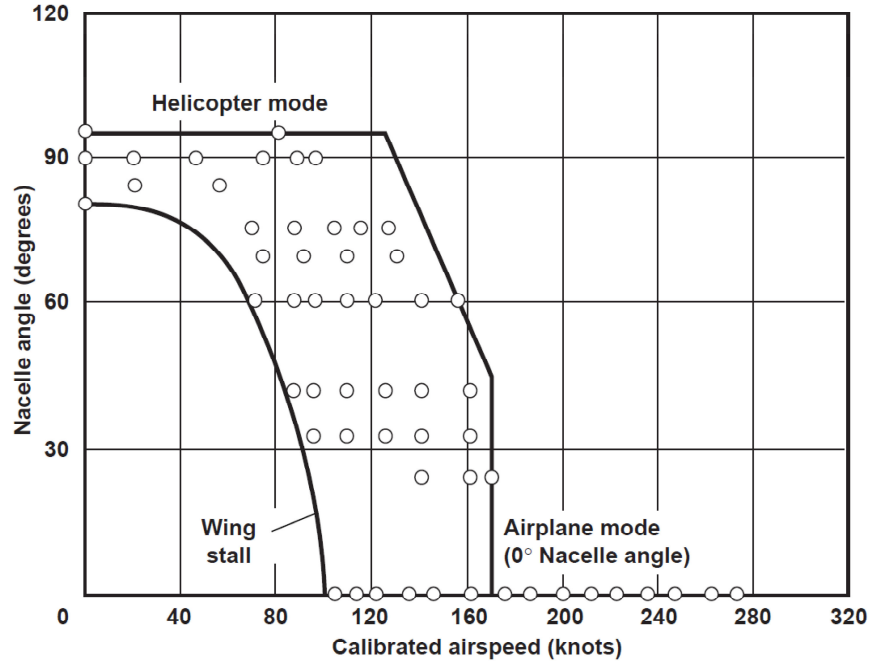


Figure 1.7: Conversion corridor

drop or other bad effects. Recovery is benign and quick. In helicopter autorotation mode, the best descent rate of 11m/s is achieved at 140km/h. At 165km/h, the descent rate increases to 20m/s. For final approaches, pilots quickly learned to use nacelle tilt angle instead of pitch inputs to control airspeed. It is different, but works very well.

Sperry Rand built the original navigation/guidance system. A digital computer provides navigation and control information to the pilot using advanced mechanical and electronic displays. The Calspan Corporation of Buffalo NY designed the Stabilization Control Augmentation System to improve its flight characteristics. The XV-15 does not incorporate fly-by-wire. Ailerons, elevator, and rudder are hydraulically boosted with a triple hydraulic system. They remain active in all flight modes.

1.3 Starting Position and Problem Statement

Due to the trends which were described above, the Centre of Aviation (ZAV) of the Zurich University of Applied Science (ZHAW) is developing a simulator model for a VTOL aircraft based on the Bell XV-15. This simulation model is designed to be used on the Research and Didactics Simulator (ReDSim) which is located at the ZHAW School of Engineering in Winterthur.

In 1988, S.W. Ferguson described the mathematical model for real-time flight simulation of the XV-15 [1]. The model developed at the ZAV is based mainly on the report of S.W. Ferguson and is implemented in MATLAB Simulink. A description for the implementation can be found in the report of F. Barra [2]. Together with the model developed, a trimming routine also provide the possibility to bring the model into a stable flight condition at the beginning of each simulation so that the initial conditions for multiple simulations are always the same. Last, a linearization of the bare A/C is given.

In preparation for this study, previous work on implementation of a stability augmentation system (SAS) was carried out. The system was set for pitch and roll axis. Additionally, a stability analysis of the model for varying airspeeds and nacelle angles was done. From this analysis it could be stated that the longitudinal and lateral stability of the aircraft is still not enough for a reasonable flight handling quality, increasing the workload of the pilot during the flight.

1.4 Project Objective

Due to considerations stated above, the main goal of this project is to develop, implement and design a Control Augmentation System (CAS) for the XV-15 model, which considers all possible nacelle angles and airspeeds, as well as to improve the already mentioned SAS (adding the yaw stability augmentation system). The implemented CAS should be tested and evaluated with pilot-in-the-loop tests.

This work could provide an improvement of the flight handling quality by fixing the stability issues discussed before.

Chapter 2

Automatic Flight Control Summary

2.1 Introduction and Theory Recapitulation

When flying an aircraft, you need to control it. This controlling can be done by humans. But often, it is much easier, safer, faster, more efficient and reliable to do so by computer. But, how is it possible to automatically control a flight? That is what this summary is all about.

2.1.1 Basic flight control concepts

Introduction automatic flight control

The system that is used to control the flight is called Flight Control System (FCS). In the early days of flying, the FCS was mechanical. By means of cables and pulleys, the control surfaces of the aircraft were given the necessary deflections to control the aircraft. However, new technologies brought with it the fly-by-wire FCS. In this system electrical signals are sent to the control surfaces. The signals are sent by the flight (control) computer (FC/FCC). In this way, the aircraft is controlled.

But what is the advantage of automatic flight control? There are several reasons. First of all, a computer has a much higher reaction velocity than a pilot. Also, it isn't subject to concentration losses and fatigue. Finally, a computer can more accurately know the state the aircraft is in. (Computers can handle huge amounts of data better and also don't need to read a small indicator to know, for example, the velocity or the height of the aircraft). However, there also is a downside to FCS. They are only designed for a certain flight envelope. When the aircraft is

outside of the flight envelope, the system can't really operate the aircraft anymore. For these situations, pilots are still needed.

Set-up of the flight control system

The FCS of an aircraft generally consists of three important parts.

- The stability augmentation system (SAS) augments to the stability of the aircraft. It mostly does this by using the control surfaces to make the aircraft more stable. A good example of a part of the SAS is the phugoid damper (or similarly, the yaw damper). A phugoid damper uses the elevator to reduce the effects of the phugoid: it damps it. The SAS is always on when the aircraft is flying. Without it, the aircraft is less stable or possibly even unstable.
- The control augmentation system (CAS) is a helpful tool for the pilot to control the aircraft. For example, the pilot can tell the CAS to 'keep the current heading'. The CAS then follows this command. In this way, the pilot doesn't continuously have to compensate for heading changes himself.
- Finally, the automatic control system takes things one step further. It automatically controls the aircraft. It does this by calculating (for example) the roll angles of the aircraft that are required to stay on a given flight path. It then makes sure that these roll angles are achieved. In this way, the airplane is controlled automatically.

There are important differences between the above three systems. First of all, the SAS is always on, while the other two systems are only on when the pilot needs them. Second, there is the matter of reversibility. In the CAS and automatic control, the pilot feels the actions that are performed by the computer. In other words, when the computer decides to move a control panel, also the stick/pedals of the pilot move along. This makes these systems reversible. The SAS, on the other hand, is not reversible: the pilot doesn't receive feedback. The reason for this is simple. If the pilot would receive feedback, the only things he would feel are annoying vibrations. This is of course undesirable.

2.1.2 Flight dynamics recap

Reference frames

To be able to express the state of the aircraft, a reference frame is needed. Several reference frames are around. The four most important ones are discussed here.

- The Earth-fixed frame of reference F_E is a right-handed orthogonal system. The Z_E axis points to the Earth's center, the X_E axis points North and the

Y_E axis points East. The origin of the system is initially positioned at the aircraft center of gravity (cog). However, the F_E reference frame is fixed to Earth. So, when the aircraft cog moves, the origin of the F_E system stays fixed with respect to the Earth.

- The body-fixed frame of reference F_B also is a right-handed orthogonal system. Its origin lies at the aircraft cog and is fixed to it. The X_B axis is parallel to the aircraft longitudinal axis and points forward. The Y_B axis is parallel to the lateral axis and points to the right. Finally, the Z_B axis points downward.
- The stability frame of reference F_S also is a right-handed orthogonal system. Its origin is fixed to the aircraft cog, just like with F_B . Also, the Y_S axis coincides with the Y_B axis. However, the X_S axis is rotated downward by the angle of attack α . To be more precise, the X_S axis is parallel to the projection of the velocity vector on the plane of symmetry of the aircraft. The Z_S axis still points downward, but it is of course also rotated by an angle α .
- Finally, there is the aircraft frame of reference F_r . Contrary to the other systems, this is a left-handed orthogonal system. Its origin is a certain fixed point on the aircraft (though not the cog). The X_r axis points to the rear of the aircraft, the Y_r axis points to the left and the Z_r axis points upward.

The equations of motion

By using the references frames, it is possible to derive the equations of motion. These equations are, however, nonlinear. So to be able to work with them more easily, they are linearized about an equilibrium position of the aircraft. After the linearization, the equations are putted in a matrix form. To use these equations for computations, they are often transformed into state space form.

The equations derivation is not given here, since the summary is not about this topic. Further details in [3].

2.1.3 Control Theory Recap: frequency domain and diagrams

The frequency domain

Let's suppose to have the state space representation of a system, but the objective is to examine the system in the frequency domain. To do this, it is necessary to put the system in the frequency domain first. To accomplish this, first step is to rewrite the state space form (defined by A, B, C, D) in the Laplace domain ($F(s)$), possibly assuming zero initial conditions for simplify matters a bit. Second

step is to eliminate the state vector $X(s)$ and rewrite the system of equations as $Y(s) = F(s)U(s)$, where $Y(s)$ is the output vector and $U(s)$ is the input vector. Thirdly, the Laplace variable s is substituted by $j\omega$, with $j = \sqrt{-1}$ the complex variable, obtaining

$$F(j\omega) = C(j\omega I - A)^{-1}B + D \quad (2.1)$$

The frequency domain of the system is examinable now. Supposing a sinusoidal input $U(s)$, with a unit magnitude and frequency ω , the result is that the output $Y(s)$ will start to oscillate as well. However, it doesn't do that in exactly the same way. Instead, the amplitude is multiplied by the gain K . Next to this, there is also a phase angle ϕ . Both parameters follow from the transfer function $F(j\omega)$ and can be found using

$$K = |F(j\omega)| \quad \text{and} \quad \phi = \arg(F(j\omega)) \quad (2.2)$$

So, if $K > 1$, the oscillation is amplified. Otherwise, it is reduced in strength. Similarly, if $\phi > 0$, the system has phase lead. Otherwise, it has phase lag.

Different kinds of diagram

The Bode diagram shows how the gain K and the phase angle ϕ vary with the frequency ω . In fact, a Bode diagram consists of two plots. Both plots have on the horizontal axis the frequency ω , on a logarithmic scale. The first plot shows the gain K in decibel (linearly). To put the gain K in decibel, the equation

$$K_{dB} = 20 \cdot \log_{10} K \quad \Longleftrightarrow \quad K = 10^{\frac{K_{dB}}{20}} \quad (2.3)$$

can be used.

The second plot shows the phase angle ϕ (also linearly).

Next to the Bode diagram, there is also the Nyquist diagram (also known as the polar plot) and the Nichols diagram.

2.1.4 Control Theory Recap: system properties

Controllability

Let's examine a system in state space form. In other words, the system can be described by $\dot{x} = Ax + Bu$ and $y = Cx + Du$.

The system, or equivalently the pair (A, B) , is said to be state controllable if, for any initial state $x(0) = x_0$, any time $t_1 > 0$ and any final state x_1 , there exists an input

$u(t)$ such that $x(t_1) = x_1$. Otherwise the system is said to be state uncontrollable. To find out whether a system is state controllable, the controllability matrix R , defined as

$$R = \begin{bmatrix} B & AB & A^2B & \dots & A^{n-1}B \end{bmatrix} \quad (2.4)$$

must be of full rank. In other words, all its rows are linearly independent.

Varying the poles and zeros of the open loop transfer function

Let's examine a basic closed loop system with transfer function $F(s)$. Adding a constant gain K into the system, the transfer function turns from

$$F(s) = \frac{G(s)}{1 + G(s)H(s)} \quad \text{into} \quad F(s) = \frac{KG(s)}{1 + KG(s)H(s)} \quad (2.5)$$

where

- $G(s)$ is the plant
- $H(s)$ is the control system

By varying this gain K , the properties of the system will vary. This is displayed by a root locus plot, which shows how the poles of the closed loop transfer function vary with K .

Sometimes, however, is possible to wind up in a situation, where it is allowed to choose one pole p_{var} of the open loop transfer function $G(s)H(s)$. This situation is very similar to the case where the gain K is chosen. To show this, defining

$$G(s)H(s) = \frac{1}{s - p_{var}} Q(s)^1 \quad (2.6)$$

this will turn the closed loop transfer function into

$$F(s) = \frac{G(s)}{1 + G(s)H(s)} = \frac{\frac{G(s)}{s - p_{var}}(s - p_{var})}{1 - \frac{p_{var}}{s + Q(s)}} = \frac{G_1(s)}{1 + G_1(s)H_1(s)} \quad (2.7)$$

In the last equation, the modified transfer function $G_1(s)$ and $H_1(s)$ are defined as

¹ $Q(s)$ defined by $G(s)$ and $H(s)$ poles and zeros.

$$G_1(s) = \frac{G(s)}{s + Q(s)}(s - p_{var}) \quad \text{and} \quad H_1(s) = -\frac{p_{var}}{G(s)(s - p_{var})} \quad (2.8)$$

Something interesting is now appreciable. Previously, the denominator of the closed loop transfer function was $1 + KG(s)H(s)$. By varying K , the poles varied. This time the denominator is $1 - p_{var}(s + Q(s))^{-1}$, so varying p_{var} is just like varying a gain K .

The same can be done varying zeros. Choosing a zero z_{var} of the open loop transfer function, then $G(s)H(s) = (s - z_{var})P(s)^2$ is obtained. The closed loop transfer function now turns into

$$F(s) = \frac{\frac{G(s)}{1 + sP(s)}}{1 - \frac{z_{var}P(s)}{1 + sP(s)}} = \frac{G_2(s)}{1 + G_2(s)H_2(s)} \quad (2.9)$$

Again, varying z_{var} is like varying the gain K .

This system feature (on which compensators are based) will be use to influence the closed loop system properties.

2.2 Adjusting System Properties

Making an aircraft stable is one thing. But giving it a satisfactory behaviour and being able to control it, that is quite a different matter. This section's focus is looking at some parameters which characterize a system. Then, the way these parameters are influenced is presented.

2.2.1 Important system parameters

For every system, there are several parameters that mention something about the system. Some parameters give hints about the stability of the system. Others are good to know for other reasons.

Phase and gain margins

Let's again examine the system with transfer function $F(s) = G(s)/(1 + G(s)H(s))$. In the frequency domain, if the term $G(j\omega)H(j\omega)$ ever becomes -1 , then the

² $P(s)$ defined by $G(s)$ and $H(s)$ poles and zeros.

system becomes unstable. So, the interest is in the points where $|G(j\omega)H(j\omega)| = 1$ and $\arg(G(j\omega)H(j\omega)) = -180^\circ$. The frequency at which $\phi = \arg(G(j\omega)H(j\omega)) = -180^\circ$ is called the phase crossover frequency $\omega_{\phi=-180^\circ}$. Similarly, the frequency at which $K = |G(j\omega)H(j\omega)| = 1$ (or $K_{dB} = 0$) is called the gain crossover frequency $\omega_{K=1}$.

It's good to know how close the instability is. So, supposing a phase angle of $\phi = -180^\circ$ (thus the frequency is equal to the phase crossover frequency $\omega_{\phi=-180^\circ}$), the gain margin GM is now defined as

$$GM = \frac{1}{|G(j\omega_{\phi=-180^\circ})|} = \frac{1}{K_{\phi=-180^\circ}} \quad (2.10)$$

A gain margin of $GM < 1$ (or similarly, $GM_{dB} < 0$) indicates instability. As a rule of thumb, a $GM_{dB} > 6dB$ is preferred.

Similarly, supposing a gain of $K = 1$ (thus the frequency is equal to the gain crossover frequency $\omega_{K=1}$), the phase margin PM is now defined as

$$PM = 180^\circ + \arg(G(j\omega_{K=1})) = 180^\circ + \phi_{K=1} \quad (2.11)$$

A phase margin of $PM < 0^\circ$ indicates instability. As a rule of thumb, a $30^\circ < PM < 60^\circ$ is preferred.

The phase and gain margins can also be found in the various plots discussed before. To find them, first the point where $\phi = -180^\circ$ (for the gain margin) or $K = 1$ (for the phase margin) has to be detected, followed by the gain/phase angle. Using the definition for the gain margin/phase margin, the corresponding value can be found. In this way, it's possible to identify the ultimate gain K_{ult} , which is defined as the gain K at the phase crossover frequency. It can be found from the gain margin, using

$$K_{ult} = GM = 10^{\frac{GM_{dB}}{20}} \quad (2.12)$$

The phase and gain margins can, however, be misleading. It may happen that the phase and gain margins appear 'safe', but there still is a value of ω for which $G(j\omega)H(j\omega)$ comes close to -1 . Therefore, instead of looking at phase and gain margins, it is often wise to simply look at the Nyquist plot of $G(j\omega)H(j\omega)$ and see if it comes close to -1 . If not, then the system appears to be quite alright.

Other frequency domain parameters

There are more parameters that are related to the frequency domain. Most of these parameters can easily be derived from the Bode plot. A couple of them are discussed.

Let's examine a Bode diagram. In this Bode diagram, there is a frequency region in which the system performs satisfactory. This region is usually a region with a more or less constant gain K_0 . The point(s) where the gain drops below $3dB$ less than this constant gain K_0 is called the cutoff frequency. The slope of the Bode plot at this point is called the cutoff rate. Also, the frequency range in which the system performs satisfactory (being the frequency range between the cutoff frequencies) is called the bandwidth ω_b .

In a Bode diagram, there is often a peak at which the gain K is at a maximum. This phenomenon is called resonance. The corresponding maximum value of the gain K is denoted by the resonance peak M_p . The frequency at which this resonance occurs is called the resonance frequency ω_p .

The last important parameter for the frequency domain is the delay time. The delay time $t_d(\omega)$ for a given frequency ω is given by

$$t_d(\omega) = -\frac{d\phi}{d\omega} = -\frac{d \arg(G(j\omega))}{d\omega} \quad (2.13)$$

Time domain parameters

In the time domain, there are also several relevant parameters. Let's suppose to have a system in which the output $y(t)$ needs to follow the input $u(t)$. Also, suppose to put a step function of size k on the input (though usually $k = 1$ is selected). So, for $t < 0$, $u(t)$ is zero, instead for $t > 0$, $u(t) = k$.

Of course, in the time domain, time matters. So, let's examine some characteristic times. First, the delay time t_d is defined such that $y(t_d) = 0.5y_{ss}$ ³. In other words, at the delay time the system is halfway with adjusting itself to the new input value. The rise time t_r definition is related to $t_{r,initial}$ and $t_{r,final}$. These parameters are defined such that $y(t_{r,initial}) = 0.1$ and $y(t_{r,final}) = 0.9$. The rise time is now given by $t_r = t_{r,final} - t_{r,initial}$. Thirdly, the settling time t_s is the time it takes for the system to come and stay close to the steady state output. So, for all $t > t_s$, $|y(t) - y_{ss}| < 0.02y_{ss}$ is desired (of course, the parameter 0.02 can be varied. A value of 0.05 is often used as well).

Next to these time-parameters, there are also ones not related to time. For example, there is the (maximum) overshoot M_p . This is the difference between the maximum

³ y_{ss} is for steady-state

value of $y(t)$ and its steady state value y_{ss} ($M_p = \max(y(t) - y_{ss})$). And finally, there is the apparent time constant τ . To grasp its meaning, suppose that the output is given by a function of the form $y(t) = y_{ss} - Ae^{(-\alpha t)} \cos(\omega t + \phi)$. The parameter τ is now defined as $\tau = \frac{1}{\alpha}$. In other words, it is the time it takes until the amplitude of the oscillation has reduced to 37% of its value.

Error specifications

When designing a system, there are usually requirements. These requirements can also concern the error which the system has. To examine the error, first simply assume that $H(s) = 1$. Thus $F(s) = G(s)/(1 + G(s))$. The open loop transfer function $G(s)$ of the system can be rewritten as

$$G(s) = K \frac{s^a \prod_{i=1}^{m-a} (s + z_i)}{s^b \prod_{j=1}^{j=n-b} (s + p_j)} = K_{mod} \frac{\prod_{i=1}^{m-a} (\tau_{z,i} s + 1)}{s^l \prod_{j=1}^{j=n-b} (\tau_{p,j} s + 1)} \quad (2.14)$$

In other words, the open loop transfer function has m zeroes and n poles. A number a of these zeroes is equal to zero. Similarly, a number b of the poles is zero as well. The parameter $l = b - a$ denotes the type of the system. If $l = 0$ system type is 0, if $l = 1$ system type is 1, and so on.

The system output $Y(s)$ should follow the system input $U(s)$. So, the error $E(s)$ is defined as

$$E(s) = U(s) - Y(s) = U(s) - U(s)F(s) = U(s) - U(s) \frac{G(s)}{1 + G(s)} = \frac{U(s)}{1 + G(s)} \quad (2.15)$$

To find the eventual error $e(\infty)$ of the system, the final value theorem⁴ is applied. It implies that

$$e(\infty) = \lim_{t \rightarrow \infty} e(t) = \lim_{s \rightarrow 0} sE(s) = \lim_{s \rightarrow 0} \frac{sU(s)}{1 + G(s)} = \frac{sU(s)}{1 + \frac{K_{mod}}{s^l}} \quad (2.16)$$

Now, giving inputs to this system, it is possible to find the error, obtaining the following results

- First, a step input is considered. Thus, $u(t) = 1$ (for $t > 0$) and $U(s) = \frac{1}{s}$. For type 0 systems, there is a steady state error of $e(\infty) = \frac{1}{1 + K_{mod}}$. However, for type 1 and beyond, the error is zero (by the way, this error is called a position error).

⁴The final value theorem is a theorem used to relate frequency domain expression to the time domain behavior as time approaches infinity.

- Second, a ramp input is considered. So, $u(t) = t$ (for $t > 0$) and $U(s) = \frac{1}{s^2}$. This time, type 0 systems give an infinite error: it diverges. Type 1 systems give a steady state error of $e(\infty) = \frac{1}{K_{mod}}$. Type 2 systems and beyond give a zero error (this error is called a velocity error).
- Third, a parabolic input is considered. So, $u(t) = \frac{1}{2}t^2$ (for $t > 0$) and $U(s) = \frac{1}{s^3}$. This time, type 0 and type 1 systems give an infinite error. Type 2 systems give a steady state error of $e(\infty) = \frac{1}{K_{mod}}$. Type 3 systems and beyond give a zero error (this error is called an acceleration error).

The general trend can easily be understood. So, the type of the system determines which kind of position, velocity and acceleration errors the system has.

2.2.2 Controllers - time domain

By varying the (proportional) open-loop gain K of the system, we can already vary its properties by quite a bit. But, sometimes varying this gain is not enough. In that case, we need a compensator or a controller.

PID Control

Let's examine a basic feedback loop with $H(s) = 1$. In this feedback loop, the output signal $Y(s)$ is fed back to the system. Usually, the signal that is fed back is proportional to the output. Thus, a proportional controller is considering: $K(s) = K_p$, where K_p is the proportional gain, $K(s)$ is the controller function. A proportional controller generally reduces the rise time t_r , increases the overshoot M_p and reduces the steady state error e_{ss} .

Sometimes, however, it may be convenient to get the derivative of the output as feedback signal. In this case, a derivative controller is used: $K(s) = K_D s$, where K_D is the derivative gain. A derivative controller reduces the overshoot M_p and settling time t_s .

Finally, the integral controller could be also used: $K(s) = \frac{1}{s} K_I$, where K_I is the integral gain. An integral controller reduces the rise time t_r and sets the steady state error e_{ss} to zero. However, it increases the overshoot M_p and the settling time t_s .

These controllers are usually combined. This results in a PID controller:

$$K(s) = K_p + \frac{K_I}{s} + K_D s = \frac{K_D s^2 + K_p s + K_I}{s} \quad (2.17)$$

By using the PID controller, the parameters t_r , t_s , M_p and e_{ss} could be influenced in many ways, just varying the gains K_p , K_D and K_I . But which gains have to be chosen? For that, tuning rules are used.

PID controllers are detailed in section 2.5.1.

The Ziegler-Nichols tuning rules

There are two variants of Ziegler-Nichols tuning rules: the quarter decay ratio method and the ultimate sensitivity method. For both methods, $K(s)$ is defined as

$$K(s) = K_p \left(1 + \frac{1}{T_I s} + T_D s \right) \quad (2.18)$$

- Quarter decay ratio method. These tuning rules should give a decay ratio of 0.25 (the decay ratio is the ratio of the magnitudes of two consecutive peaks of an oscillation). First, the response of the original system to a unit step input will be examined. From this, lag $L \approx t_d$ (which is the time until the system really starts moving) is defined, as well as the slope $R \approx y_{ss}/t_r$, which is the average slope of the system response during its rise time.

Based on the values of L and R , the gains are chosen. For only proportional gain, then $K_p = \frac{1}{RL}$. For PI controller, then $K_p = \frac{0.9}{RL}$ and $T_I = \frac{L}{0.3}$. Finally, for a PID controller, then $K_p = \frac{1.2}{RL}$, $T_I = 2L$ and $T_D = 0.5L$. These rules should then roughly give a decay ratio of 0.25. Although some additional tuning is often necessary/recommended.

- Ultimate sensitivity method. First, the original system with a gain equal to the ultimate gain $K_p = K_{ult}$ is considered. In other words, K_p is chosen such that the system has continuous oscillations without any damping. The corresponding ultimate period of these oscillations is now denoted by P_u . This does mean that the ultimate sensitivity method can only be used when continuous oscillations can be achieved. In other words, the root locus plot has to cross the imaginary axis at a point other than zero.

Based on the values of K_{ult} and P_u , the gains are chosen. For only proportional control, then $K_p = 0.5K_{ult}$. For PI controller, then $K_p = 0.45K_{ult}$ and $T_I = \frac{P_u}{1.2}$. Finally, for a PID controller, then $K_p = 0.6K_{ult}$, $T_I = \frac{1}{2}P_u$ and $T_D = \frac{1}{8}P_u$. Again, additional tuning is often necessary/recommended.

2.2.3 Compensators - frequency domain

Three kinds of compensators

There are three important kinds of compensators. These are the lead compensator, the lag compensator and the lead-lag compensator, respectively given by the transfer functions

$$D_1(s) = K(s + z), \quad D_2(s) = \frac{K}{s + p}, \quad D_3(s) = K \frac{s + z}{s + p} \quad (2.19)$$

Let's look at these compensators individually.

The lead compensator offers PD control. This causes it to speed up the response of a system. In other words, the rise time t_r goes down. Also, the overshoot M_p becomes less. The lead compensator does have a problem though. It increases the gain of the system at high frequencies. In other words, with a lead compensator high frequencies are amplified. This is generally not very good.

The lag compensator offers PI control. This means that it improves the steady state accuracy (if it is needed to have $e_s \approx 0$, then a lag compensator comes in handy). The PI controller reduces high-frequency noise. As such, it can be used as a low-pass filter⁵.

The lead-lag compensator combines the lead and the lag compensator. In this way, the negative effects of the lead compensator can be compensated for. First, a lead compensator can be used to speed up the response of the system. Then a lag compensator is also added, such that the high frequency effects are limited. This lag compensator is made such that its effects on the biggest part of the system are negligible.

In the lead-lag compensator, the lead compensator is the most important part. However, we can also put it together such that the lag compensator is the most important part. In this case, we often call the compensator a lag-lead compensator.

Tuning the compensators

Using lead and lag compensators is like adding zeros and poles to the system. But when doing this, an important question arises: where do we put the zeros and poles? For this, the root locus plot could be used. So, now a nice rule of thumb

⁵This is a filter that only lets low frequencies pass.

derives: poles push the locus away, whereas zeros attract the locus. But there are also more precise rules to place the zeros and poles.

Supposing to set up a lead compensator. Thus the zero has to be chosen. It is often wise to put this zero in the neighbourhood of the natural frequency ω_N which you want the system to have. This natural frequency can roughly be determined from the parameters t_r and/or t_s using the approximate equations

$$t_r \approx \frac{1.8}{\omega_N} \quad \text{and} \quad t_s \approx \frac{4.6}{\zeta \omega_N} \quad (2.20)$$

In this equation, the value of ζ can be often be determined from the required value of the overshoot peak M_p , according to

$$\zeta \approx 0.7 \quad \text{when} \quad M_p \approx 5\%$$

$$\zeta \approx 0.5 \quad \text{when} \quad M_p \approx 15\%$$

$$\zeta \approx 0.3 \quad \text{when} \quad M_p \approx 35\%$$

Table 2.1: $\zeta - M_p$ relationship

To compensate for high frequency effects, a pole could be added (as a lag compensator). This pole, however, should be relatively far away from the zero. A rule of thumb is to place the pole 5 to 20 times closer from the origin as the zero. Thus, $z \approx (5 \text{ to } 20) \cdot p$.

An in-deep and detailed explanation about compensators is presented in section 2.5.2.

2.3 System Performance Specifications

Previously, how to influence the parameters of a system has been considered. In this section, the requirements which an aircraft should have are investigated. First, the way the requirements are built up is examined, later on, which parameters are subject to these requirements.

2.3.1 Requirements on handling qualities

Flying quality requirements

Most countries have regulating agencies (like the *EU-OPS* for Europe and the *FAR* for the US). These agencies specify flying quality requirements. These requirements are the minimum acceptable standard of the flying (or handling) qualities of an aircraft. They define rules subject to which the stability, control and handling of the aircraft must be designed.

The flying quality requirements differ per aircraft class. Small light airplanes are class I, medium weight airplanes are class II, big heavy airplanes are class III and high manoeuvrability airplanes are class IV. Next to this, there are also separate criteria per flight phase. Category A concerns non-terminal flight phases that require rapid manoeuvring, precision tracking or precise flight path control (e.g. air combat/terrain following). Category B is about non-terminal flight phases that require gradual manoeuvring, less precise tracking and less accurate flight path control (e.g. climb, descent and cruise). Finally, category C relates to terminal flight phases that require gradual manoeuvring and precision flight path control (e.g. take-off and landing).

Aircraft manufacturers must demonstrate a compliance with the specifications. This is done by using flight tests. In these tests, the flying quality of the aircraft is rated. This is often done based on the *Cooper-Harper* scale. In this scale, a 1 means the aircraft has excellent handling qualities, and the pilot workload is low. On the other hand, a 10 means that there are major deficiencies in the handling quality of the aircraft. A test is never performed for just an aircraft or just a control system. It is always performed for the combination of the aircraft and the control system.

Flight requirements are generally specified for three levels of flying quality. Level 1 means that the flying qualities are clearly adequate for the respective flight phase. Level 2 means that the flying qualities are still adequate, but there is an increase in pilot workload and/or degradation in mission effectiveness. In level 3, the flying qualities are degraded. However, the airplane can still be controlled, albeit with an inadequate mission effectiveness and a high or limiting pilot workload. Airplanes must be designed to satisfy level 1 flying quality requirements with all systems in their normal operating state. Within this thesis work, we will try to satisfy this requirement.

Handling qualities

Flying quality requirements are present to make sure aircraft have handling qualities. But what do these qualities mean? Flying qualities concern how well a task can be fulfilled and how the aircraft responds to inputs. Important parameters that influence these qualities include the stability of the aircraft and the flight control system (FCS) characteristics. Let's take a closer look at these two parameters.

With stability, we mean how easy it is to establish an equilibrium flight condition, without the aircraft having a tendency to diverge. There are two kinds of stabilities. With static stability, we mean that every deviation causes an opposing force/moment. However, the deviation does not have to be eliminated. It could simply be the case that a new equilibrium position is created. With dynamic stability we also mean that every deviation from the equilibrium position is eliminated. In other words, the system returns to the original equilibrium position. It is usually preferable to have an aircraft stable. However, if an aircraft is too stable, then it's not manoeuvrable anymore: it's too hard to get it out of its equilibrium position. So, this isn't a positive thing either.

There are three ways in which the FCS can have a bad effect on the flying qualities. First, something can occur between the cockpit and the actuators (e.g. there may be a lag in the signal that is sent to an actuator). Second, there can also be a lag in an actuator itself (e.g. when the ailerons takes a long time to deflect). And finally, the displays in the cockpit can lag. Because this is undesirable, requirements are made concerning these lags. Next to this, also control system break-out forces are important. These are the forces which the pilot must apply before his actions have any effect at all.

Giving an airplane the right handling qualities usually isn't easy. It often has a bad effect on the performance and weight of the aircraft. Therefore, trade-offs often need to be made between the handling quality and the performance of the aircraft. That is, if trade-offs can be made. Requirements on the handling qualities are simply present and they have to be followed.

2.3.2 Parameters subject to requirements

Longitudinal flight requirements

Now let's look at some actual requirements for aircraft, first on the longitudinal flight, then on the lateral flight.

In longitudinal flight, there are requirements on the control forces which the pilot

needs to exert. These forces are often indicated by the stick force F_S . In a manoeuvring flight, the gradient $\partial F_S / \partial n$ with respect to the load factor n is important. It should fall within limits. Also, there should be no significant nonlinearities in it. Next to this, when the airplane configuration changes a bit (e.g. flaps are deployed), the control forces shouldn't change either.

When the aircraft changes its speed, no strange things may happen either. The stick-force-speed-gradient $\partial F_S / \partial V$ must be stable and must meet other specs. Also, the return-to-trim-speed-behaviour must meet certain requirements. During take-off and landing (with fixed trim controls) the control force must be within certain limits. Also, during a dive, the control force may not exceed certain values. These values also depend on whether the aircraft is equipped with a stick or a wheel. Also, the allowable values depend on whether it concerns pushing or pulling the wheel/stick.

Next to control forces, also the dynamic behaviour of the aircraft is important. Let's consider the phugoid requirements first. The phugoid must have a certain prescribed damping ζ . And if the eigenmotion is allowed to be unstable (for example, during a level 3 flying quality situation), then there will be a requirement on the time to double amplitude $T_{2,ph}$. This time can be found, by using

$$A_{ph} e^{-\zeta_{ph} \omega_{n,ph} (t_1 + T_{2,ph})} = 2 A_{ph} e^{-\zeta_{ph} \omega_{n,ph} t_1} \quad \Rightarrow \quad T_{2,ph} = \frac{\ln 2}{-\zeta_{ph} \omega_{n,ph}} \quad (2.21)$$

In the above equation, A_{ph} is the amplitude of the phugoid motion, ζ_{ph} the damping ratio and $\omega_{n,ph}$ the natural frequency.

Similar to the phugoid, there are also short period motion requirements. These requirements of course concern the damping ratio ζ_{sp} . But for the short period motion also the natural frequency $\omega_{n,sp}$ is quite important. However, for (highly) augmented airplanes, these requirements are not used. Instead, the control anticipation parameter (CAP) is used, which is defined as

$$CAP = \frac{\dot{q}(t=0)}{n_z(t=\infty)} = \frac{\omega_{n,sp}^2}{n_\alpha} \quad (2.22)$$

In this equation, $n_\alpha = \partial n / \partial \alpha$ is the gust- or load-factor- sensitivity. By using flight dynamics equations, expressions/approximations can be calculated for $\omega_{n,sp}$ and n_α , after which the CAP can be found.

Finally, the aircraft must have flight path stability. This means that there are requirements on the derivative $\partial \gamma / \partial V_P$. The term ∂V_P here denotes the changes

in velocity that are caused by pitch control only (e.g. engine throttle effects are not taken into account).

Lateral flight requirements

There are several requirements for lateral flight as well. First, the focus is on lateral control forces. These concern both the (sideways) forces on the stick and the forces on the rudder pedals. The force requirements depend on the situation (for example, there are separate requirements for the situation where one engine isn't functioning anymore). It also matters whether it concerns a short/temporary force or a prolonged force.

Now let's examine the Dutch roll. For this eigenmotion, of course the damping ratio ζ_d is very important, as well as the natural frequency $\omega_{n,d}$. Therefore, there are certain minimum values for these parameters. There are also requirements on the product $\zeta_d \omega_{n,d}$, and depending on the roll angle ϕ and the sideslip angle β , more complicated requirements can be put on the damping and frequency.

For the spiral eigenmotion, divergence is usually allowed. Now, the time $T_{2,s}$ until a double amplitude is reached (with cockpit controls free) is an important parameter. For the roll mode, the roll mode time constant T_R is important. A maximum value is usually specified.

Stability and manoeuvrability also matter. How quickly can an airplane reach a certain roll angle? Or alternatively, in a given time, what maximum roll angle can be achieved? And is the aircraft directionally stable? In other words, it is required that $C_{n,\beta} > 0$. Next to this, it is also desired/required that $C_{Y,\beta} < 0$ and $C_{l,\beta} < 0$.

The Gibson criterion

The Gibson criterion is a special criterion to prevent certain aircraft behaviour. It is mainly relevant when a pilot is trying to change the pitch rate of the aircraft. The Gibson criterion can be split up into the dropback criterion and the phase rate criterion. We'll examine the dropback criterion first.

Let's suppose to have a certain pitch angle. For reaching another pitch angle, the pilot deflects the elevator, until he achieves the desired pitch. Then, he lets go of the control surfaces. What happens next? If the vehicle goes back to a situation with a smaller pitch angle, then *dropback* (DB) occurs. However, if the pitch angle continues to increase, then *overshoot* (OS) occurs (dropback can thus be seen as negative overshoot and vice versa).

The dropback criterion concerns dropback. Important parameters are the maximum pitch rate q_m , the steady state value of the pitch rate q_s and the pitch rate overshoot ratio q_m/q_s . The dropback criterion now describes a region in which the values of DB/q_s and q_m/q_s should be. Basically, zero dropback is optimal. However, some dropback is preferred to overshoot. Acceptable pitch rate overshoot values are $1 \leq q_m/q_s \leq 3$.

The phase rate criterion is present to prevent/reduce pilot induced oscillations (PIOs). A PIO can occur when the pilot continuously tries to compensate for something, but by doing so only contributes to oscillations. Important parameters now are the frequency at 180° phase lag $\omega_{\phi=-180^\circ}$ and the phase rate at 180° phase lag $(\partial\phi/\partial\omega)_{\phi=-180^\circ}$. The phase rate criterion now demands that

$$\omega_{\phi=-180^\circ} \approx 1 \text{ Hz} \quad \text{and} \quad \left(\frac{\partial\phi}{\partial\omega} \right)_{\phi=-180^\circ} \leq 100 \text{ deg/Hz} \quad (2.23)$$

The optimum for the parameters is for $\omega_{\phi=-180^\circ}$ to be somewhere between 1 and 1.4 and for $(\partial\phi/\partial\omega)_{\phi=-180^\circ}$ to be somewhere between 60 Hz and 90 Hz. In this case, then the chance that a PIO occurs is really low.

2.4 Control Augmentation System (CAS)

In the previous work, the stability augmentation system was implemented. This system can be seen as the inner loop of the aircraft control system. In this chapter, the focus is on the outer loop: the control augmentation system. When a certain pitch angle, velocity, roll angle, heading, or something similar has to be kept, then a CAS is used. In this way, the pilot workload can be reduced significantly. First, holding longitudinal parameters are examined, then, the lateral once as well.

In the next subsections, the basic layout of the CAS (on longitudinal and lateral-directional axis) is presented. In chapter 3 his implementation, with detailed information regarding the controller, is given.

2.4.1 Basic longitudinal control augmentation system

Holding the pitch attitude is the aim on the longitudinal axis. It will be carried out in the next chapter. The altitude, the airspeed and the climb/descent rate hold are also introduced, as they can be implemented in future works.

Holding the pitch attitude

The pitch attitude hold mode prevents pilots from constantly having to control the pitch attitude. Especially in turbulent air, this can get tiring for the pilot.

This system uses the data from the vertical gyroscope as input (feedback). It then controls the aircraft through the elevators. An overview of the system can be seen in figure 2.1.

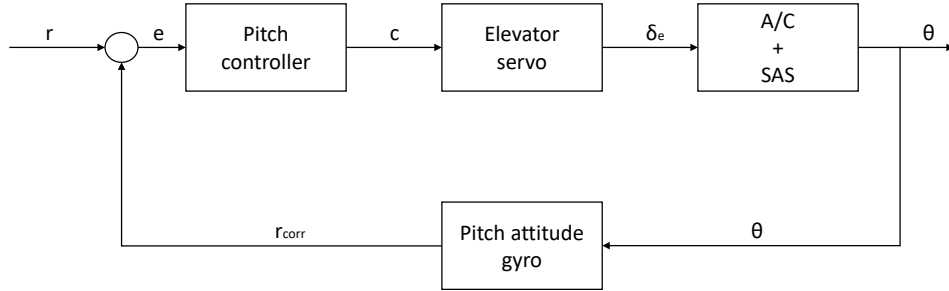


Figure 2.1: An overview of the pitch attitude holding system

where

- r is the reference signal
- e is the error signal
- r_{corr} is the feedback signal
- θ is the pitch angle
- δ_e is the elevator deflection
- c is the command signal

The design of the control block involves choosing the right gains of a PID controller (K_p, K_i, K_d) or placing poles and zeros of a compensator. As a result of the controller design, the SAS of the aircraft could need to be adjusted.

Holding the altitude

The altitude hold mode prevents pilots from constantly having to maintain their altitude. The input (feedback) comes from the altimeter. The system then uses the elevator to control the altitude.

The altitude parameter h can be derived using

$$\dot{h} = V \sin \gamma \approx V \gamma \quad \Rightarrow \quad h(s) = \frac{V}{s} \gamma(s) = \frac{V}{s} (\theta(s) - \alpha(s)) \quad (2.24)$$

Using a constant gain for the altitude controller can lead the phugoid to become unstable (this can happen if a low gain is used, and if the original phugoid was already not so damped). To prevent this situation from occurring, several options are possible like using a vertical acceleration feedback or lead-lag compensation.

It usually turns out that an integral action is not necessary.

Holding the airspeed

The airspeed hold mode holds a certain airspeed. It uses the airspeed sensor as input and it controls the throttle.

The reference value of the velocity V is often set at the autopilot control panel. Alternatively, it can be derived from the throttle input. For example, if the pilot manually pushes the throttle forward, the FCC increases the desired (reference) velocity V .

Usually, only a proportional gain is used.

Holding the climb or descent rate

The flight path angle hold mode is similar to the pitch attitude hold mode. In this control system, the flight path angle/climb rate is kept constant. As input (feedback), the flight path angle is used, but γ can't be measured directly. So, γ is calculated as

$$\gamma = \theta - \alpha \quad (2.25)$$

The flight path angle hold mode eventually uses the elevators to control the flight path angle.

Usually, the derivative action is not required. Transient behaviour is mostly acceptable when adjusting the flight path angle. A steady state error, however, is more troubling. So integral actions are often used.

2.4.2 Basic lateral control augmentation system

Holding the roll angle, together with the sideslip suppressor, is the aim on the lateral-directional axis. These will be carried out in the next chapter. The heading hold is also introduced, as it can be implemented in future works.

Holding the roll angle

The roll angle hold mode prevents the pilot from constantly having to adjust/control the roll angle during a turn. It uses the roll angle gyro as sensor and it effects the ailerons. An overview of the system can be seen in figure 2.2.

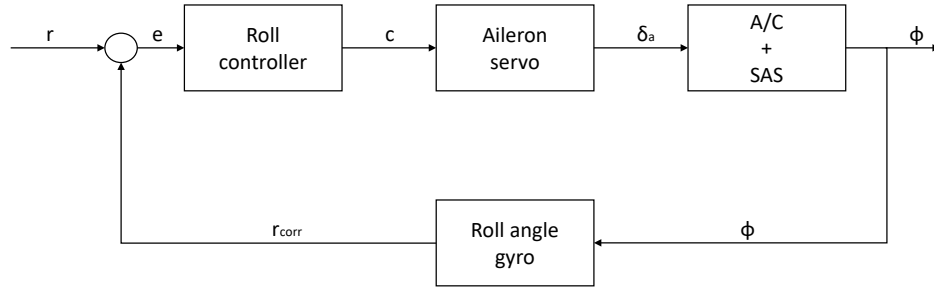


Figure 2.2: An overview of the roll angle holding system

where

- r is the reference signal
- e is the error signal
- r_{corr} is the feedback signal
- ϕ is the roll angle
- δ_a is the aileron deflection
- c is the command signal

When modelling the aircraft, it is often assumed that rolling is the only degree of freedom, in order to simplify matters. Thus, the transfer function between $\phi(s)$ and $\delta_a(s)$ becomes

$$\frac{\phi(s)}{\delta_a(s)} = \frac{-L_{\delta_a}}{s(s - Lp)} \quad (2.26)$$

Nevertheless, it is often worth while to check whether the behaviour of the full model (without the simplifications) is much different from that of the reduced model. It can, for instance, occur that the Dutch roll becomes unstable in the full model, whereas the reduced model doesn't indicate this.

Suppressing the sideslip angle

The coordinated roll angle hold mode is an extension of the roll angle hold mode. It also tries to make sure that the sideslip angle β is equal to zero. This should result in a coordinated turn⁶, thus giving the aircraft less drag and the passengers more comfort. A turn is said to be 'coordinated' when the lateral acceleration n_y and the sideslip velocity (v), hence the sideslip angle (β), are zero. In any turn, sideslip angle occurs if the rate of yawing (r) is different from the value given by

$$r = \frac{g}{U_0} \sin(\phi) \quad (2.27)$$

The turn will not be coordinated in that case. Therefore, this suppressor control system maintains the sideslip angle close to zero during any maneuver, with proper rudder deflections.

The coordinated roll angle hold mode uses the sideslip sensor (vane-type sideslip sensor) as input (feedback). Alternatively, it is possible to use also the lateral acceleration n_y as input to the rudder, obtaining the same effect.

Holding the heading angle

The heading angle control mode controls the heading. It does this by giving the aircraft a roll angle. In fact, it sends a signal to the (coordinated) roll angle hold mode, telling it which roll angle the aircraft should have. This roll angle is maintained until the desired heading is achieved. As sensor, this system uses the directional gyro. Its output effects the ailerons (the latter is obviously, since the system controls the roll angle hold mode).

2.5 Dynamic Compensation

In this section, more details about PID and LEAD-LAG compensators are presented.

2.5.1 PID regulators

How a PID regulator is built is shown in figure 2.3 (R is the reference signal).

⁶This controller is usually called coordinated roll angle hold mode.

⁷ U_0 is the longitudinal flight velocity.

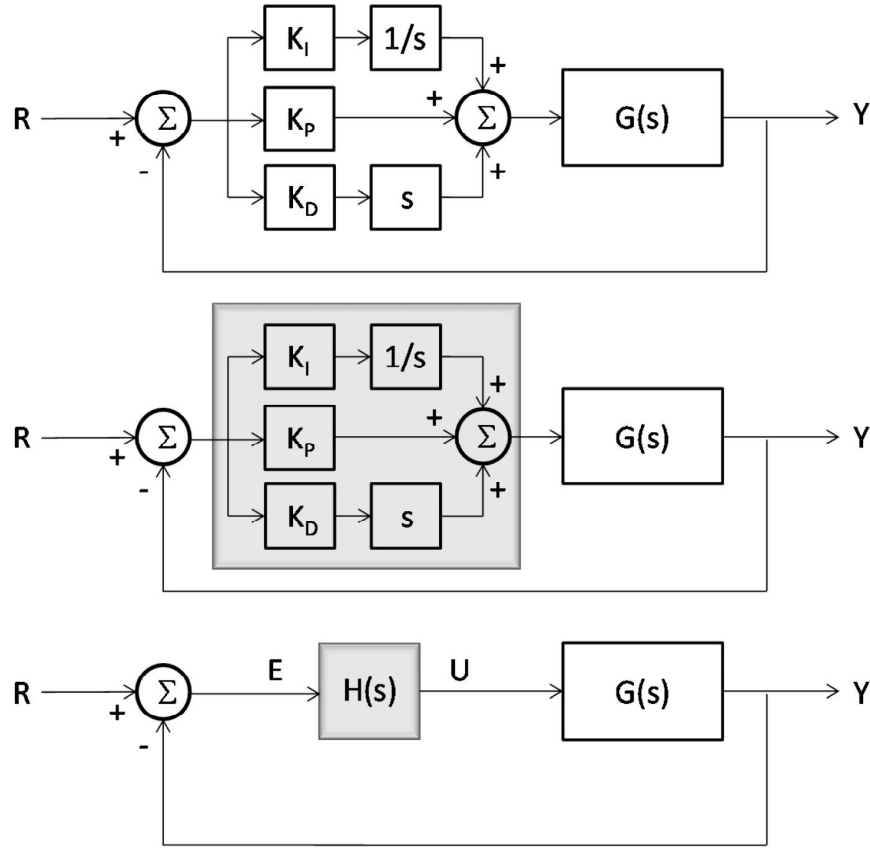


Figure 2.3: PID compensator

Looking at figure 2.3, it is clearly that

$$u(t) = K_P e(t) + K_I \int e(\tau) d\tau + K_D \frac{d}{dt} e(t) \quad (2.28)$$

$$U(s) = \left(K_P + K_I \frac{1}{s} + K_D s \right) E(s) = H(s) E(s) \quad (2.29)$$

where

$$H(s) = K_P + K_I \frac{1}{s} + K_D s = \frac{K_D s^2 + K_P s + K_I}{s} \quad (2.30)$$

Strictly speaking a PID regulator introduced a pole at the origin and two zeros in the feedforward loop.

The PID (Proportional, Integral and Derivative) controller produces a control signal that consists of the weighted sum of three terms:

- The P-term produces a signal that is proportional to the error between the actual and the desired value of the to-be-controlled variable. It achieves the basic feedback compensation control, leading to a control input whose purpose is to make the to-be-controlled variable increase when it is too low and decrease when it is too high.
- The I-term feeds back the integral of the error. This term results in a correction signal whenever this error does not converge to zero. When properly tuned, this term achieves robustness, good performance not only for the nominal plant but also for plants that are close to it, since the I-term tends to force the error to zero for a wide range of the plant parameters. To understand how the I-term works we have to analyze the steady state error formulation

$$e_{ss} = \lim_{t \rightarrow \infty} e(t) = \lim_{s \rightarrow 0} sE(s) = \lim_{s \rightarrow 0} s \frac{R(s)}{1 + G(s)H(s)} \quad (2.31)$$

and the e_{ss} table

System Type	Step	Ramp	Parabolic
0	$\frac{A}{1 + K_p}$	∞	∞
1	0	$\frac{A}{K_v}$	∞
2	0	0	$\frac{A}{K_a}$

Table 2.2: Steady state error e_{ss} table

where

- A is the signal amplitude
- K_p is the position error
- K_v is the velocity error
- K_a is the acceleration error

The I-term make the position error $K_p = \lim_{s \rightarrow 0} G(s)H(s)$ tend to infinity and cancel the steady state error of a type 0 system tracking a step input.

- The D-term acts on the derivative of the error. It results in a control correction signal as soon as the error starts increasing or decreasing, and it can thus be expected that this anticipatory action results in a fast response. Be aware that the derivation process can lead to unexpected results when the signal is noise-corrupted: in this case it is important to filter the error signal with a low-pass filter in order to remove higher frequency noise components. As low-pass filtering and derivative control can cancel each other out, the amount of filtering is limited.

Some applications may require using only one or two actions to provide the appropriate system control. This is achieved by setting the other parameters to zero. A PID controller will be called a PI, PD, P or I controller in the absence of the respective control actions.

Parameter	Rise time	Overshoot	Settling time	Steady-state error	Stability
K_P	Decrease	Increase	Small change	Decrease	Degrade
K_I	Decrease	Increase	Increase	Eliminate	Degrade
K_D	Minor change	Decrease	Decrease	No effect (to be checked)	Improve if K_D small

Table 2.3: Effect of increasing a parameter independently

According to 2.3, it would be incredibly effective rise selectively K_I , for example, at low frequency to cancel the steady state error, while limiting its effect at high frequency, where it has the undesirable effect of increasing the overshoot. PID regulator, though, do not have this feature.

2.5.2 Lead and lag compensators

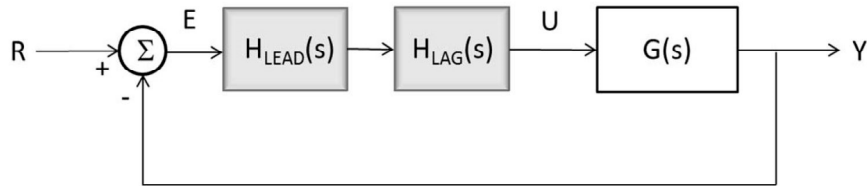


Figure 2.4: Lead-lag compensator

Lead-lag compensators work exactly like PID regulators but in a much smarter way as the effect of each term can be modulated over the frequency range. To

explain this interesting feature we have to analyze, separately, the Bode diagram of the two filters, the lead compensator and the lag compensator, which can be used singularly or as a system. Lead and lag compensator are defined with the same equation:

$$H(s) = \frac{s + z}{s + p} \quad (2.32)$$

Where p and z represent the constant values of a pole and a zero. The difference between lead and lag compensator lies in the order of magnitude of the ratio z/p .

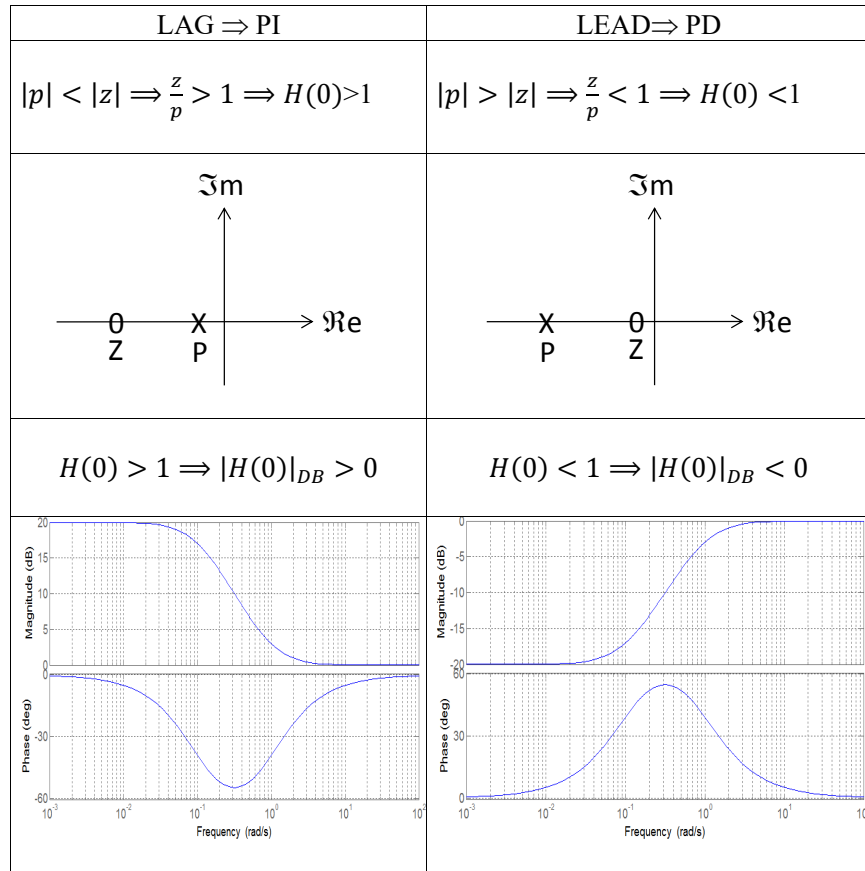


Figure 2.5: Effect of ratio z/p

The LAG compensator works as a PI filter, but the integral part is particular effective just where is strictly necessary, namely at low frequency where it increases the gain as to reduce the steady-state error. The drawback is a phase margin reduction at high frequency, which could jeopardize the phase margin specification.

The LEAD compensator works as a PD filter and is particularly effective at high frequency, where it is necessary to decrease the rise time. The drawback is a loss of the static gain which leads to an increase of the steady state error.

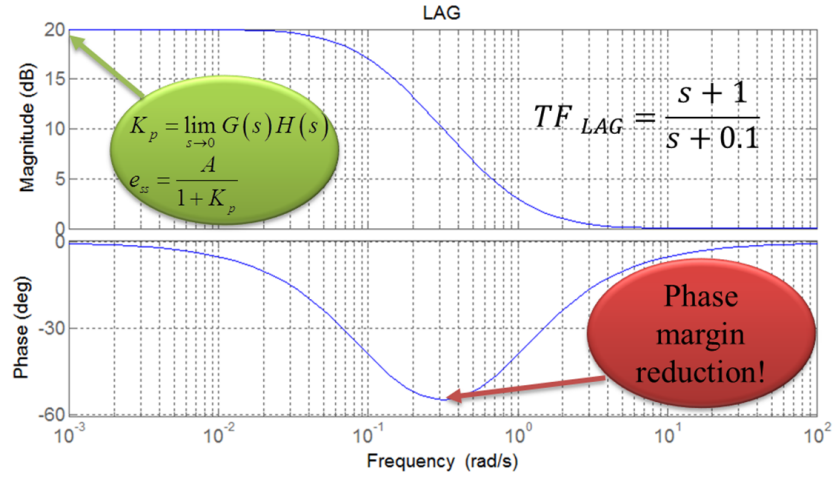


Figure 2.6: Frequency analysis of the LAG compensator

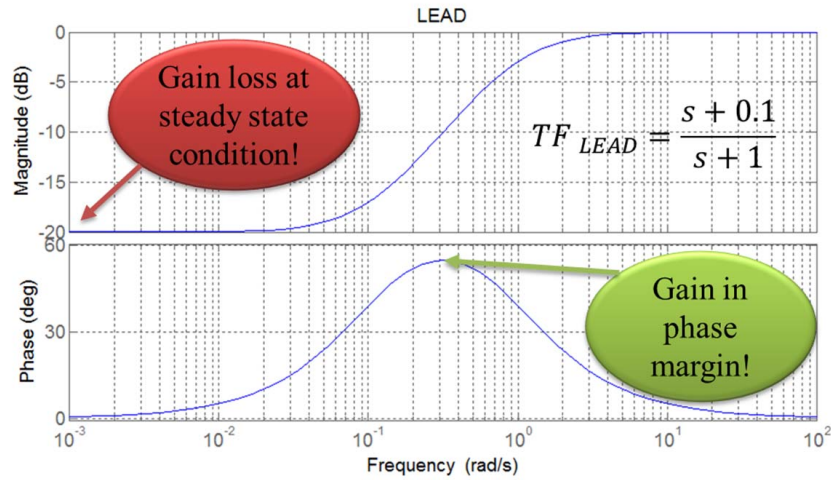


Figure 2.7: Frequency analysis of the LEAD compensator

If used together, the lead and lag compensators work as a PID filter, provided the relative poles and zeros do not cancel with each other. The design of the lead-lag compensator consists in defining a proper choice of poles and zeros, as to meet the control specification. The test-case illustrated in the next chapter will show how poles and zeros of a lead-lag compensator can be properly placed.

Chapter 3

Control Augmentation System Development and Implementation

In the following chapter the methodical approaches and the developed CAS is described. The chapter is divided into sections about the XV-15 Simulink model, the review on the exiting SAS, the development and implementation of the CAS and the gain-scheduled method.

3.1 XV-15 Simulink Model

The following section provides an overview of the XV-15 simulation model that was developed at the ZHAW, in order to understand the work carried out. The mathematical basis for the model is the work of Ferguson in 1988. The practical implementation as a MATLAB Simulink model was developed by a project team from the Centre for Aviation (ZAV). The model was designed to run on the "Research and Didactics Simulator" (ReDSim) located at the ZHAW in Winterthur. The ReDSim is a flight simulator equipped with helicopter and airplane controls, a simple digital cockpit, and a virtual environment.

3.1.1 Model overview

In the following subsections an overview of the model components and their functions are given. It should be mentioned that the following description is deliberately kept general and only serves the understanding of the context for the development of the control augmentation system (CAS). A complete description of the model

would exceed the scope of this thesis.

The block diagram in figure 3.1 shows the main components of the XV-15 model. It consists of five subsystems: the pilot interface, the flight control computer (FCC), the actuation system, the aircraft dynamics (A/C), and sensor dynamics. For a better understanding the block diagram is simplified and the connections are illustrated as bus signals.

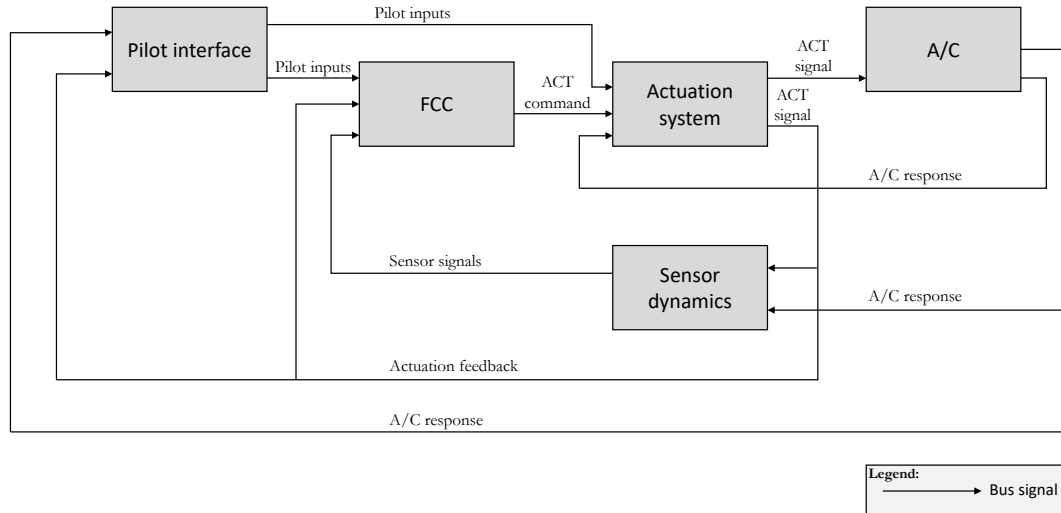


Figure 3.1: Model Overview

3.1.2 Pilot interface

The pilot interface represents the interface of the model to the pilot, thus to the hardware of the flight simulator. Relevant input sources are the interfaces for the controls, as cyclic stick, collective lever, pedals and multiple switches. The pilot interface requires the aircraft response from the aircraft dynamics and actuation feedback from the actuation system. The output signals of the pilot interface are linked to the FCC and the actuation system.

3.1.3 Flight control computer

The flight control computer described below represents the basis for the implementation of the CAS. Usually, the task of a flight control computer is to determine how to move the actuators at each control surface to provide the desired response while also providing a finer control for stability. The term is often used in context

with fly-by-wire systems. In the XV-15 model the flight control computer contains the "MIXER", the "SAS", the "Collective governor", the "NAC"¹ block, while the "CAS" has to be implemented.

The main inputs of the FCC block are the pilot commands (control inputs) and the feedback of the actuation system and sensor signals. The mixer inside the FCC is peculiar of a tilt-rotor model (as well as helicopter models), as it mixes the control inputs based on the nacelle angle. Since there is not only an airplane and helicopter mode, but also a conversion corridor where the nacelle angle is varied between 0° and 90°, the mixer basically consolidates the pilot inputs with the different controls, based on the current nacelle angle. In general, this means that the pilot input must be converted into the deflection of the control surfaces (elevator, ailerons, and rudder) or into the control input for the rotors (collective / cyclic controls) based on nacelle angle.

The SAS has the purpose of counteracting disturbances during flight. If disturbances like wind gusts occur there are also changes on the roll, pitch, and yaw rates. In the current model, the first two measured rates (roll and pitch) are fed into the SAS block which processes this data and creates commands for the control surfaces which then counteracts the unwanted rate change of the aircraft. So, a yaw damper is not implemented, but a positive effect on the directional stability, when using a roll SAS, is assumed, due to coupling between the axes. In the previous work, a finding of the stability analysis is that there is a relation between the stability behaviour and the nacelle angle, which means that the stability around all axes behaves differently when changing the nacelle angle. This conclusion relies also on Ferguson's implementation of a SAS. Moreover, a dependency of the stability on the airspeed can be seen. It follows that the stability changes due to the current nacelle angle as well as due to the airspeed.

Last, the collective governor supplies θ_0 angle to the mixer, resulting in the collective pitch angle request, while the NAC block produces the nacelle rotation command.

Since the implementation of a CAS is the aim of this thesis, a detailed description can be found further.

¹NAC is for nacelle

3.1.4 Actuation system

The actuation system simulates the dynamics of the actuators and transforms the input signals into deflections or actuation signals for the aircraft dynamics. Thus, the pilot inputs for the flaps, the landing gear, the thrust, the brakes, and the mixed pilot commands from the FCC are processed inside the actuation system.

Specifically, the input signals are processed as requests for moving aircraft components and are converted inside the actuators into states, which are then used as commands in the aircraft dynamics. Usually, there is a delay (which depends on the type of actuator) between the pilot input and the actuation response.

3.1.5 Aircraft dynamics

The aircraft dynamics contains all mathematical and physical basics to determine and process the aircraft dynamics, as the rotor dynamics, the aerodynamics, weight and balance, the landing gear dynamics, and the impact of gravity. These are then used for the equations of motion to simulate the flight behaviour of the aircraft. The input of the aircraft dynamics includes almost all signals processed in the model and is directly connected to the actuation system. The output is the so-called aircraft response, which holds the information regarding flight behaviour of the aircraft.

3.1.6 Sensor dynamics

In general, the dynamics of the real aircraft sensors is simulated inside the sensor dynamics. For example, the measurement of the airspeed is given by the dynamics of a pitot tube, introduced in the model. The most relevant processed signals are the angles of pitch, roll and yaw, their respective rates, and the calibrated airspeed.

3.1.7 Sign convention

The sign convention used in the model corresponds to the sign convention used by Ferguson [1]. In the following considerations, the body axis system in the body reference frame is assumed and the pilot position is used as a reference point.

The maximum/minimum inputs of the primary controls are defined as follows in table 3.1

Lateral stick (roll control)	-4.8 to 4.8 <i>in</i> (full left to full right)
Longitudinal stick (pitch control)	-4.8 to 4.8 <i>in</i> (full back to full front)
Pedals (yaw control)	-2.5 to 2.5 <i>in</i> (full left pedal to full right pedal)

Table 3.1: Inputs range

The sign convention is defined as follows

- positive lateral stick input leads to positive roll moment
- positive longitudinal stick input leads to negative pitch moment
- positive pedal input leads to positive yaw moment

3.1.8 Linearization

The current rotor dynamics inside the aircraft dynamics is using a multi-blade model, which means that the forces and moments generated by the rotor are expressed individually for each blade. These are then transmitted to the hub, which creates a more realistic modelling of the rotors. For this technique periodic loads are involved as the forces and moments are functions of the azimuthal position of each blade in time. This results in a periodic solution of the trim condition rather than a steady state solution. In consequence the linearization becomes more complex due to increase of mathematical complexity of the rotor model.

Luckily, the linearization of the bare A/C was implemented in the previous works. It is crucial for applying the control linear theory.

In the next section, a simply but effective model is implemented on Simulink, in order to obtain the whole model linearized (A/C, together with SAS, sensors and actuation system). This is the starting point for the development of the CAS.

3.2 Basic Development and Review on SAS

In the following subsection the development process of the linearized model is described. Next, an update of the SAS is accomplished.

3.2.1 Model linearization

As stated before, a control linear theory requires a linear model. In such cases, the system linearization is related to a single equilibrium point (trim condition). The linearized aircraft model is then decoupled into two sets of equations: longitudinal equations that involve the variable of speed, angle of attack, pitch attitude, pitch rate and altitude, and lateral-directional equations that involve sideslip angle, bank angle, roll and yaw rates. According to this design philosophy, the longitudinal CAS and the lateral-directional one will be design independently. This design concept simplifies the development of the CAS and at the same time is accurate.

Thus, the model to be linearized (through a MATLAB routine) consists of the bare linearized A/C² and the simplified sensors and actuators models, defined by linear-continuous transfer functions (figure 3.2).

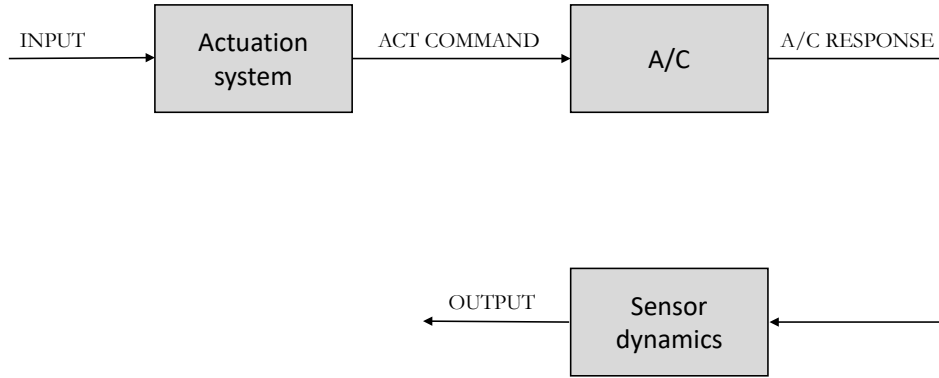


Figure 3.2: Block diagram for open loop system

The operating point, chosen for a first cut design, refers to $140kts$ and nacelle angle of 0° (XV-15 in airplane mode³). However, the following considerations apply to any other flight condition.

The linear model behaviour is compared with the whole XV-15 nonlinear model input response, in order to asses if the two matches. This can be also checked with the root locus plot, paying attention to the poles and zeros location.

²The initial conditions are set to zero.

³With some further parameter setting, such as the desired altitude and flight attitude, the initial trim conditions are calculated with the trim routine, which is provided.

Next, the linearized SAS is developed (figure 3.3). Is is based on the current XV-15 whole model too.

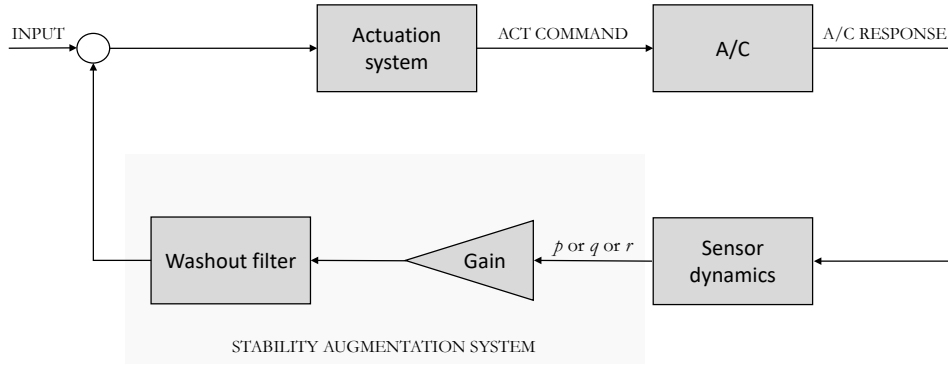


Figure 3.3: Block diagram for closed loop system

The model behaviour, with the stability augmentation system switched ON, is finally checked. The system response is not satisfactory at all. Thus, an improvement of the stability augmentation system is required.

3.2.2 Stability augmentation system re-design

It is a common practice in the analysis of nonlinear systems and in feedback control design to assume that the equilibrium point (or the operating point) of the system is accurately known or does not change over the operating regime. However, models of physical dynamical systems are in general uncertain. Therefore, static feedback control is ineffective in addressing problems where the operating point is not accurately known or there is parameter drift. Moreover, static state feedback changes the operating conditions of the open-loop system. This results in wasted control effort and may also result in system performance loss.

To overcome these problems, washout filter is used in many applications. A washout filter is a high pass filter that washes out steady state inputs, while passing transient inputs. The main benefit of using washout filters is that all the equilibrium points of the open-loop system are preserved. Thus, one can concentrate on the design of controllers emphasizing the increase in performance achieved for a particular operating point, without the potential for affecting the location of other equilibria. In addition, washout filters facilitate automatic following of a targeted operating point, which results in vanishing control energy once stabilization is achieved and

steady state is reached.

In continuous-time setting, the transfer function of a typical washout filter is

$$G(s) = \frac{s}{s + d} \quad (3.1)$$

Although washout filters have been successfully used in many control applications, there is no systematic way for choosing the constants of the washout filters and the control parameters, but, as a rule of thumb, d (the reciprocal of the filter time constant) satisfies $d > 0$ for a stable washout filter. Furthermore, in discrete-time setting⁴ (i.e. in digital control of dynamic systems), for a stable washout filter, the filter constant satisfies $0 < d < 2$.

Thus, the washout filter, related to the previous works, is to be considered unsatisfactory, due to $d = 4$. It leads to a poor response (figure 3.4) as the open loop properties (SAS switches off) are not preserved.

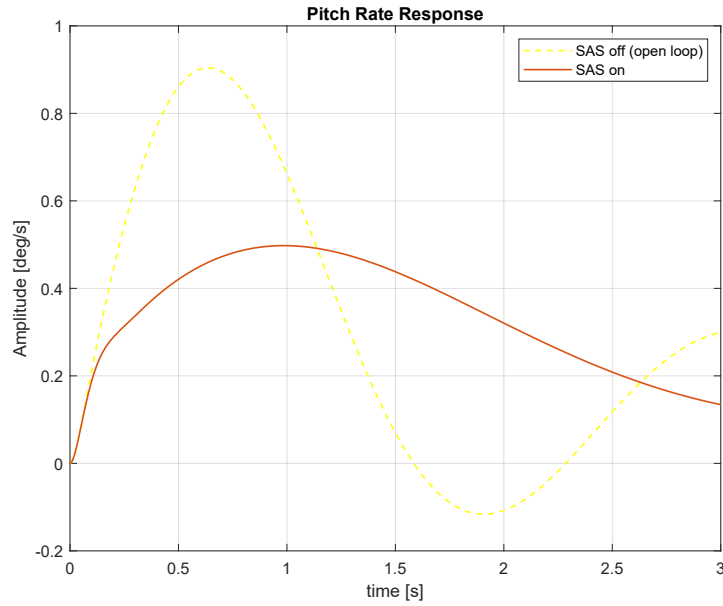


Figure 3.4: Pitch rate response to -0.1 *in* input

So, the time constant τ ($\tau = \frac{1}{d}$) is quite important. For too high values, the pilot will still have to fight the stability augmentation system, while for too low values,

⁴Sampled-data system are designed in section 3.5.2.

the stability augmentation system itself doesn't work, because the washout circuit simply adjusts too quickly. Due to the previous considerations, an in-deep research for choosing the best value of the washout filter constant is out of the topic of this thesis. So, a conventional value (on pitch, as well as roll and yaw axis) is considered

$$\tau = 4 \text{ s} \quad \Rightarrow \quad d = 0.25 \frac{1}{\text{s}} \quad (3.2)$$

The two different filters behaviour is shown in figure 3.5.

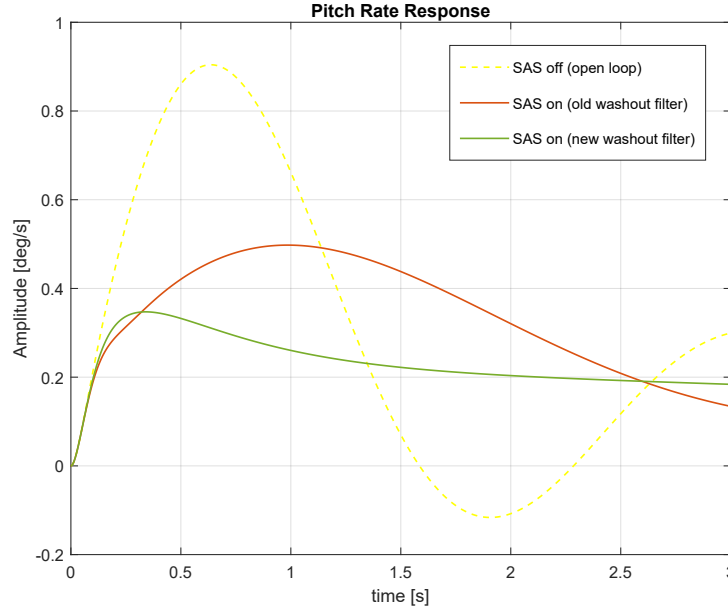


Figure 3.5: Pitch rate response - comparison

Changing the filter constant leads to resize the SAS gains. Many empirical attempts (as based on MATLAB Simulink simulations) were done to find a good compromise between performance and retain the open loop properties. Finally, the simulations on the whole XV-15 model (with the CAS implemented) led to an optimum *scaled gain*, which multiplies the previous existing gain of the SAS, as in figure 3.6. The scaled gains are given in table 3.2.

Pitch gain	Roll gain	Yaw gain
0.65	0.3	0.25

Table 3.2: Scaled gains

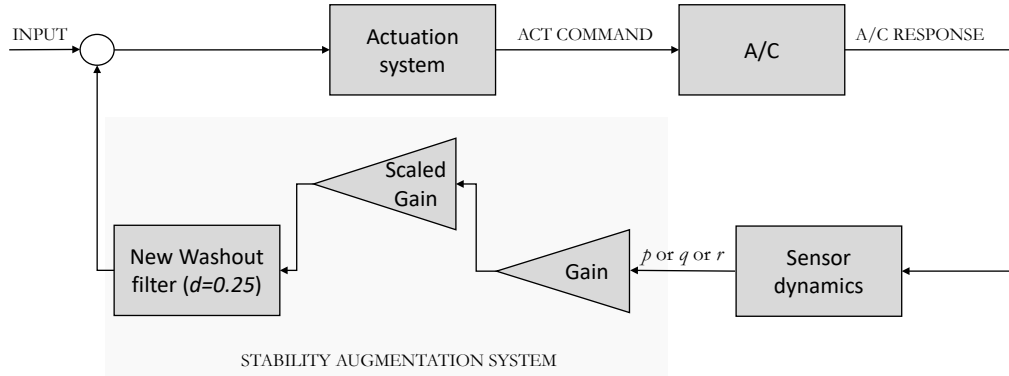


Figure 3.6: Latest SAS linearized model

Moreover a simple but effective yaw damper SAS was accomplished, which gains changes with the nacelle angle, as shown in figure 3.7. This was implemented since the beginning of the thesis work, so a yaw scaled gain was considered too.

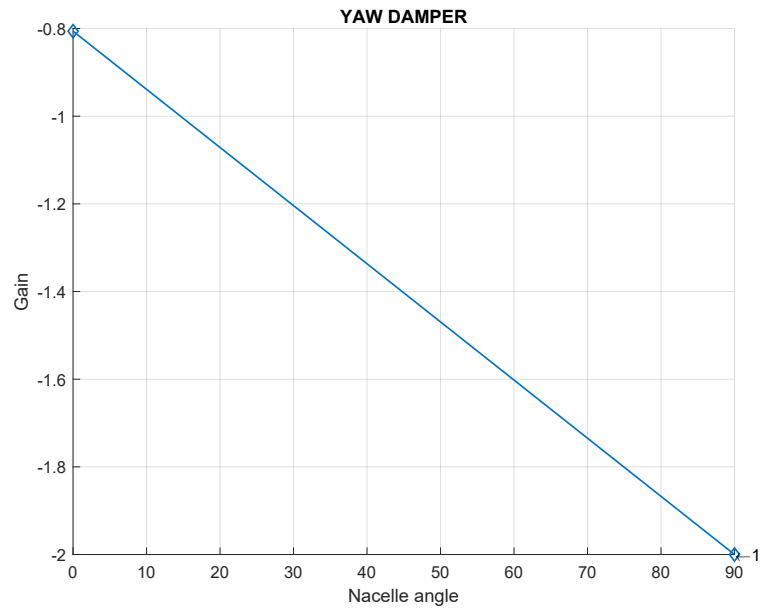


Figure 3.7: Yaw damper gains

3.2.3 Results

The system response to a step input is shown in the following figures. Trim conditions are still set to $140kts$ and nacelle angle equals to 0° .

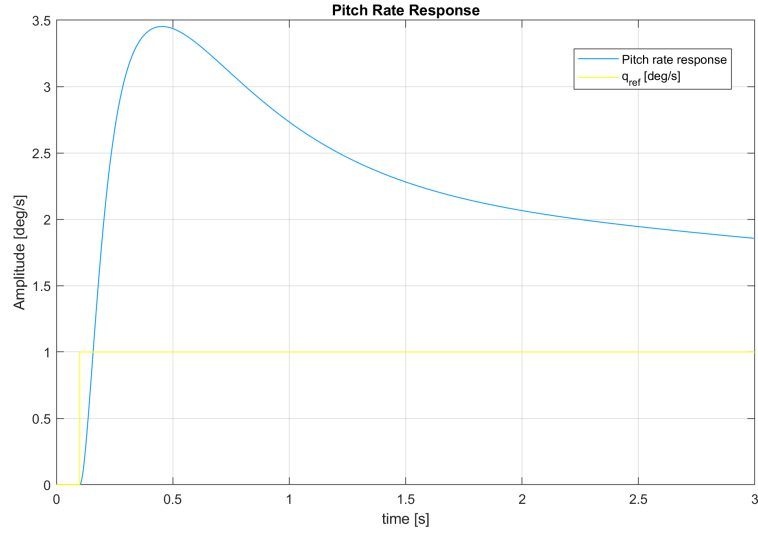


Figure 3.8: Pitch rate response to a step input

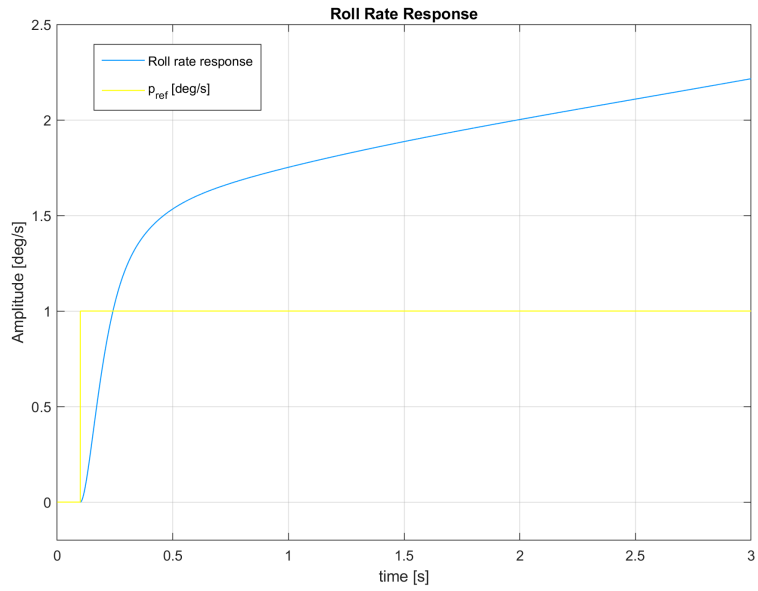


Figure 3.9: Roll rate response to a step input

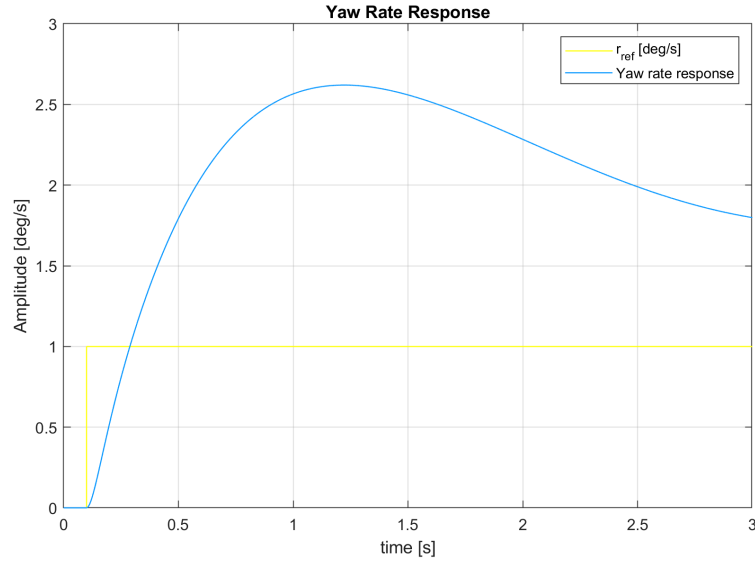


Figure 3.10: Yaw rate response to a step input

The system response shows that a tacking system (CAS) shall be considered in order to satisfy handling qualities requirements.

3.3 Control Augmentation System Implementation

Control augmentation system is a common part of modern airplane control and is best characterized as a form of tracking control. In this section, a linear-continuous time CAS is to be designed that augments both stability and control, providing dramatic improvements in aircraft handling qualities.

The kind of controller (PID or LEAD-LAG compensator) will be developed in the next section.

3.3.1 Longitudinal motion controller

The longitudinal control consists on hold the pitch rate (q) and the pitch angle (θ). The control implemented for the pitch angle works as a chain: the pitch hold generates the reference for the pitch rate hold. The pitch rate hold then generates the actuator position. This architecture makes sure that both pitch and pitch rate are controlled, in airplane mode as well in helicopter mode.

Pitch rate hold

The pitch rate hold control loop, implemented as illustrated in fig. 3.11, is responsible for maintaining the pitch rate according to the desired reference value q_{ref} . The vehicle's current angular velocity on the y axis q_{SnS} (measured by sensors SnS) is used to feed the CAS controller (as in eq. 3.3), generating an increment on the elevator or on the control input for the rotors (cyclic control), depending on the XV-15 current flight mode. This signal is added to the SAS output ($PSAS$), before getting to the actuator (ACT).

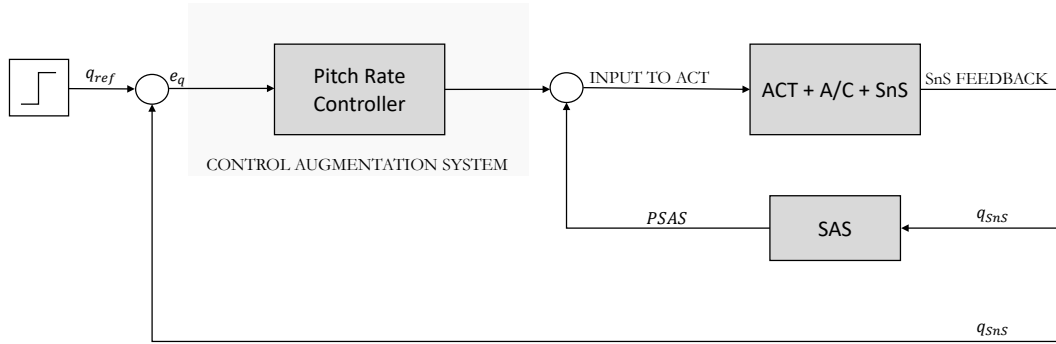


Figure 3.11: Pitch rate hold control system

$$e_q = q_{ref} - q_{SnS} \quad (3.3)$$

where e_q is the error between the desired pitch rate (q_{ref}) and the current one (q_{SnS}).

Pitch hold

Pitch attitude hold is generally implemented for level flight condition. The reference variable is θ_{ref} and sensor used for feedback is attitude reference gyroscope which generates the error signal e_θ (eq. 3.4), feeding the pitch controller. This controller is on the top of the longitudinal control chain, as shown in figure 3.12.

$$e_\theta = \theta_{ref} - \theta_{SnS} \quad (3.4)$$

where θ_{SnS} is the current pitch.

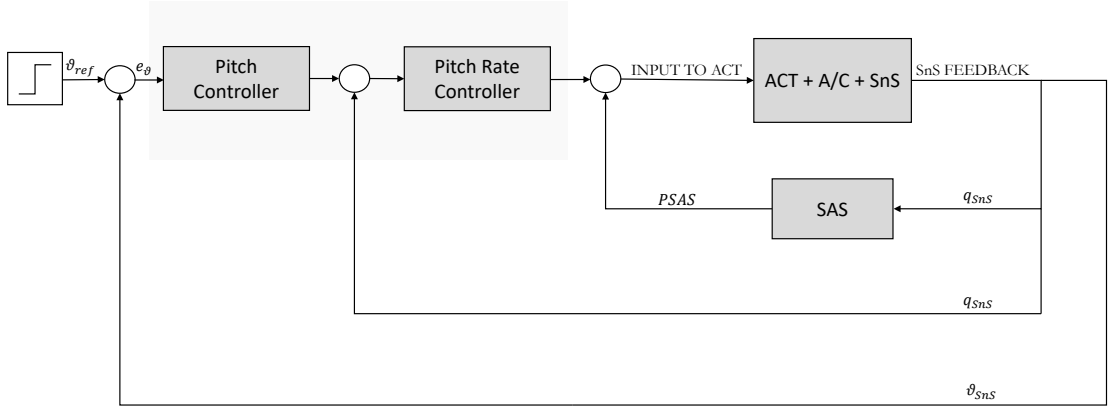


Figure 3.12: Pitch hold control system

3.3.2 Lateral-Directional motion controller

The lateral control consists on hold the roll rate (p) and the roll angle (ϕ). The control implemented for the roll angle works as a chain, similar to the pitch hold system: the roll hold generates the reference for the roll rate hold. The roll rate hold then generates the actuator position. This architecture makes sure that both roll and roll rate are controlled, in airplane mode as well in helicopter mode.

The directional control consists on hold the yaw rate (r) in helicopter mode, while in a turn coordinator controller in airplane mode.

Roll rate hold

The roll rate hold, illustrated in figure 3.13, is responsible for changing and keeping the vehicle's roll rate stable according to the input value, the reference roll rate p_{ref} . It presents two feedback lines: one of these, the current angular velocity on the x axis p_{SnS} , feeds the roll rate controller. The second provides a signal ($RSAS$) generating the exact amount of aileron or control input for the rotors (cyclic control) that must be applied on the vehicle.

$$e_p = p_{ref} - p_{SnS} \quad (3.5)$$

where e_p is the error between the desired roll rate (p_{ref}) and the current one (p_{SnS}).

Roll hold

Design of bank angle hold controller is shown in figure 3.14. This outer control loop provides a roll references angle ϕ_{ref} as the input signal to the inner loop (roll rate

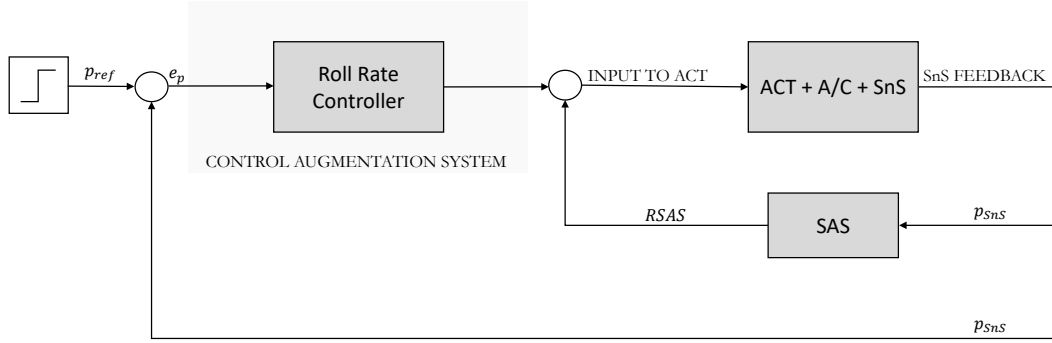


Figure 3.13: Roll rate hold control system

hold), that generates the appropriate command to the ailerons or cyclic control in order to the vehicle behaves as desired. The third feedback line, the current roll ϕ_{SnS} , feeds the roll controller.

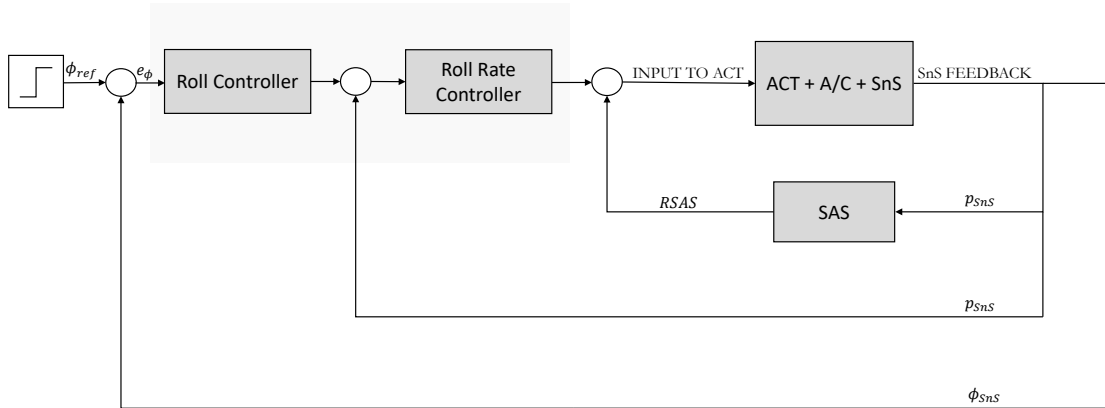


Figure 3.14: Roll hold control system

$$e_{\phi} = \phi_{ref} - \phi_{SnS} \quad (3.6)$$

where e_{ϕ} is the error between the desired roll angle (ϕ_{ref}) and the current one (ϕ_{SnS}).

Yaw rate hold

This controller changes the aircraft's yaw rate and holds it in the assigned reference value r_{ref} . It provides the control of the yaw rate by pedals, which give input for

the rotors (cyclic control). The vehicle's current angular velocity on the z axis r_{SnS} feeds the yaw rate controller. The CAS output is putted into the actuator, together with the directional SAS output ($YSAS$).

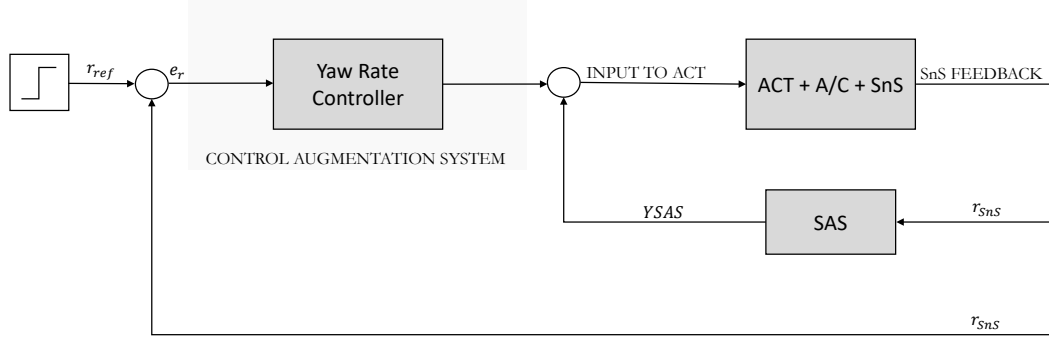


Figure 3.15: Yaw rate hold control system

$$e_r = r_{ref} - r_{SnS} \quad (3.7)$$

where e_r is the error between the desired yaw rate (r_{ref}) and the current one (r_{SnS}).

Turn coordinator controller

During turnings, an undesired sideslip angle may occur if the flight is not coordinated. The function of turn-coordinator (figure 3.16) is to suppress the sideslip angle with appropriate deflections of rudder, as this controller works in airplane mode. A turn is said to be 'coordinated' when the lateral acceleration (n_y) and the sideslip velocity (v), hence the sideslip angle (β), are zero. The condition for a coordinated turn is that the rate of change of the sideslip angle ($\dot{\beta}$) is zero. In any turn, sideslip angle occurs if the rate of yawing (r) is different from the value given by eq. 3.8. The turn will not be coordinated in that case. Therefore, this suppressor control system maintains the lateral acceleration close to zero during any maneuver, with proper rudder deflections, feeding a turn controller (the reference input is simply zero).

$$r = \frac{g}{U_0} \sin(\phi) \quad (3.8)$$

where

- g is the gravitational acceleration

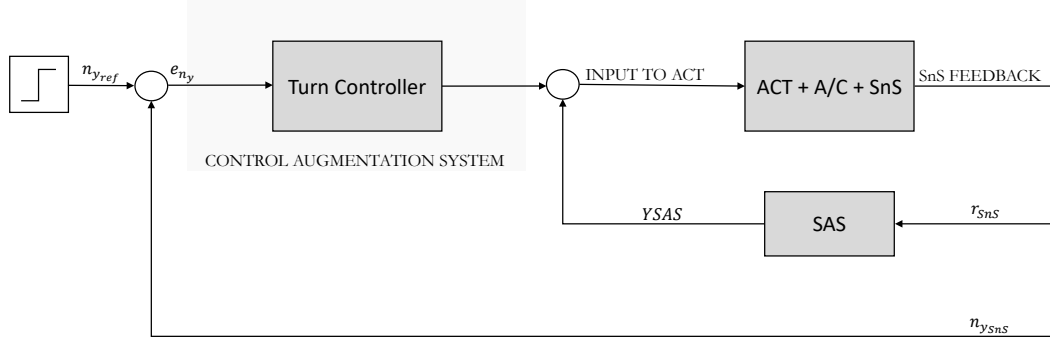


Figure 3.16: Turn coordinator control system

- U_0 is the flight velocity

Furthermore, the controller allows to track the lateral acceleration n_y when the pilot commands the pedal.

3.4 Gain Evaluation

The following section describes the methods for gains evaluation.

The operating point refers to 140kts and 0° of nacelle angle (XV-15 in airplane mode), as in the previous section. These trim conditions were used as initial conditions for the simulations. In consequence, it is guaranteed that the aircraft is in a stable position at the beginning of each simulation. The achieved initial conditions have been verified and checked initially by analysing a short trim condition test.

3.4.1 PID Controller

A PID controller, which is a commonly employed controller in closed-loop control systems, is designed according to Ziegler-Nichols method (Ultimate sensitivity method). A prerequisite for the use of this method is that it is applied to closed control loops and that the system must not be damaged by the eventual use of too high gains during evaluation.

Step inputs are applied to stimulate the system. Then the controller gain is gradually increased by observing the respective output (e.g. the step is performed on the reference pitch rate q_{ref} , so the current pitch rate q_{SnS} is observed). The gain

is then achieved, according to the simulations outcomes.

Results are shown for each motion controller, as detailed below, together with proportional K_p and integral K_I gain values (K_D is not assessed, due to the SAS already gives a derivative action). The simulation time on MATLAB Simulink was set to $t = 3s$.

Pitch rate hold

The controller is implemented as in figure⁵ 3.17, with

- $K_{pq} = 0.4$
- $K_{Iq} = 0.2$
- $K_{FFq} = -0.35$
- $K'_{pq} = -0.5$

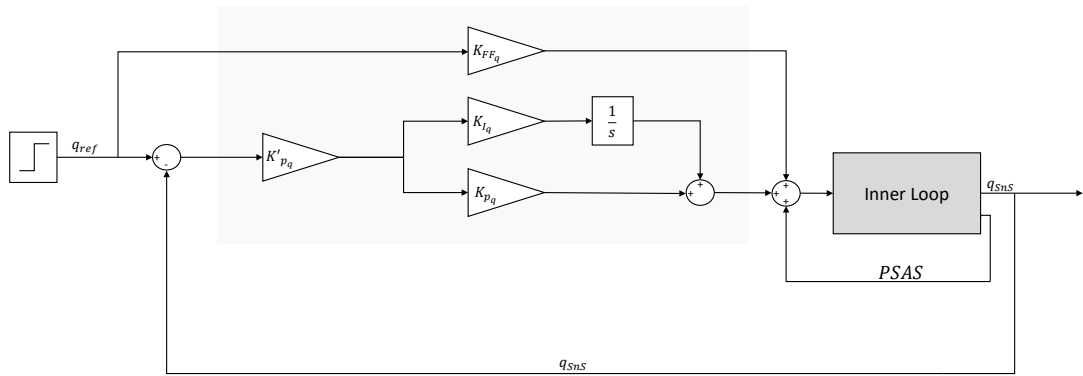


Figure 3.17: Pitch rate control system implementation

The system response to a step input is shown in figure 3.18.

Pitch hold

The controller is implemented as in figure 3.19, with

- $K_{p\theta} = 4.8$

The system response to a step input is shown in figure 3.20.

⁵Inner loop includes ACT, A/C, SnS and SAS

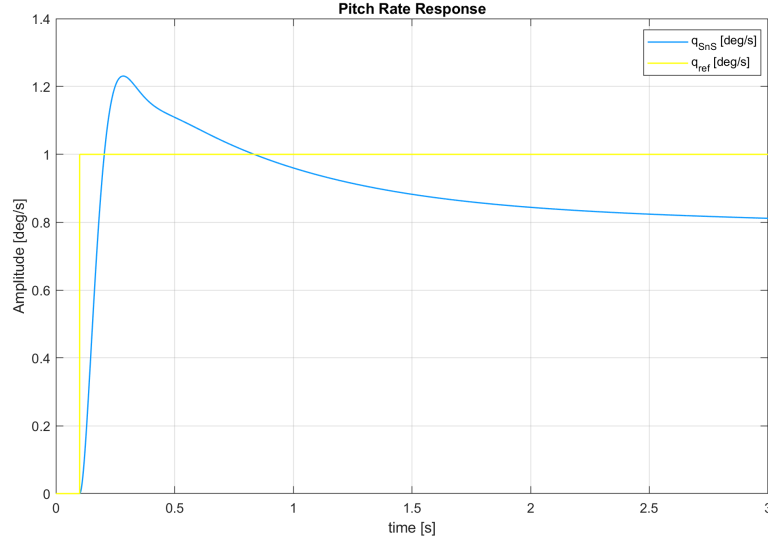


Figure 3.18: Pitch rate response

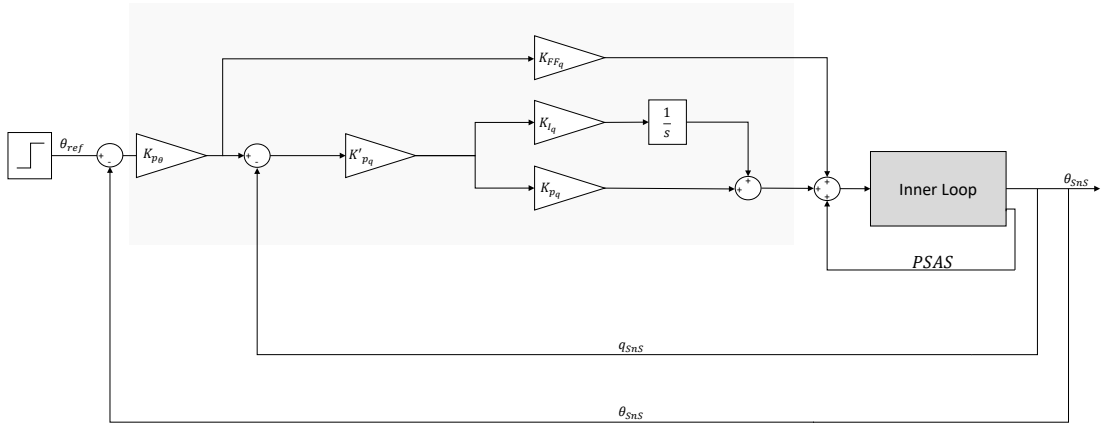


Figure 3.19: Pitch control system implementation

Roll rate hold

The controller is implemented as in figure 3.21, with

- $K_{p_p} = 0.7$
- $K_{I_p} = 0.64$
- $K_{FF_p} = 0.35$

The system response to a step input is shown in figure 3.22.

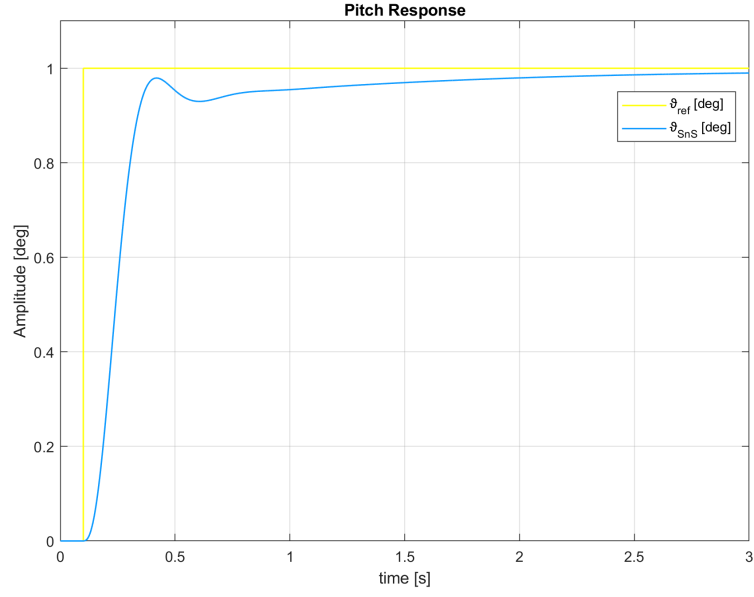


Figure 3.20: Pitch response

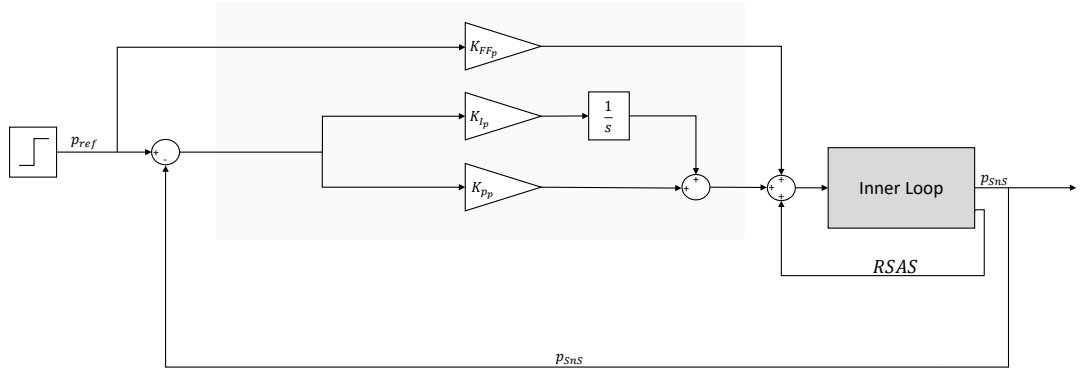


Figure 3.21: Roll rate control system implementation

Roll hold

The controller is implemented as in figure 3.23, with

- $K_{p_\phi} = 2.4$

The system response to a step input is shown in figure 3.24.

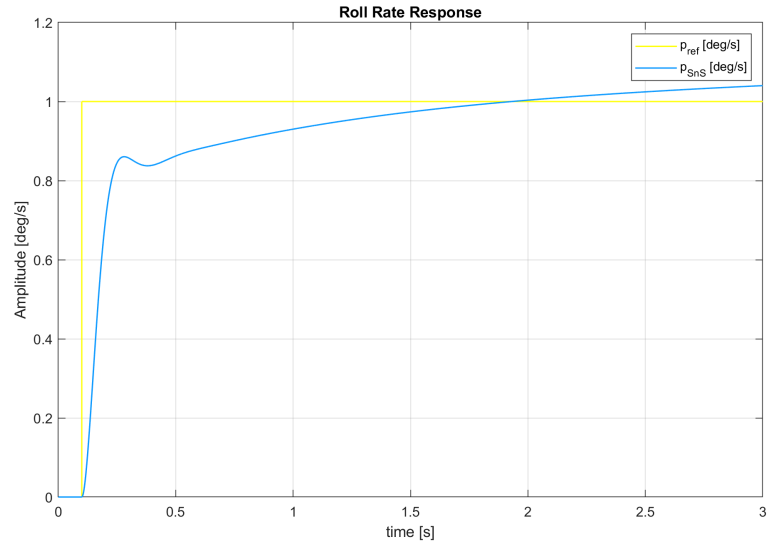


Figure 3.22: Roll rate response

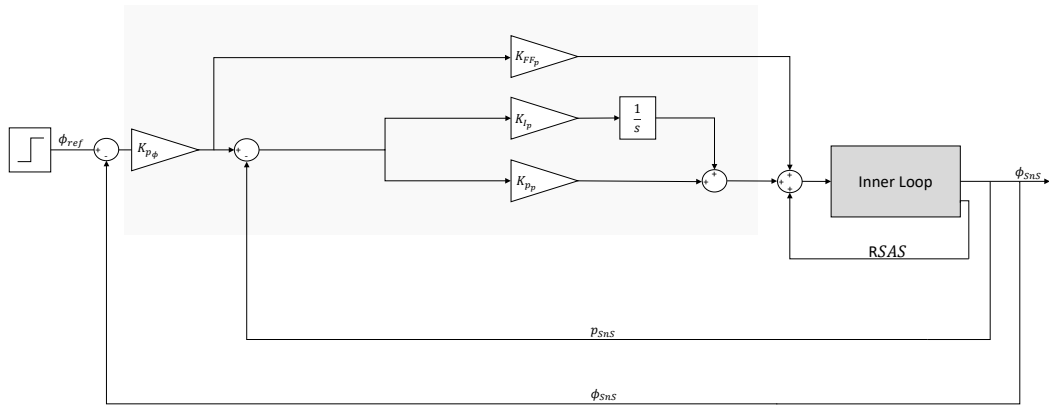


Figure 3.23: Roll control system implementation

Turn hold

The controller is implemented as in figure 3.25, with

- $K_{p_{n_y}} = 14$
- $K_{I_{n_y}} = 12$
- $K_{FF_{n_y}} = 3$

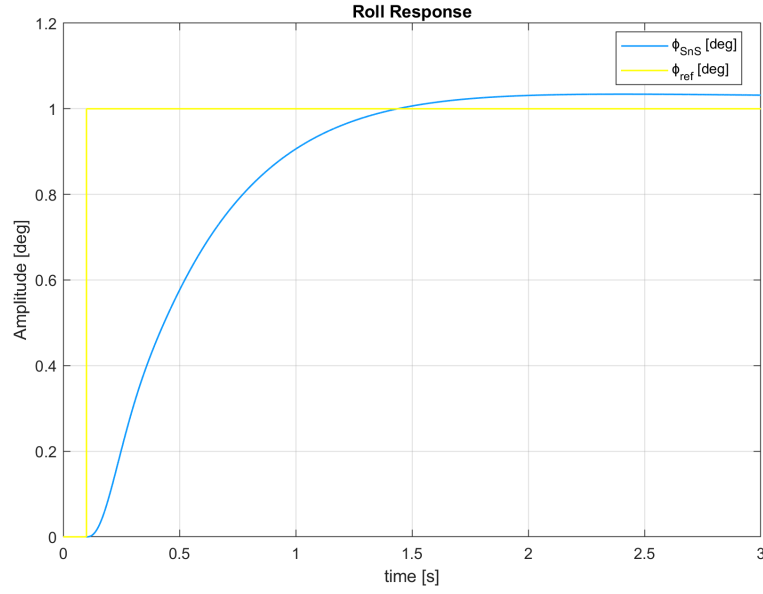


Figure 3.24: Roll response

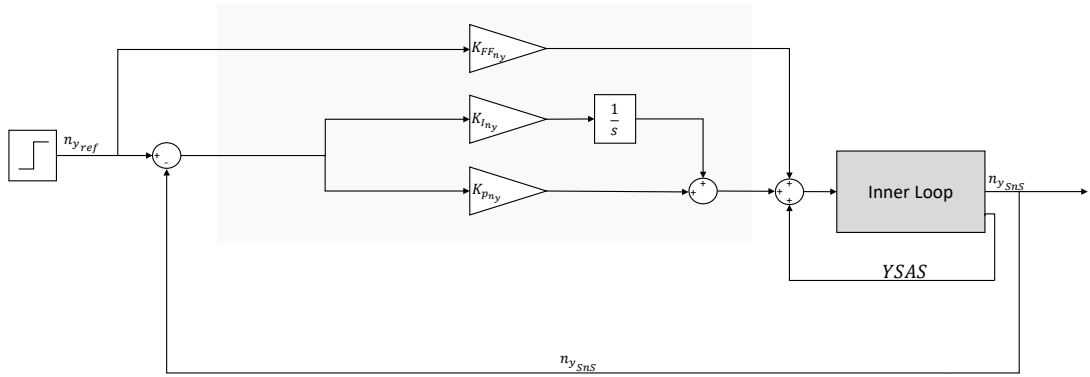


Figure 3.25: Turn hold control system implementation

The system response (showing a non-minimum phase behaviour) to a step input is shown in figure 3.26.

Yaw rate hold

The controller is implemented as in figure 3.27, with

- $K_{pr} = 1.6$

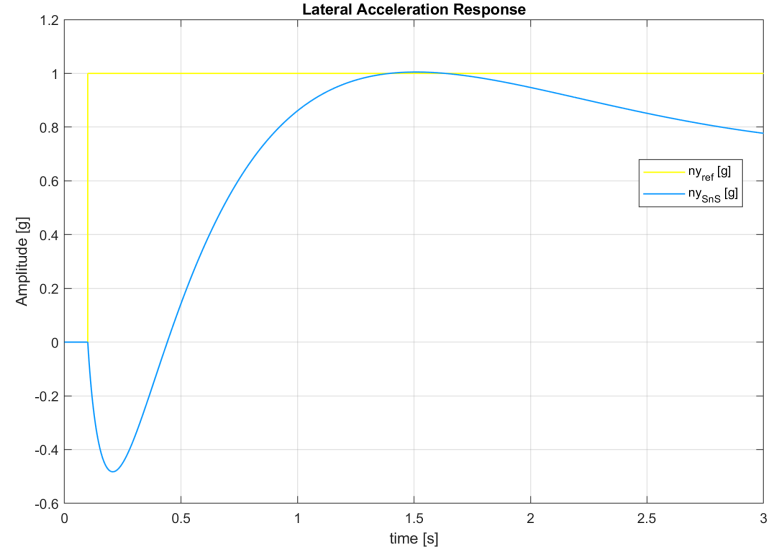


Figure 3.26: Lateral acceleration response

- $K_{I_r} = 0.9$

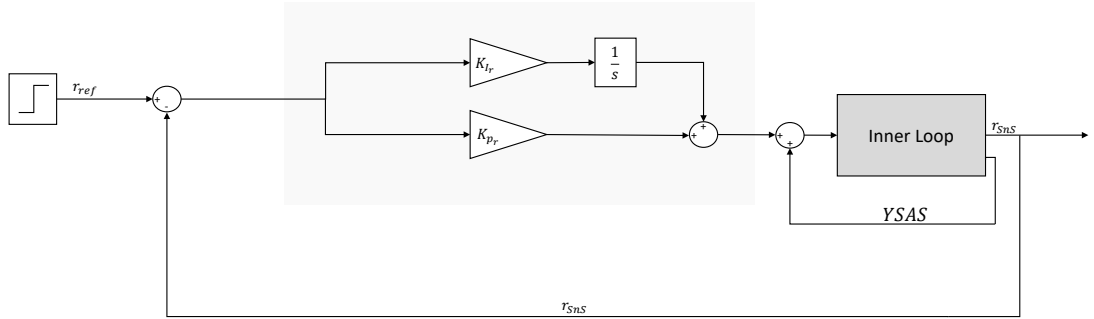


Figure 3.27: Yaw rate control system implementation

The system response to a step input⁶ is shown in figure 3.28.

⁶Initial conditions are set differently: 40kts and 90° of nacelle angle (XV-15 in helicopter mode).

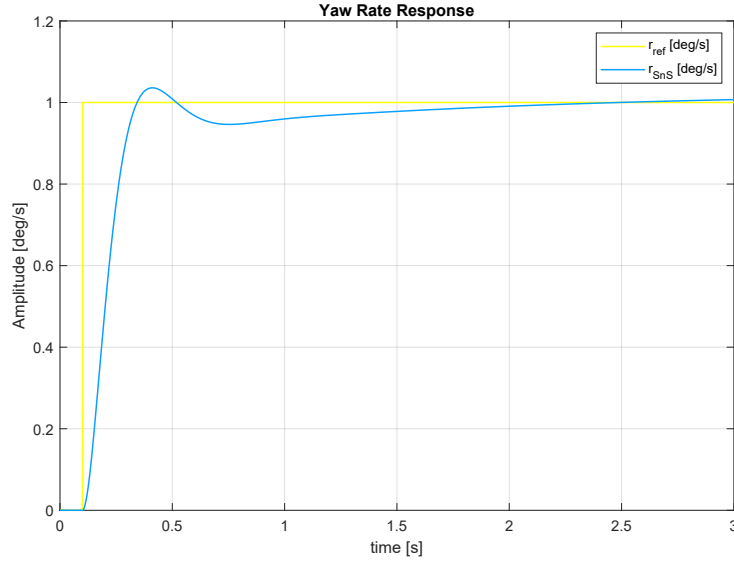


Figure 3.28: Yaw rate response

Considerations

The systems outcome show quite good results, although it would be better sometimes to make the response faster as well as to improve damping and steady-state error. Mostly, the pitch rate response is not satisfactory. This leads to prove and test the lead-lag compensator features, as to meet the handling qualities.

3.4.2 LEAD-LAG compensator - Case study

This paragraph provides a case study for a lead-lag compensator design. This was implemented on the pitch axis (making use of MATLAB Simulink). Same steps can be taken on lateral-directional axis.

Problem statement

Consider the open loop system shown in figure 3.2. The linearization allows to define the open loop SISO transfer function (longitudinal input to pitch rate q). As stated before, the plant itself needs a (longitudinal) stability augmentation system, leading to the block arrangement in figure 3.3. This shapes the inner loop (figure 3.29).

The goal arranged is to satisfy the following specification:

- Steady state error to a step response $< 5\%$

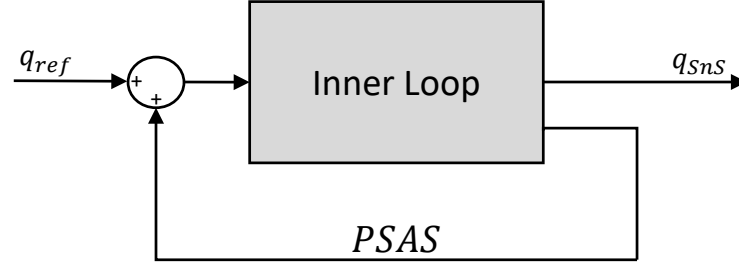


Figure 3.29: Inner Loop

- Peak time $t_p < 1.5s$
- Maximum first overshoot $M_p < 10\%$

This specification can be interpreted into useful guidelines for designing a compensator using either the root locus or frequency response method as follows.

Peak time: $t_p = \frac{\pi}{\omega_d}$ where ω_d is the damped frequency of the (closed loop) system.

$$\omega_d = \frac{\pi}{1.5} = 2.09 \text{ rad/s} \quad (3.9)$$

$$\text{Peak overshoot: } M_p = e^{\frac{-\zeta\pi}{\sqrt{1-\zeta^2}}}$$

$$\ln(M_p) = \frac{-\zeta\pi}{\sqrt{1-\zeta^2}} = -2.3 \Rightarrow \zeta = 0.59 \quad (3.10)$$

Now $\omega_d = \sqrt{1-\zeta^2} \cdot \omega_n$, where ω_n is the (closed loop) system natural frequency.

$$\omega_n = \frac{2.09}{\sqrt{1-0.59^2}} = 2.59 \text{ rad/s} \quad (3.11)$$

$$\text{Phase margin: } \zeta \approx \frac{PM}{100} \Rightarrow PM \approx 59^\circ$$

Summarising, our design guidelines are:

$$\omega_n = 2.6 \text{ rad/s} \quad \zeta = 0.6 \quad PM = 60^\circ \quad (3.12)$$

Stage 1: Open loop system

First we ask whether the inner loop system itself satisfies the specification. Assume that the inner loop transfer function (G_{il}) can be multiplied by a constant gain K as show in figure 3.30.

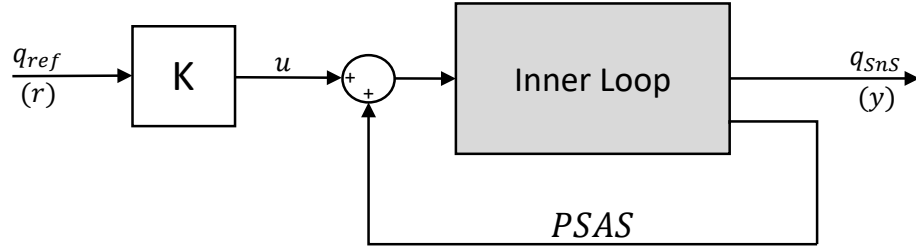


Figure 3.30: Block diagram for inner loop system with constant gain

Then

$$y = K \cdot G_{il} \cdot r \quad (3.13)$$

Setting the gain $K = -0.35$ (relying on the proportional value found in the previous subsection) gives the transfer function response as in figure 3.31.

Although the response is well-damped and easily satisfies peak time criterion, it falls over time. This indicates that a closed loop solution is desirable.

Stage 2: Closing the loop

The block diagram for the system with unity feedback is shown in figure 3.32.

To start with, we try a simple form of compensator by retaining $H(s) = 1$ and considering the effect of various values of the gain K (trial and error method).

From figure 3.33 it is evident that the gain ($K = -0.72$) has reduced the system performance. It has also made the response faster but this is not really required.

Stage 3: Using a LAG-LEAD compensator

First, the steady state error can be improved by the use of a lag compensator. The principle is to selectively increase the gain of the system at low frequency (which affects steady state error) but keeping its value at high frequency unchanged (so that stability and speed of response are not affected). To avoid affecting the phase margin, the compensator must not contribute significant phase margin at ω_n . The transfer function for the compensator is:

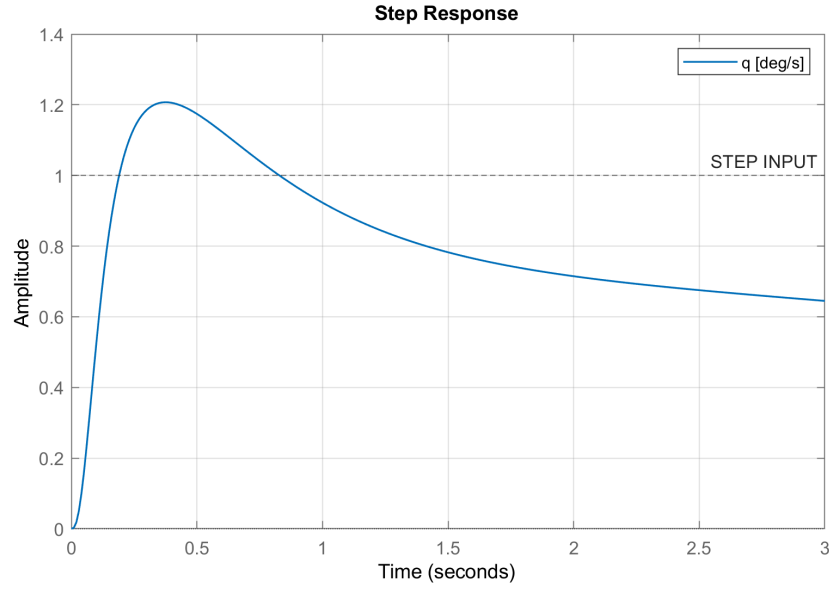


Figure 3.31: Inner loop step response

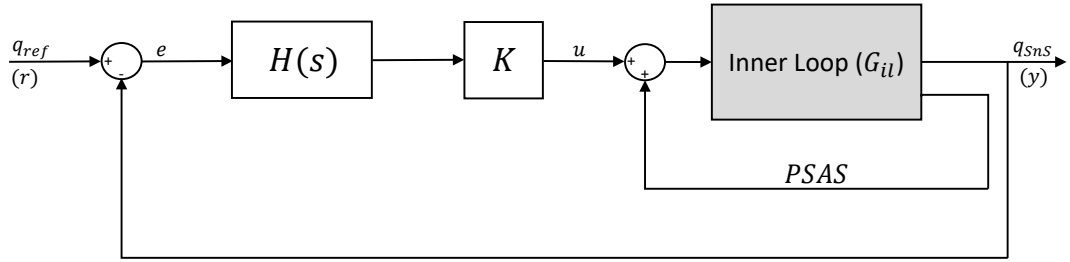


Figure 3.32: Block diagram for closed loop system

$$H_1(s) = \frac{s + z}{s + p} \quad (3.14)$$

Note that the low frequency gain (i.e. as $s \Rightarrow 0$) is given by z/p . As a first guess, let's place the zero at 3rad/s so that the phase lead it contributes has mostly cancelled out the phase lag contributed by the pole to leave the phase margin relatively unaffected in ω_n . As described in the previous chapter, a rule of thumb is to place the pole 5 to 20 times closer from the origin as the zero. Thus, $p = z/20$ is chosen.

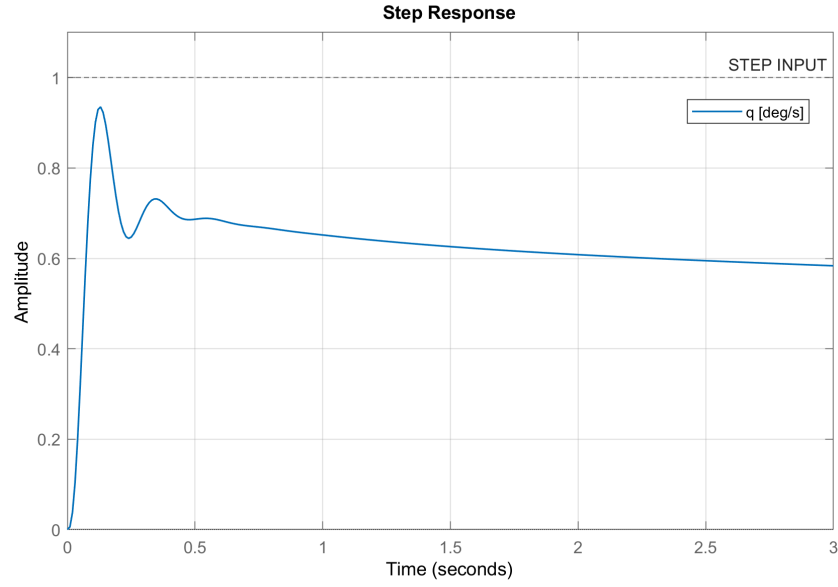


Figure 3.33: Step response

$$p = \frac{3}{20} = 0.15 \quad (3.15)$$

Thus

$$H_1(s) = \frac{s + 3}{s + 0.15} \quad (3.16)$$

The frequency response shown in figure 3.34.

The next step is to cascade the compensator with the inner loop and the gain value $K = -0.35^7$, so that

$$G_0 = K \cdot H_1 \cdot G_{il} \quad (3.17)$$

Figure 3.35 shows that G_0 has about 94.4° of phase lag, i.e. 85.6° of phase margin, at a crossover frequency of about 9.73 rad/s . This does not seem to be too bad (although the system response could be too fast), so let us look at the closed loop step function.

⁷This gain, found in stage 1, predicts a good speed of response. Alternatively, it is possible to obtain the gain from the bode plot of the open loop transfer function, as will be developed later.

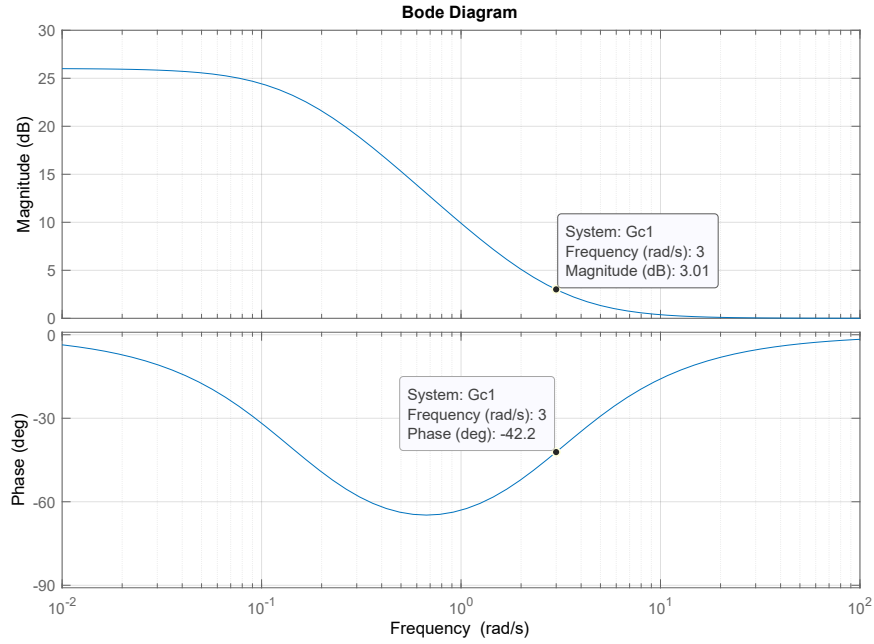


Figure 3.34: Bode plot for the lag compensator with the pole in -0.15 and the zero in -3

Figure 3.36 shows that the damping is too high. This indicates that some further action needs to be taken to improve the speed of response and the damping but without adversely affecting the steady state error.

Stage 4: Performance improvement

Careful inspection of 3.37 shows that, if we wish to decrease the speed of response by moving the crossover frequency from 9.73 rad/s to 2.6 rad/s , then we must decrease the gain at 2.6 rad/s by 6 dB . Doing so would, however, leave a phase margin of 126.4° , which is too high, as stated before.

Let us use another compensator to restore the phase margin at 2.6 rad/s back to 60° , i.e. we need to put in an additional $\approx 66^\circ$ of phase lag. The following expressions are an useful guideline for locating the pole and zero (further details in appendix B)

$$\omega_{max} = \sqrt{|z||p|} \quad (3.18)$$

$$\frac{z}{p} = \frac{1 - \sin \phi_m}{1 + \sin \phi_m} \quad (3.19)$$

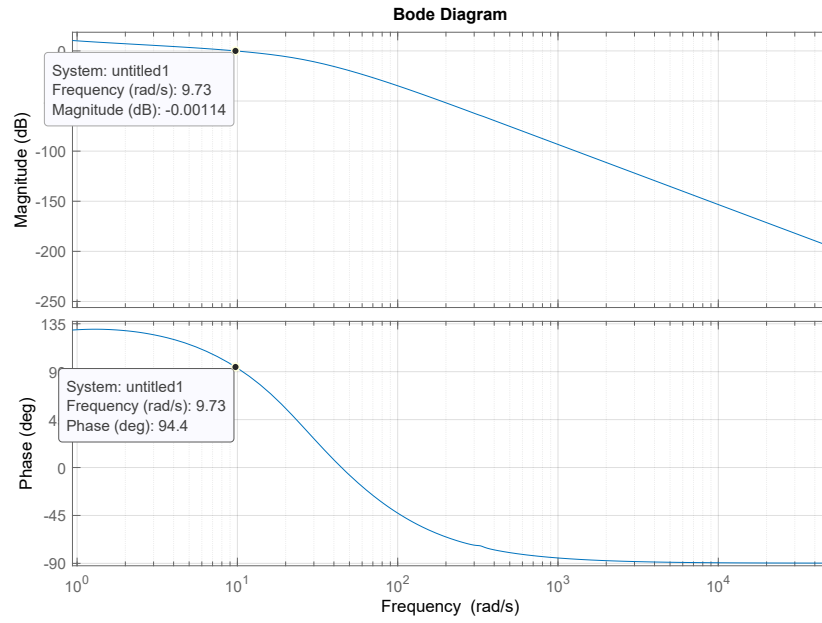


Figure 3.35: Bode plot of open loop transfer function G_0

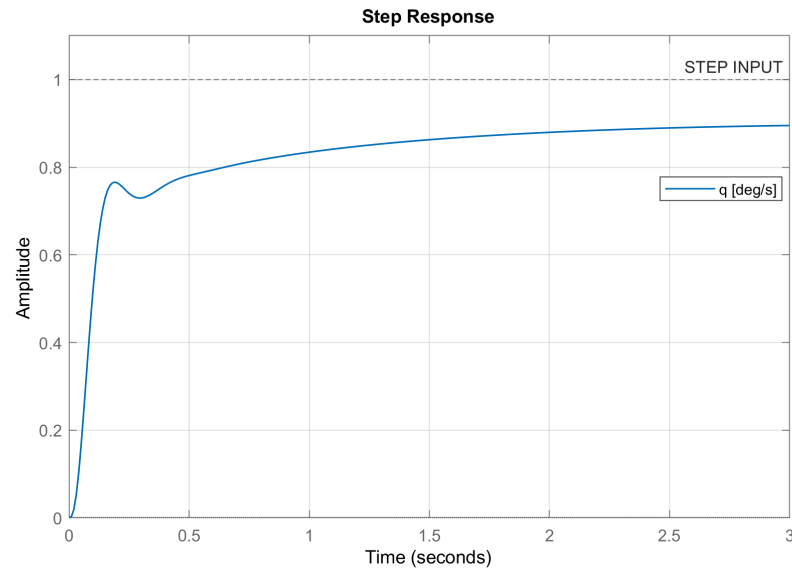


Figure 3.36: Step response with lag compensator included

where ω_{max} is the frequency at which the maximum phase lag/lead occurs and ϕ_m is the maximum phase lag/lead.

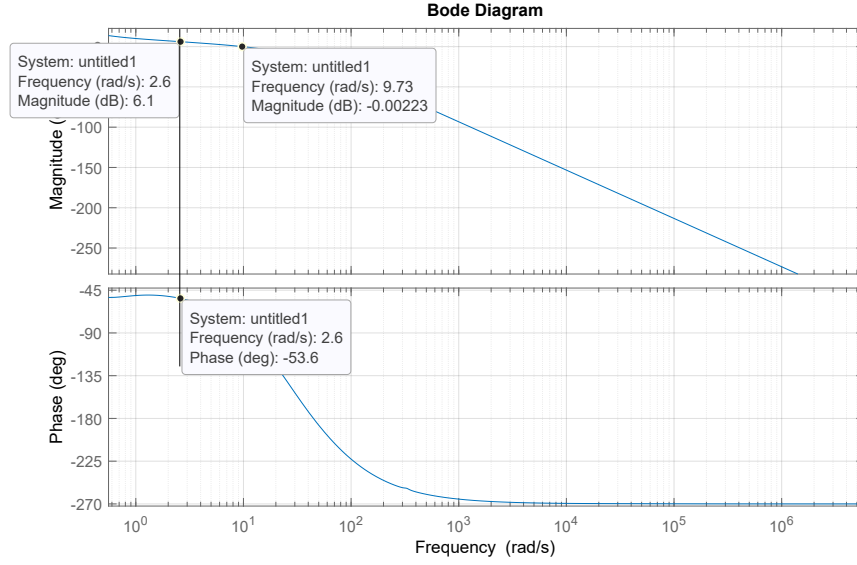


Figure 3.37: Bode plot of the open loop transfer function G_0 - action to speed up the response

Thus $\omega_{max} = 2.6$ and $\phi_m = -66^\circ$ so

$$\frac{z}{p} = 22.13 \quad \Rightarrow \quad z = 11.95 \quad p = 0.54 \quad (3.20)$$

This leads to

$$H_2(s) = \frac{s + 11.95}{s + 0.54} \quad (3.21)$$

Now we incorporate $H_2(s)$ so that $G_0 = H_1 \cdot H_2 \cdot G_{il}$. The open loop frequency response with both compensators included is shown in figure 3.38. As a rule of thumb, a $GM_{dB} > 6dB$ is preferred. So, we do indeed need an extra $\approx -20dB$ of gain to make the phase margin 60 deg.

$$K_{dB} = -20dB \Rightarrow -20 = 20 \cdot \log(K) \Rightarrow K = -0.1 \quad (3.22)$$

The result is shown in figure 3.39 where it can be seen that the steady state error is smaller than 5% with the transient response much improved. The peak overshoot is now about 15% (acceptable) and the peak time is about 0.5s.

It is concluded that an acceptable design has been accomplished. Note, however, that usually this would only be regarded as the first pass of an iterative process and that further refinement of the compensator would typically be undertaken to obtain an ‘optimum’ result, i.e. choosing

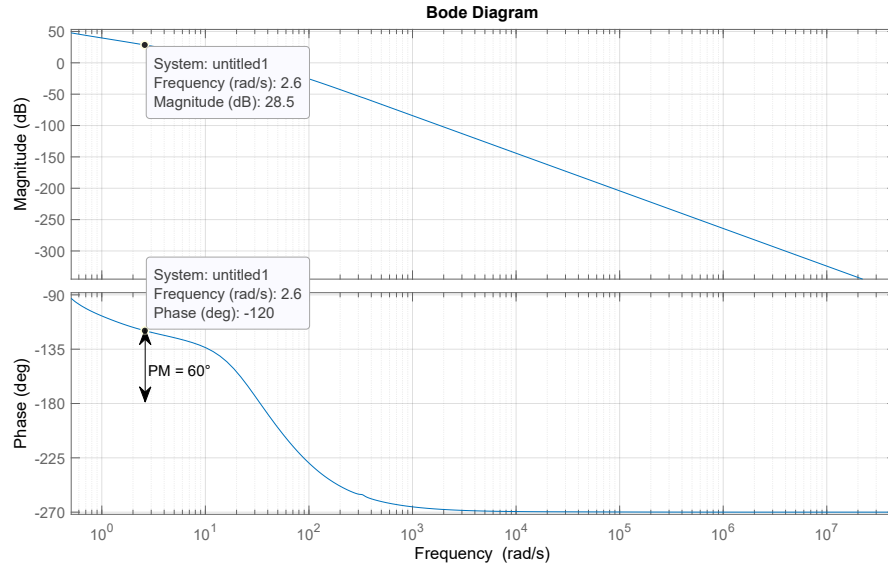


Figure 3.38: Bode plot with the both compensator included

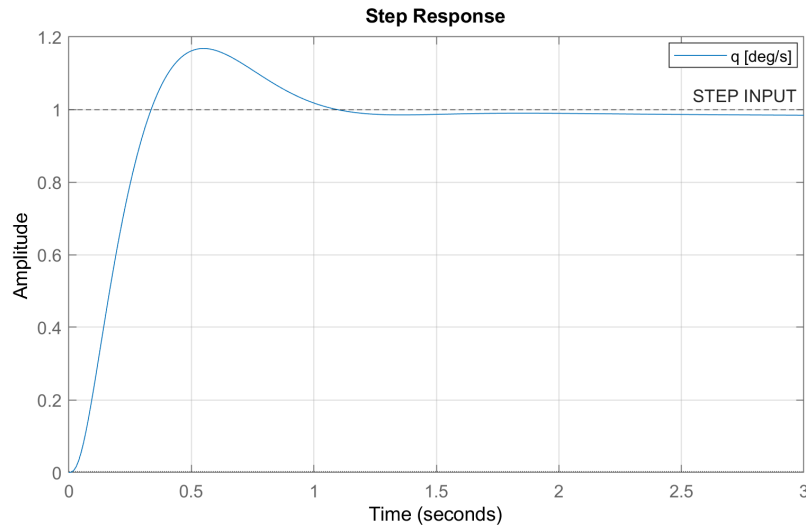


Figure 3.39: Closed loop step response with both compensators included

$$H_2(s) = \frac{s + 14}{s + 1.5} \quad \text{and} \quad K = -0.115 \quad (3.23)$$

the requirements are fulfilled (figure 3.40).

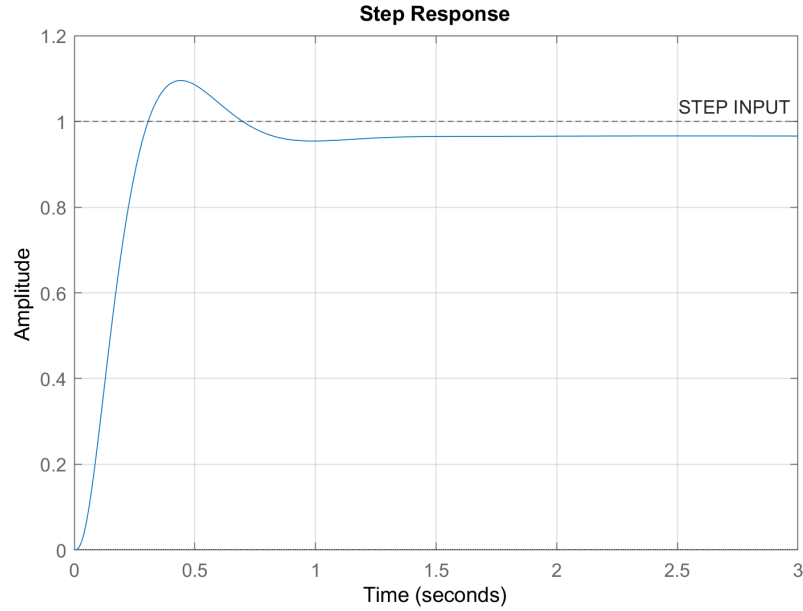


Figure 3.40: Closed loop step response (refinement)

This project method, an alternative to the PID, will be discussed in the next section.

3.5 Gain Scheduling

Realistic engineering systems (such as the XV-15 model) are often nonlinear. There are many approaches in nonlinear control system design, such as linearization, robust control, adaptive control, etc. Through linearizing the nonlinear system, the controller can be designed using the approaches of linear control theory, as in the previous sections. Therefore, linearization is the most common approach in nonlinear system design.

The limitation of the design via the linearization approach is the fact that the controller is guaranteed to work only in the neighborhood of a single operating (equilibrium) point (i.e. 140 kts and a nacelle angle of 0° was chosen), because the dynamic behavior of a system changes with the operating region. This could prove the bad dynamic response of the linear PID controller, over the time.

Thus, a typical approach to overcome this issue is gain scheduling. In many situations, how the dynamics of a system change with its operating points can be identified. The system can be modeled in such a way that the operating points are

parameterized by one or more variables, which are called scheduling variables. In such cases, the system may be linearized at several equilibrium points. A linear (and continuous) feedback controller can be designed at each point that performs satisfactorily when the system is operating near the respective operating points. A family of linear controllers can be implemented as a single controller whose parameters change by monitoring the scheduling variables, which are intended to handle the nonlinear aspects of the design problem.

So, gain scheduling is a practical method that can extend the validity of the controller operation to a set of operating points and has been proved to be a successful method in many applications in nonlinear control system design, especially in flight control systems.

Nowadays, due to the widespread use of digital hardware in controller implementation, the next step is to design a parameterized family of linear discrete-time controllers, using approaches that relate to sampled-data gain scheduling.

Last, gain-scheduled controller has to be implemented on the nonlinear model. A nonlinear system has to preserve the input-output properties of the linear closed loop systems locally, about each equilibrium point (this means that linearizations match the linear controllers performance at each operating point). Unfortunately, this property could not be satisfied in some gain-scheduled systems: this may result in a loss of performance or even instability of the feedback system.

So, the development of a sampled-data (and nonlinear) controller involves the following steps.

- Compute the constant operating points of a nonlinear plant, parameterized by constant values of a set of scheduling variables, and obtain the corresponding linearized plants. Linear controllers are then designed.
- For the family of linearized plants, design a parameterized family of linear discrete-time controllers to meet the design goals at each operating point.
- Construct a nonlinear gain scheduling controller that linearizes to the correct linear controller at each constant operating point.
- Verify the performance of the gain scheduled controller by simulation.

Considering the design of a control augmentation system, first the nonlinear equations of motion are linearized about selected operating points that capture the key modes of operations throughout the flight envelope (the set of conditions under which the vehicle is expected to fly). Linear controllers are then designed to achieve

desired stability and performance requirements for the linearizations of the plant about the selected operating points. Since these requirements must be satisfied throughout the flight envelope, the parameters of the controllers are then interpolated as a function of a gain scheduling variable (typically, this variable can be dynamic pressure, Mach number, altitude, angle of attack or a combination of the above). Finally, the scheduled controller is adequately modified for discrete-time application and implemented on the nonlinear plant.

Nevertheless, designing a gain-scheduled controller remains largely an ad hoc procedure that requires extensive computer simulations. This is due the lack of powerful analysis tools to assess the stability and performance of the resulting nonlinear time-varying feedback systems.

3.5.1 Linear system

According to the gain scheduling methodology, the first step of nonlinear gain scheduled controller design is to compute the family of constant operating points for specified steady-state flight conditions and linearize the nonlinear model about the specified flight conditions.

Since the SAS gain is simultaneously dependent on the nacelle angle and airspeed, sample point for CAS gain evaluation refers to airspeed as scheduling variable. It should be remarked that the conversion corridor of the XV-15 (figure 1.7) describes the airspeed limits for safe operation at different nacelle angles as well as the two possible operating modes (airplane/helicopter). The airspeeds, chosen as sampling points, are shown in table 3.3.

Airspeed [kts]							
0	40	100	140	180	220	260	300

Table 3.3: Sample points for CAS gain evaluation

The obtained gains are combined, shaping a 1D lookup table (linear interpolation is chosen).

The previous section showed system response for $140kts$ (nacelle angle of 0°) in airplane mode and for $40kts$ (nacelle angle of 90°) in helicopter mode. Further results (relating to different operating points) will be provided only for the nonlinear system.

3.5.2 Sampled-data system

A typical sampled-data system includes a sampler and a data-reconstruction device. The zero-order hold is usually used for data sampling and reconstruction: it is a mathematical model of the practical signal reconstruction done by a conventional digital-to-analog converter. It describes the effect of converting a discrete-time signal to a continuous-time signal.

Once the Laplace-transform of a (linear) system has been determined, it is possible to use the information contained in the function to graphically represent it and easily observe many defining characteristics: the poles and zeros can be plotted onto the z -plane, a complex plane with an imaginary and real axis referring to the complex-valued variable z . The position on the complex plane is given by $re^{j\theta}$ and the angle from the positive real axis around the plane is denoted by θ . When mapping poles and zeros onto the plane, poles are denoted by 'x' and zeros by an 'o'. Figure 3.41 shows s - and z -plane.

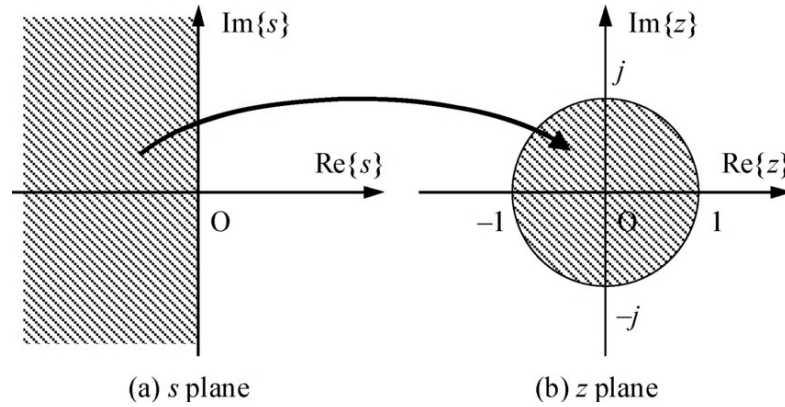


Figure 3.41: s - and z -plane

From the z -plot, it is possible to understand the magnitude of the transfer function: it will be larger when it is closer to the poles and smaller when it is closer to the zeros. This provides a qualitative understanding of what the system does at various frequencies and it is crucial for a better stability assessment.

The sampled-data controller design deals with the characteristics of the system in z -plane. However, many of the analysis and design techniques for a continuous-time system (i.e. PID/compensator) are based on the s -plane characteristics, where the

stability boundary is the imaginary axis. These techniques cannot be applied to the sampled-data system in the z -plane directly, since the stability boundary is the unit circle there. The bi-linear transformation, defined as in eq. 3.24, maps the unit circle of the z -plane into the imaginary axis of the w -plane.

$$w = \frac{2}{T} \frac{z - 1}{z + 1} \quad (3.24)$$

where T is the sample period.

The standard design techniques for a continuous-time system can be used in the w -plane. So, throughout the controllers design, the aircraft model is discretized and mapped into the w -plane from the s -plane first. The same design techniques in continuous-time controller design are used to design the pitch attitude hold, roll hold, etc. Finally the controllers are mapped into the z -plane by the bi-linear transformation.

This results in almost identical sampled-data system configuration as in continuous-time (figure 3.42). The PID controllers, as well as LEAD/LAG compensator, are designed in the w -plane with the same approach as in the s -plane.

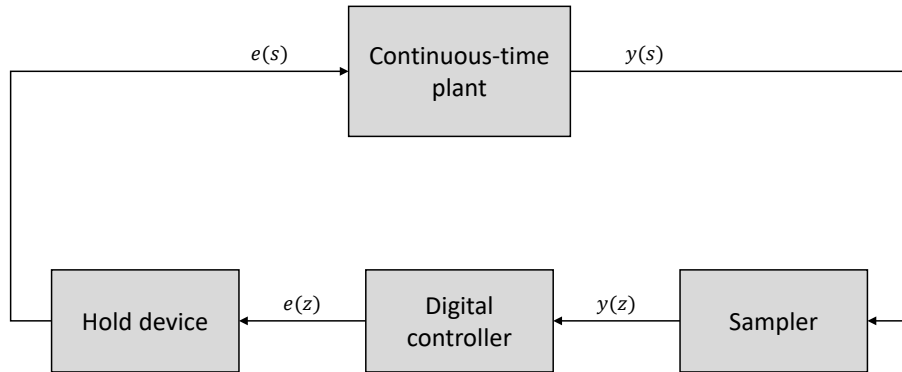


Figure 3.42: Sampled-data system

The same trim conditions were used for both continuous-time and sampled-data systems simulation, in order to check that the sampled-data ones perform as good as the continuous ones.

Longitudinal and lateral-directional (discrete) motion controllers are provided in the following paragraphs. The same linear-continuous gains are used in this project phase.

Longitudinal motion controller

The idea of the developed longitudinal motion controller (both for airplane/helicopter mode), is that the current (or trimmed) attitude is held indefinitely when the pilot flies 'hands-off', which means that the pilot does not apply any force on the control stick.

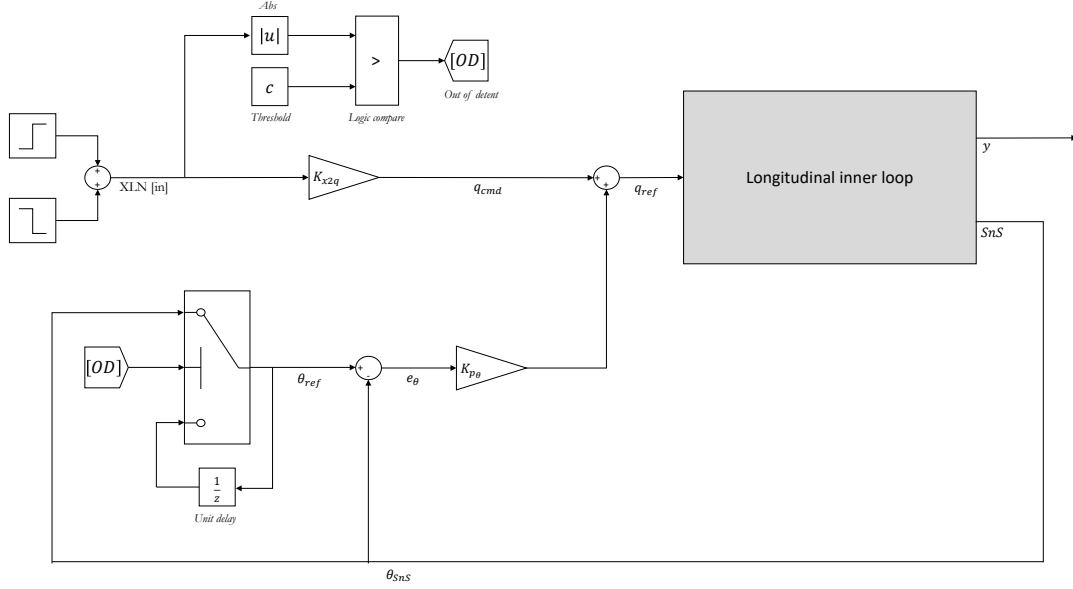


Figure 3.43: Longitudinal motion controller

The detailed discrete implementation of the designed longitudinal CAS is shown in figure 3.43, where the *longitudinal inner loop*, including the pitch rate control system (figure 3.17), gets q_{ref} , merging the commanded pitch rate q_{cmd} with $e_\theta \cdot K_{p_\theta}$. As in 3.19, the latter signal ($e_\theta \cdot K_{p_\theta}$) allows to keep the attitude, in accordance with the out-of-detent logic.

Actually, if the pilot stick longitudinal input $XLN[in]$ is below a certain threshold c (set as $0.1[in]$ for the current implementation system), thus the pilot does not apply any force to the stick, the attitude hold system is *in detent* (the pitch hold controller is active). If the pilot now moves the stick enough, so that the logical 'greater' compare detects its displacement, the attitude hold system goes *out-of-detent*. Therefore, when the stick input exceeds the threshold, the out-of-detent signal $[OD]$ becomes '1'. Conversely, the out-of-detent signal becomes '0' when the stick displacement falls below the threshold.

There are two transitional situations that need to be handled:

- Pilot is 'hands-off'. Taking the control he goes 'hands-on'. Out of detent gets true.
- Pilot is 'hands-on'. He releases the stick and goes 'hands-off'. Out-of-detent gets false.

For the first transition, when out-of-detent gets true, e_θ is zeroed. This is done by a switch. While the pilot flies 'hands-on' the reference angle θ_{ref} corresponds to the measured pitch θ_{SnS} and therefore the error is zero. For the second transition, the out-of-detent becomes false. This means that θ_{ref} corresponds to the last measured θ_{SnS} , so the error is non-zero. In this instance, the Unit Delay block holds (and delays) its input (θ_{ref}) by the sample period specified, until the out-of-detent is false.

Besides this, it must be mentioned that the same sampling time must be used in the whole FCS to guarantee its functionality. For the present implementation $T_{FCS} = 0.01 \text{ s}$ ⁸ was defined, as well as $K_{x2q} = 1$ (stick to pitch rate conversion). Note that a zero-order hold was used as 'hold device', as in figure 3.42.

The system response ($t = 8\text{s}$) for 140kts and nacelle angle set to 0° is shown in figures 3.45 and 3.46. A longitudinal step is used to stimulate the system, as in figure 3.44.

The simulations show that the sampled-data longitudinal motion controller performs as good as the continuous-time system.

Lateral-Directional motion controller (airplane mode)

The discrete implementation of the lateral-directional CAS (airplane mode) is shown in figure 3.47. The *lateral-directional inner loop* holds the roll rate control system (figure 3.21) and the turn hold (figure 3.25). Here, the pilot stick lateral input $XLT[in]$ and the pedal input $XPD[in]$ result in a certain reference roll rate p_{ref} and lateral acceleration $n_{y_{ref}}$, respectively⁹.

⁸ $T_{ACT} = 0.005 \text{ s}$ and $T_{SnS} = 0.01 \text{ s}$. The same sample periods are used for the lateral-directional motion controller too.

⁹The commanded signal (*cmd*) corresponds to the reference one (*ref*).

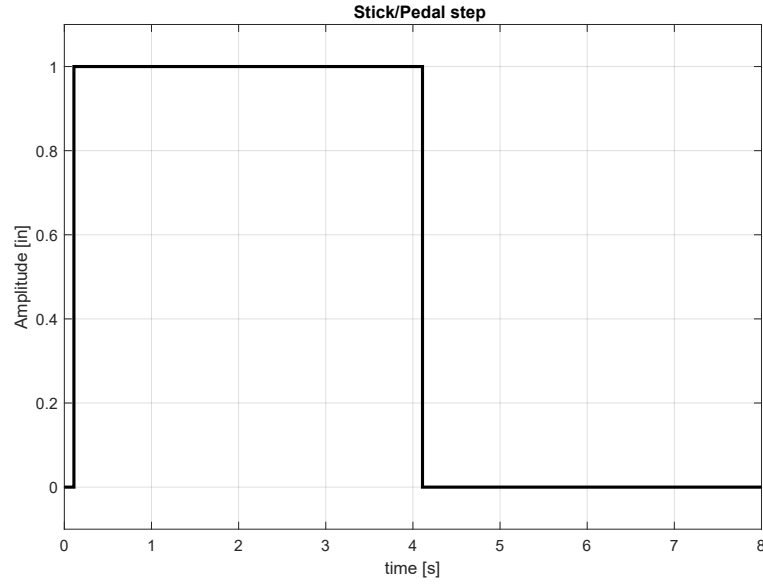


Figure 3.44: Stick/Pedal step input

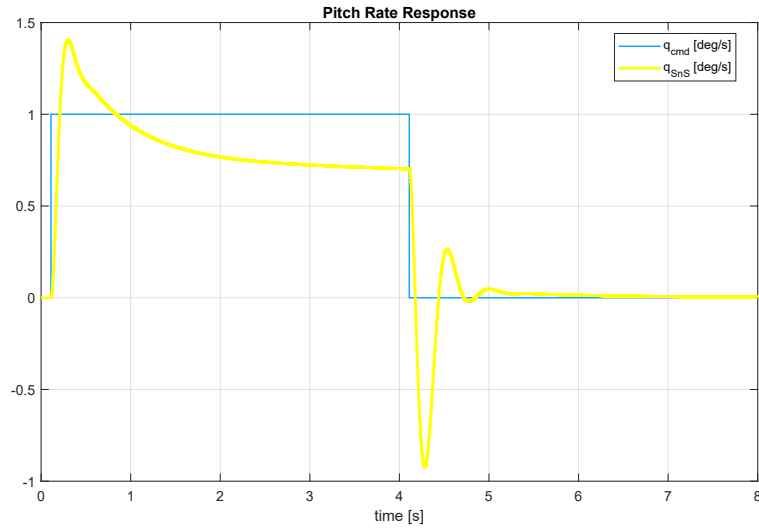


Figure 3.45: Pitch rate response

For the present implementation $K_{x2p} = 1$ (stick to roll rate conversion) and $K_{x2n_y} = 1$ (pedal to lateral acceleration conversion) were defined. Note that a zero-order hold was used as 'hold device', as in figure 3.42.

The system response ($t = 8s$) for 140kts and nacelle angle set to 0° is shown in

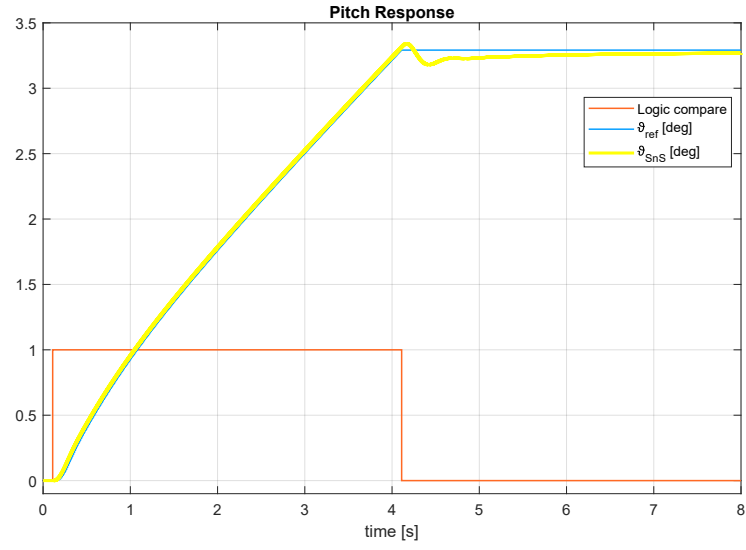


Figure 3.46: Pitch response

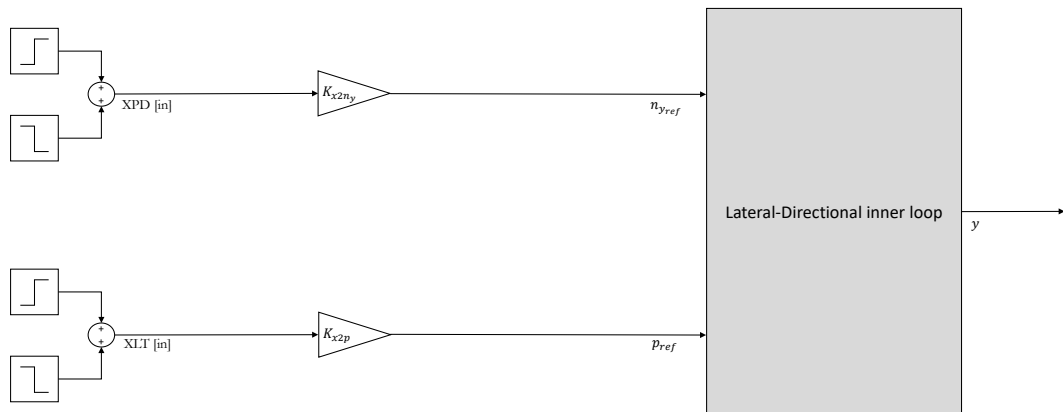


Figure 3.47: Lateral-Directional motion controller (airplane mode)

figures 3.49, 3.50 and 3.51. A lateral step is used to stimulate the system (figure 3.44) as well as a pedal step (figure 3.48).

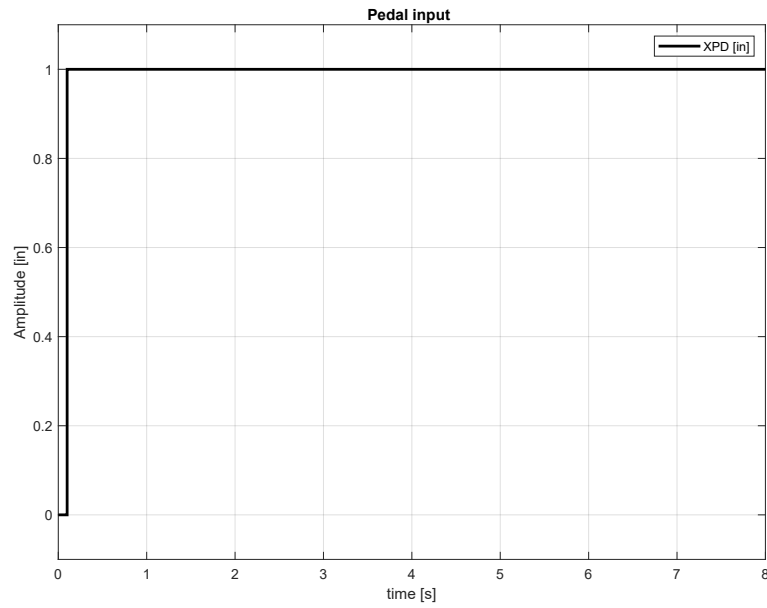


Figure 3.48: Pedal step input

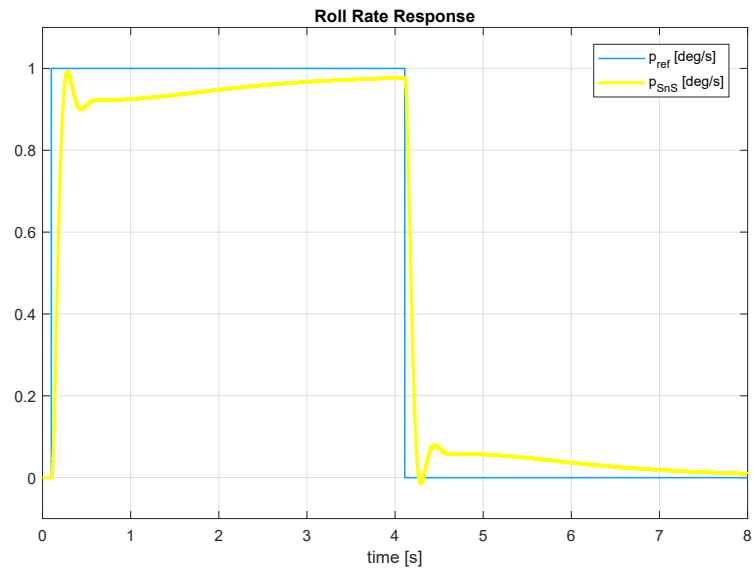


Figure 3.49: Roll rate response to a lateral step input XLT

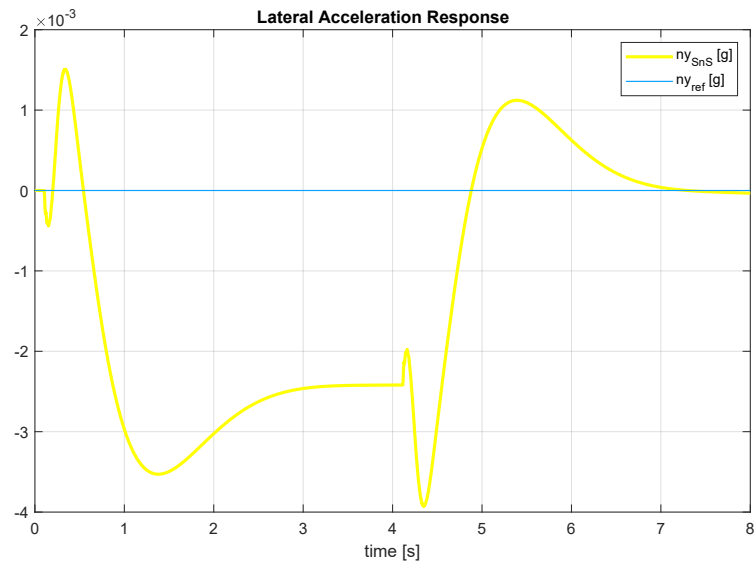


Figure 3.50: Lateral acceleration response to a lateral step input XLT

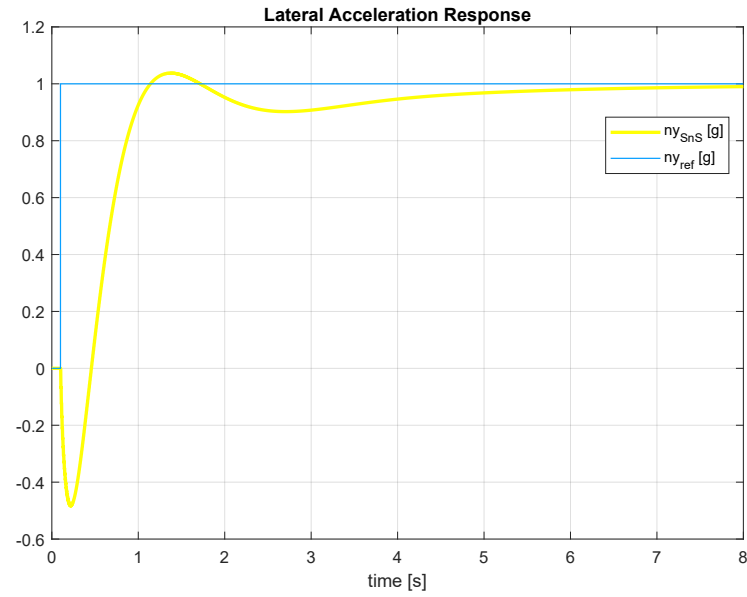


Figure 3.51: Lateral acceleration response to a pedal step input XPD

Lateral-Directional motion controller (helicopter mode)

The discrete implementation of the lateral-directional controller (helicopter mode) is shown in figure 3.52. The *lateral-directional inner loop* holds the roll rate- (figure 3.21) and yaw rate- control system (figure 3.27). Here, the pilot stick lateral input $XLT[in]$ and the pedal input $XPD[in]$ result in a certain reference roll rate p_{ref} and yaw rate r_{ref} ¹⁰, respectively.

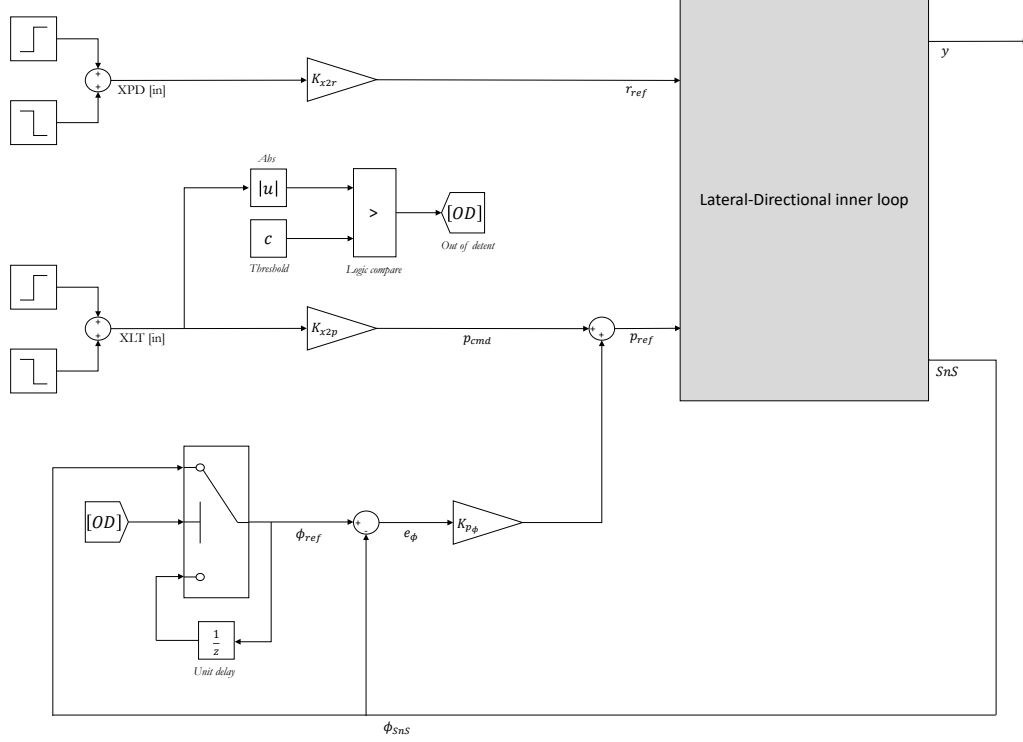


Figure 3.52: Lateral-Directional motion controller (helicopter mode)

The out-of-detent logic is the same as in the longitudinal motion control. For the present implementation $K_{x2p} = 1$ (stick to roll rate conversion) and $K_{x2r} = 1$ (pedal to yaw rate conversion) were defined. Note that a zero-order hold was used as 'hold device', as in figure 3.42.

The system response ($t = 8s$) for $40kts$ and NAC set to 90° is shown in figures 3.53, 3.54 and 3.55. A lateral and pedal step is used to stimulate the system, as in figure 3.44.

¹⁰The directional commanded signal (*cmd*) corresponds to the reference one (*ref*).

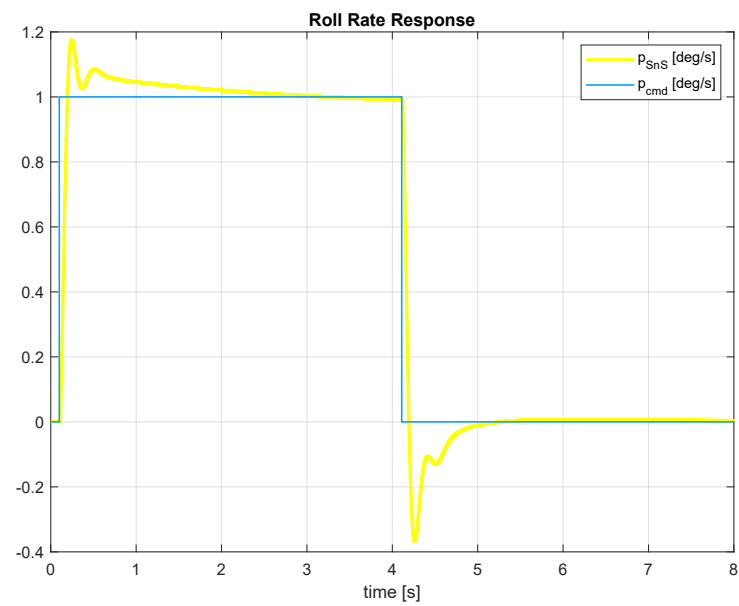


Figure 3.53: Roll rate response

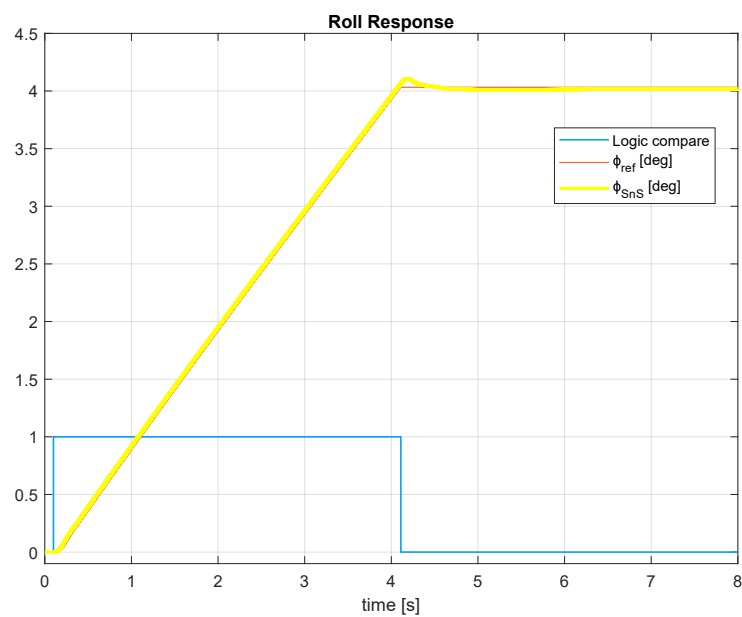


Figure 3.54: Roll response

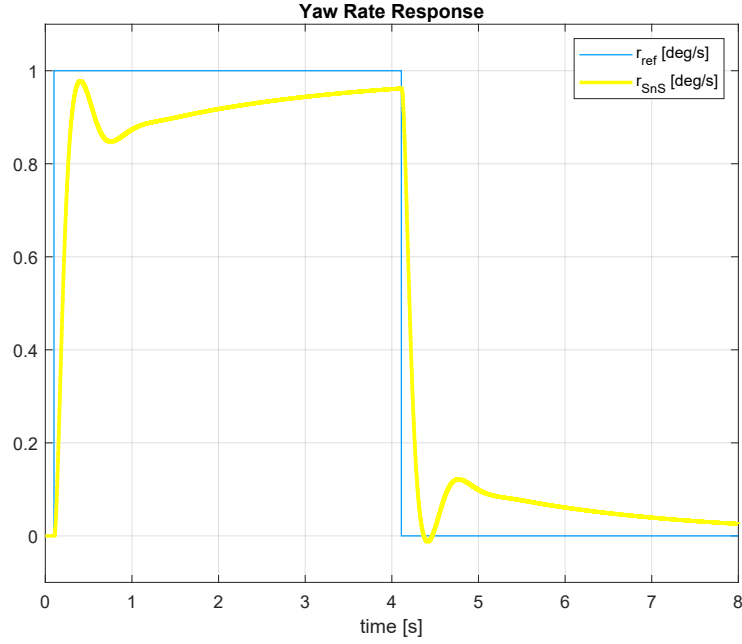


Figure 3.55: Yaw rate response

The sampled-data lateral-directional motion controller shows satisfactory performances as the continuous-time system.

3.5.3 Nonlinear system

In this paragraph, a simple method, for the implementation of gain-scheduled controllers for nonlinear system, is proposed. This method can be applied to a fairly general class of control structures that are usually referred to as tracking controllers. The key procedures are to provide integral action at the inputs to the plant and differentiate some of the measured outputs before they are feedback to the scheduled controller. The resulting system is easy to obtain and its structure is similar to that of the original linear controller. Furthermore, despite the use of differentiators, this scheme does not introduce additional noise amplification.

It is important to emphasize that a potential weak point of this method, namely the requirements that some of the outputs be differentiated, can be dealt with in practice by using suitable approximations: in the case of digital computers, differentiation could be replaced by taking the difference between present and previous values of the measured outputs.

Thus, the problem addressed here is to find a gain-scheduled (nonlinear) controller

for the nonlinear plant G so that the *linearization property*¹¹ is satisfied at each equilibrium point α .

Let G_l be the closed-loop linear system, G the nonlinear closed-loop system and $G_k(\alpha)$ denote its linearization at α . Therefore, the controller implementation problem considered can be stated as follow: find a gain-scheduled controller C such that for each equilibrium point of G the following properties hold:

- (I) the feedback systems $G_k(\alpha)$ and $G_l(\alpha)$ have the same closed-loop eigenvalues.
- (II) the closed-loop transfer functions related to $G_k(\alpha)$ and $G_l(\alpha)$ are equal.

Following these rules of thumb, the nonlinear controllers are carried out. The integral action¹² as well as the difference between current and previous values of the measured outputs were already implemented on the linear and discrete models, so it is expected that the linearization property is preserved¹³.

Thus, the implemented nonlinear CAS (appendix A) is almost the same as the sampled-data one, although the gains related to the sample points are replaced with lookup tables (linear interpolation was accomplished), in order to handle the whole flight envelope control. Moreover, a simple but effective Relay block is used as switch between airplane and helicopter mode, for the lateral-directional motion controller.

The developed 'PID-based' controllers, as well as the 'compensator-based' one, were evaluated with simulations on MATLAB Simulink and compared to the linear model for the same trim condition and command input. The PID showed better results than the linear system, due to the following considerations:

- Although both nonlinear and linear systems perform satisfactorily at the operating point, the linear one cannot hold the performance when the commanded input (e.g. pitch rate command) is far from the operating point. This is

¹¹At any given operating point, the linearization of the feedback system consisting of the gain-scheduled controller and the nonlinear plant (frozen-time system) exhibits the same internal and input-output properties as the feedback interconnection of the linearized plant and the corresponding linear controller.

¹²The integral action in the nonlinear model of the XV-15 is provided by a self-made integrator (developed by the ZHAW team).

¹³Due to the limited available time, the two properties stated in (I) and (II) could not be checked. Nevertheless, the proposed rules provide a good basis for further researches in order to be pursued.

because the dynamic behavior of nonlinear system changes with the operating range. The gain scheduled nonlinear controller performs its job well in a larger operating range.

- The XV-15 whole model is more detailed than the linearized model developed in this chapter (e.g. the actuators and the sensors implemented are more realistic than the transfer functions used in the linear system).

Therefore, it was preferred to use PID based techniques, for this first cut design, as PID control technique is popular for its simplicity, handling desired multiple specifications simultaneously and it easy to implement.

As conclusion, it is important to remark that in practical applications, gain-scheduled controllers are often switched on after an initial phase where the plant is steered by an operator (manual mode) or by a linear time-invariant controller. It is then important to initialize properly the states of the gain scheduled controller at the time of the switching.

Chapter 4

Results

The following chapter presents the results of the gain evaluation and the scheduling tests, performed on MATLAB Simulink, in order to check the functionality of the implemented CAS, as well as quantifying the effects of all the modifications introduced by the author and described in the previous chapters. This goal has been pursued by means of two different activities:

- On one hand, system response from offline simulations have been assessed. Furthermore, the outputs comparison between CAS on and off gave a first indication for an improvement or degradation of the handling qualities.
- On the other hand, a series of pilot-in-the-loop tests has been carried out, to evaluate the pilots' perception of the aircraft model and assess the fidelity of the simulation to a real piloting experience.

4.1 Gain Evaluation

The following section lists the evaluated gains for the implemented CAS. Due to the large amount of raw data, only the nonlinear gains are shown, achieved assessing the offline simulations outputs.

In the following figures, sample points (3.3) are plotted as bullets •.

The resulting CAS gains are shown as a function of the calibrated airspeed.

4.1.1 Gain Scheduling - Longitudinal CAS

Airspeed [kts]	0	40	100	140	180	220	260	300
Gain Value	0.55	0.55	0.45	0.45	0.40	0.35	0.15	0.12

Table 4.1: K_{p_q} evaluated gain

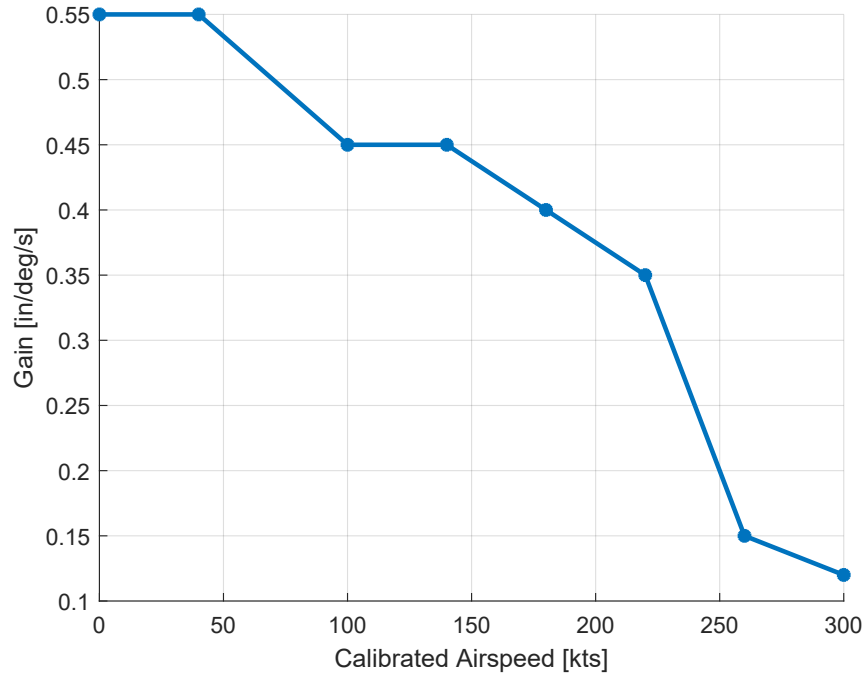


Figure 4.1: K_{p_q} evaluated gain throughout XV-15 flight envelope

Airspeed [kts]	0	40	100	140	180	220	260	300
Gain Value	0.50	0.50	0.20	0.20	0.20	0.20	0.15	0.10

Table 4.2: K_{I_q} evaluated gain

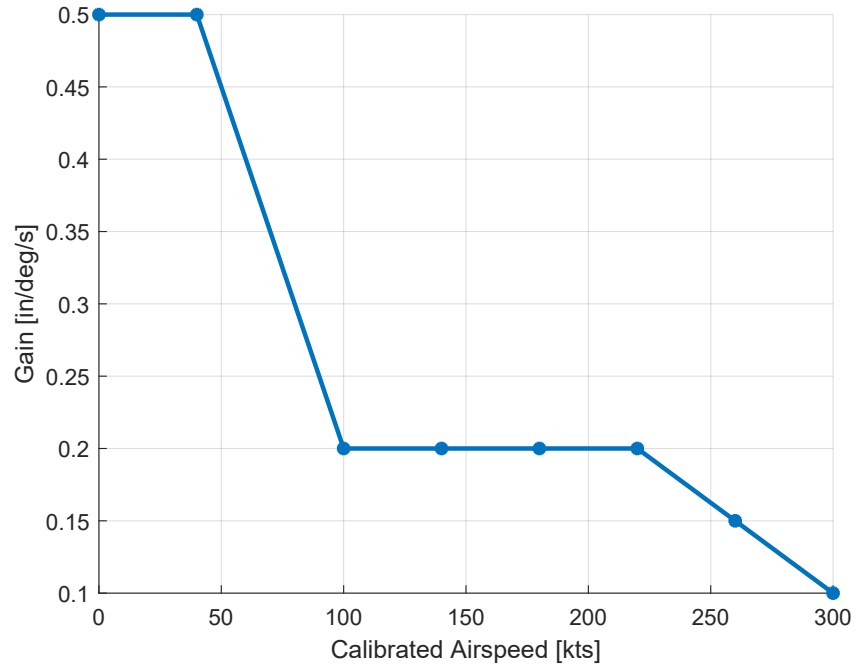


Figure 4.2: K_{I_q} evaluated gain throughout XV-15 flight envelope

Airspeed [kts]	0	40	100	140	180	220	260	300
Gain Value	-0.40	-0.40	-0.40	-0.40	-0.10	-0.05	0.00	0.00

Table 4.3: K_{FF_q} evaluated gain

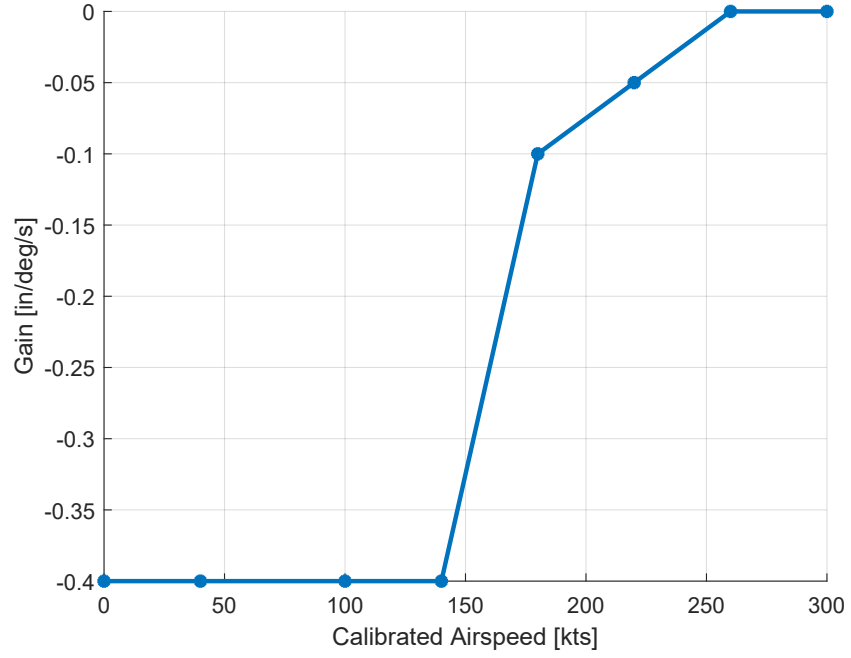


Figure 4.3: K_{FF_q} evaluated gain throughout XV-15 flight envelope

Airspeed [kts]	0	40	100	140	180	220	260	300
Gain Value	-0.48	-0.48	-0.48	-0.48	-0.48	-0.48	-0.48	-0.48

Table 4.4: K'_{pq} evaluated gain

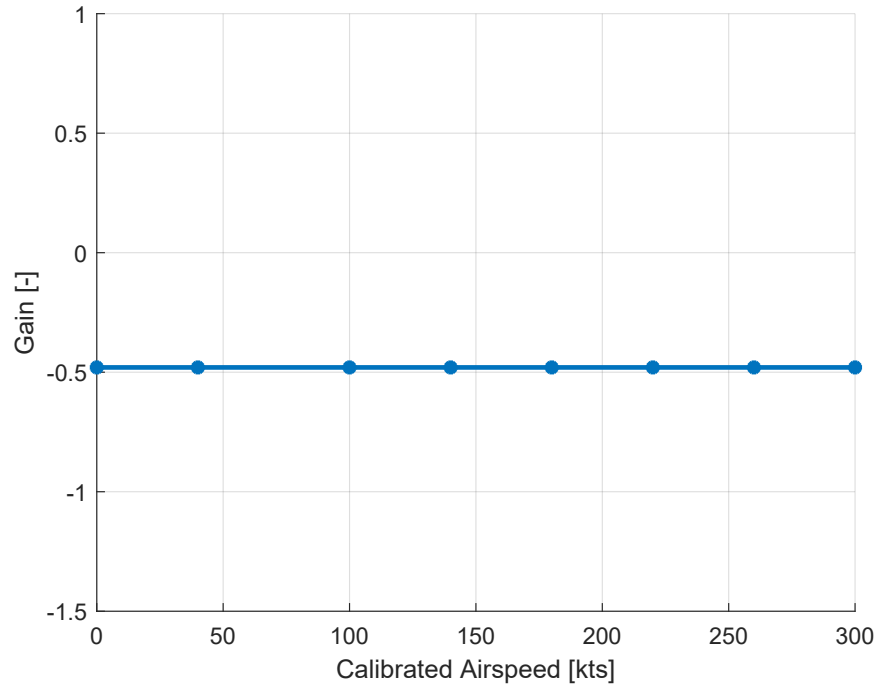


Figure 4.4: K'_{pq} evaluated gain throughout XV-15 flight envelope

Airspeed [kts]	0	40	100	140	180	220	260	300
Gain Value	6.00	6.00	4.80	4.80	7.20	8.40	9.60	10.80

Table 4.5: K_{p_θ} evaluated gain

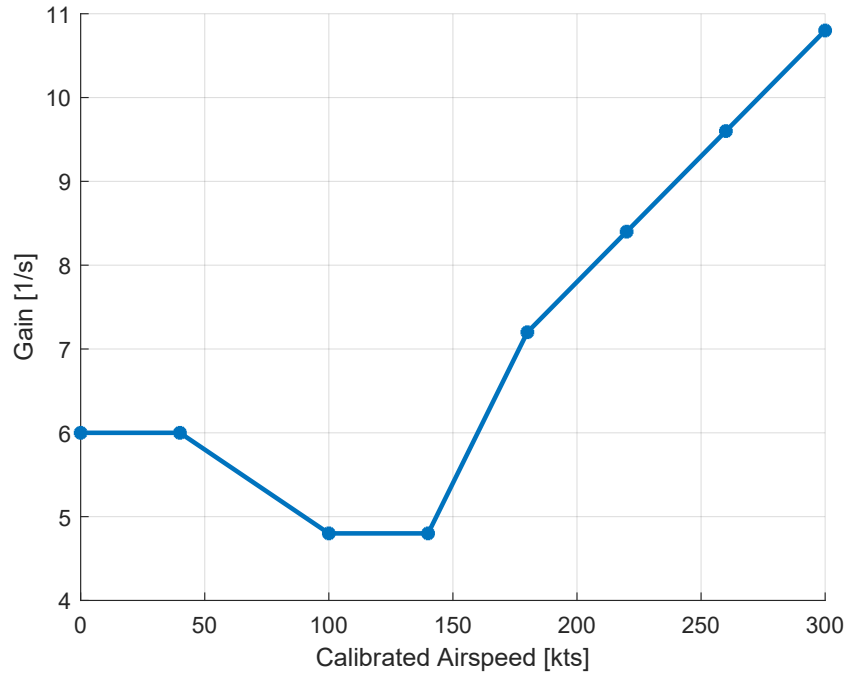


Figure 4.5: K_{p_θ} evaluated gain throughout XV-15 flight envelope

4.1.2 Gain Scheduling - Lateral CAS

Airspeed [kts]	0	40	100	140	180	220	260	300
Gain Value	0.50	0.50	0.70	0.70	0.30	0.20	0.10	0.10

Table 4.6: K_{pp} evaluated gain

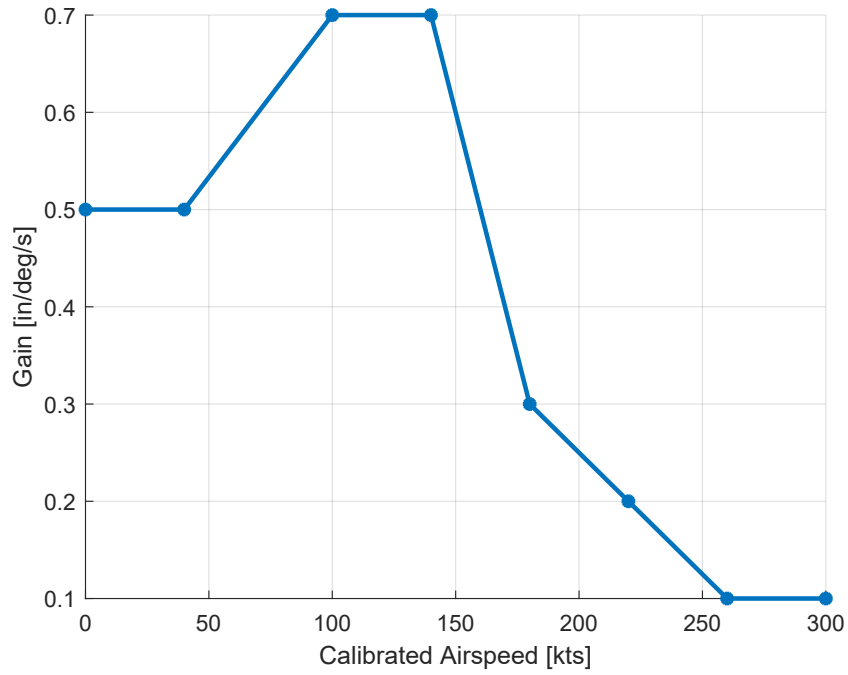


Figure 4.6: K_{pp} evaluated gain throughout XV-15 flight envelope

Airspeed [kts]	0	40	100	140	180	220	260	300
Gain Value	0.25	0.25	0.64	0.64	0.60	0.60	0.60	0.60

Table 4.7: K_{I_p} evaluated gain

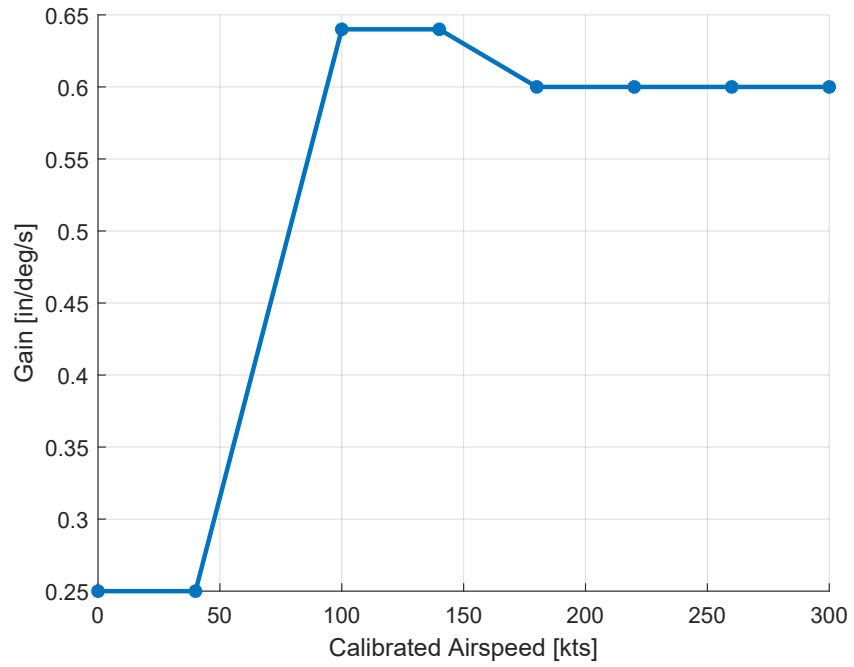


Figure 4.7: K_{I_p} evaluated gain throughout XV-15 flight envelope

Airspeed [kts]	0	40	100	140	180	220	260	300
Gain Value	0.40	0.40	0.35	0.35	0.35	0.25	0.25	0.25

Table 4.8: K_{FF_p} evaluated gain

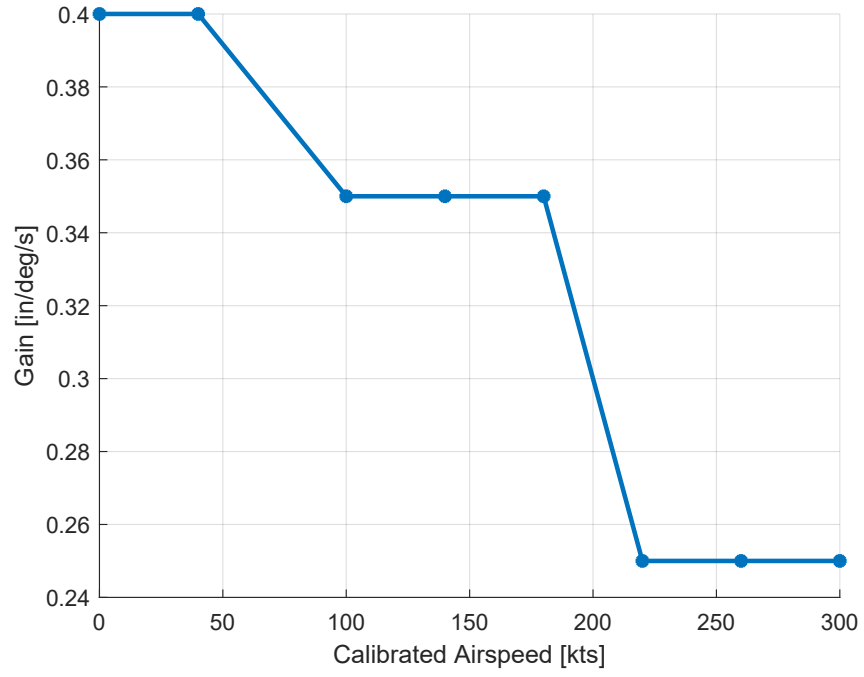


Figure 4.8: K_{FF_p} evaluated gain throughout XV-15 flight envelope

Airspeed [kts]	0	40	100	140	180	220	260	300
Gain Value	5.00	5.00	2.40	2.40	6.00	6.00	6.00	6.00

Table 4.9: K_{p_ϕ} evaluated gain

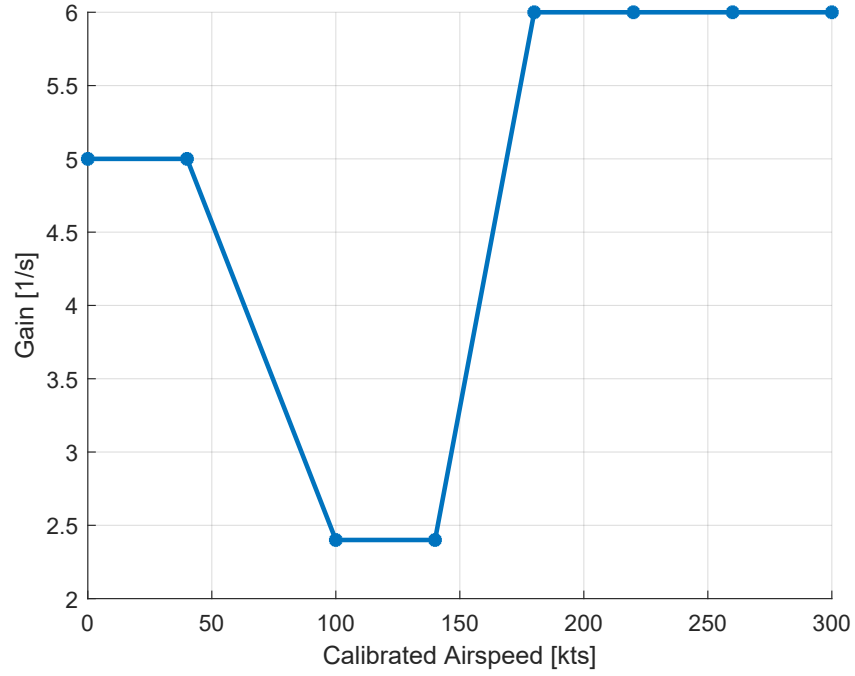


Figure 4.9: K_{p_ϕ} evaluated gain throughout XV-15 flight envelope

4.1.3 Gain Scheduling - Directional CAS

Airspeed [kts]	0	40	100	140	180	220	260	300
Gain Value	12.60	12.60	12.60	12.60	8.10	6.30	3.60	2.70

Table 4.10: $K_{p_{n_y}}$ evaluated gain

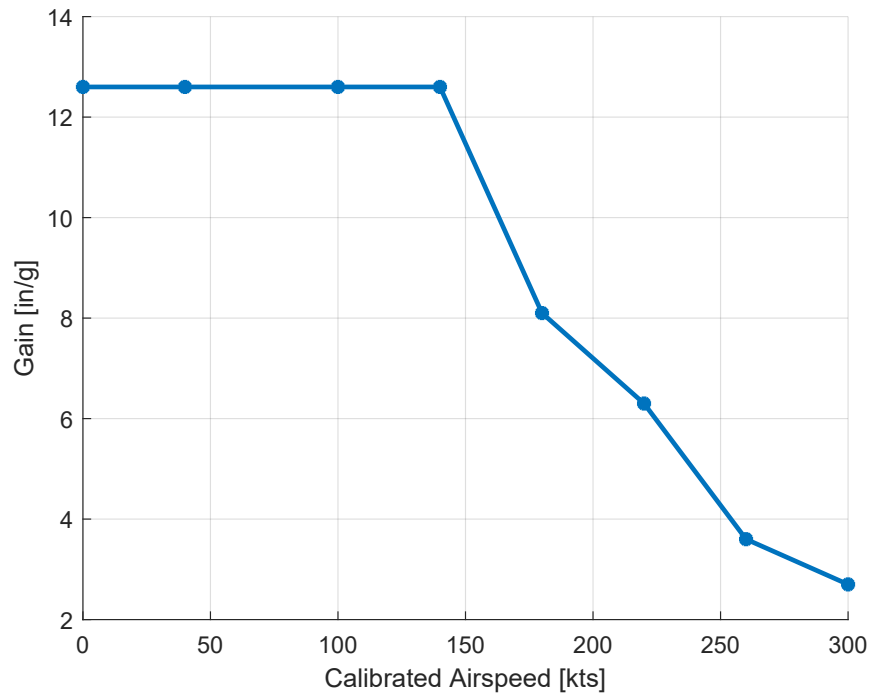


Figure 4.10: $K_{p_{n_y}}$ evaluated gain throughout XV-15 flight envelope

Airspeed [kts]	0	40	100	140	180	220	260	300
Gain Value	10.80	10.80	10.80	10.80	6.30	4.50	1.80	1.35

Table 4.11: $K_{I_{ny}}$ evaluated gain

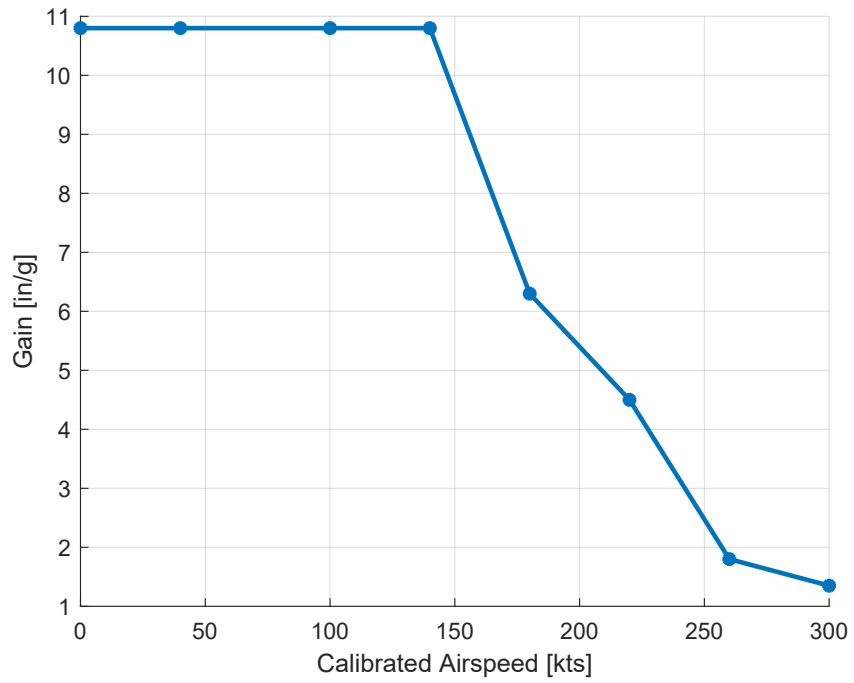


Figure 4.11: $K_{I_{ny}}$ evaluated gain throughout XV-15 flight envelope

Airspeed [kts]	0	40	100	140	180	220	260	300
Gain Value	3.00	3.00	3.00	3.00	3.00	3.00	3.00	3.00

Table 4.12: $K_{FF_{ny}}$ evaluated gain

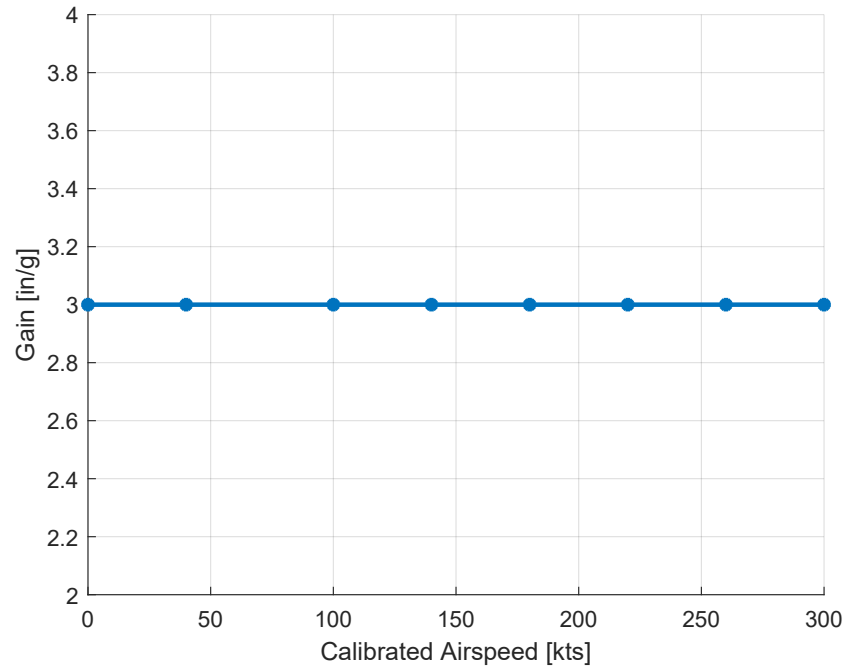


Figure 4.12: $K_{FF_{ny}}$ evaluated gain throughout XV-15 flight envelope

Airspeed [kts]	0	40	100	140	180	220	260	300
Gain Value	1.60	1.60	1.60	1.60	1.60	1.60	1.60	1.60

Table 4.13: K_{pr} evaluated gain

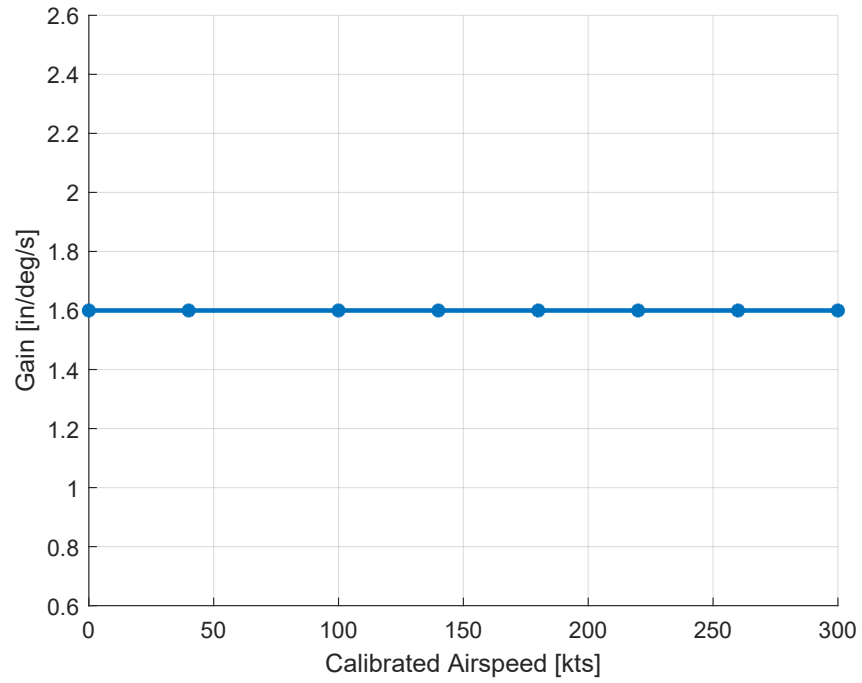


Figure 4.13: K_{pr} evaluated gain throughout XV-15 flight envelope

Airspeed [kts]	0	40	100	140	180	220	260	300
Gain Value	0.90	0.90	0.90	0.90	0.90	0.90	0.90	0.90

Table 4.14: K_{I_r} evaluated gain

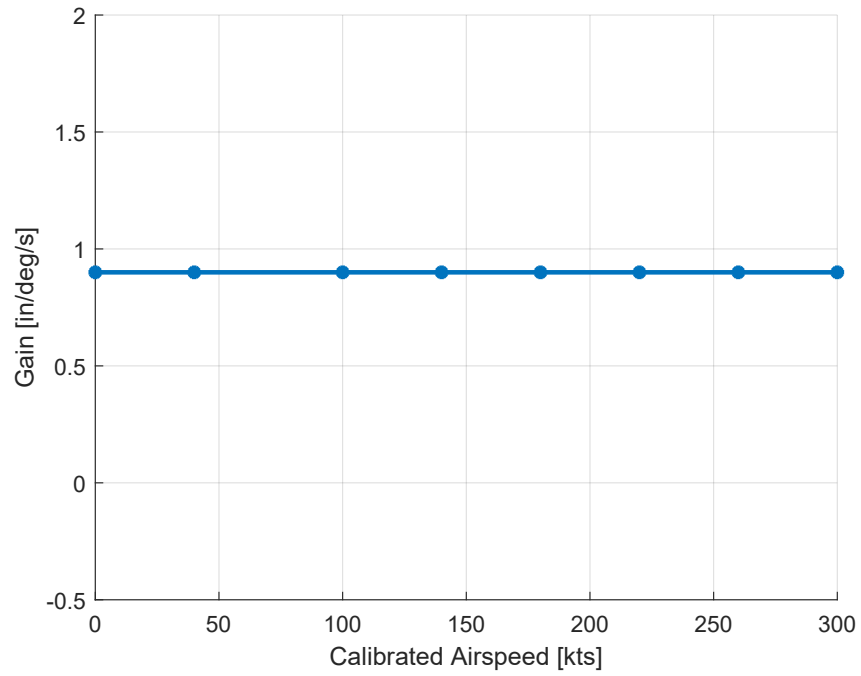


Figure 4.14: K_{I_r} evaluated gain throughout XV-15 flight envelope

4.2 Scheduling Test

In the following section the results of the scheduling tests are shown. To be brief, only the model response for *0kts*, *40kts*, *140kts* and *200kts* is presented. The simulation time is set to *8s*, while the stick/pedal step input is put to *0.50in*.

Due to the limited available time, the stick/pedal to command input conversion¹ was set considering the expected rate/acceleration to a full stick/pedal displacement (as in 3.1).

$$K_{x2q} = \frac{-25^{\circ/s}}{4.8in} \approx -5.20 \frac{\circ/s}{in}$$

$$K_{x2p} = \frac{30^{\circ/s}}{4.8in} \approx 6.25 \frac{\circ/s}{in}$$

$$K_{x2r} = \frac{50^{\circ/s}}{2.5in} \approx 20 \frac{\circ/s}{in}$$

$$K_{x2n_y} = \frac{0.50g}{2.5in} \approx 0.20 \frac{g}{in}$$

Last, an overview of the improvements carried out is detailed showing how the system reacts with CAS off, as well as with the previously implemented SAS model.

¹Note that positive longitudinal stick input leads to negative pitch moment.

4.2.1 Helicopter mode

The following results relate to a nacelle angle of 90° . The angle of sideslip (AoS), as well as the out-of-detent logic and the heading (Ψ), is shown in the following figures.

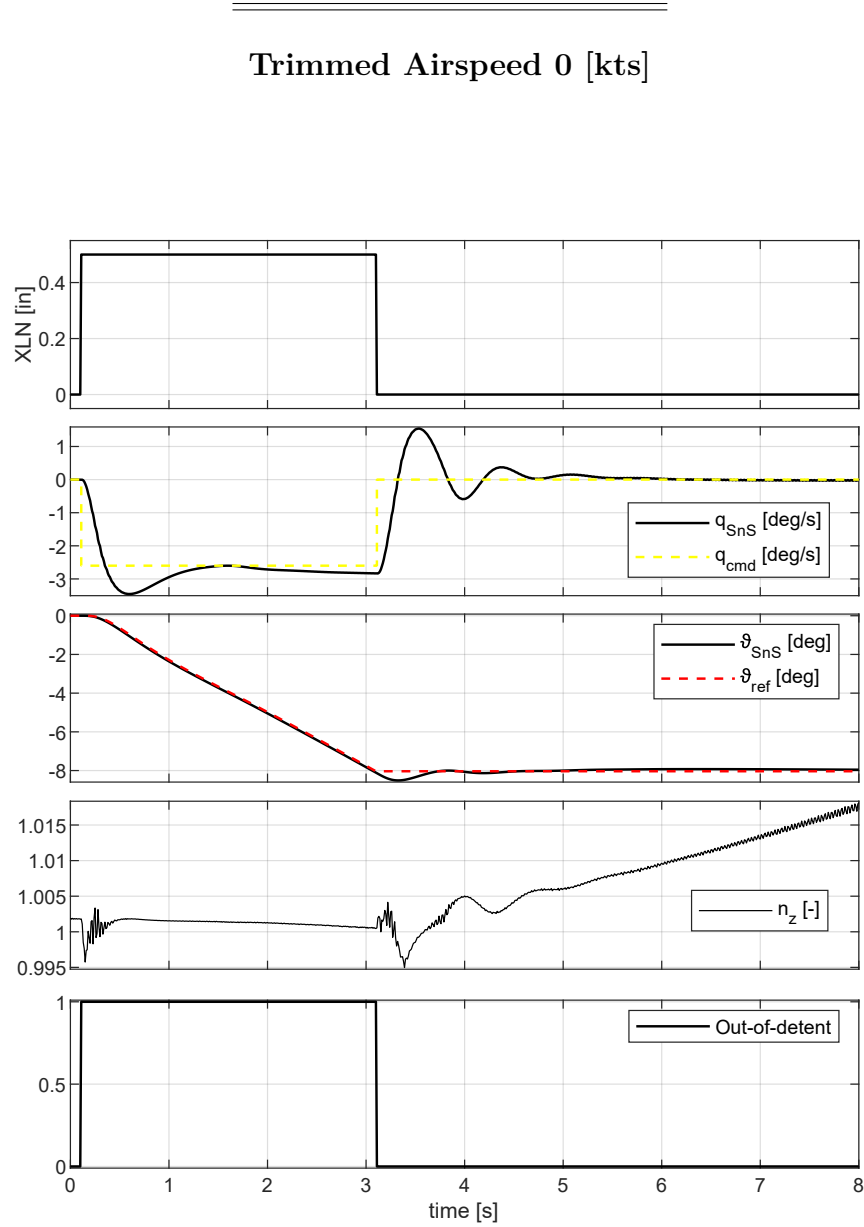


Figure 4.15: XV-15 model response to a longitudinal step input

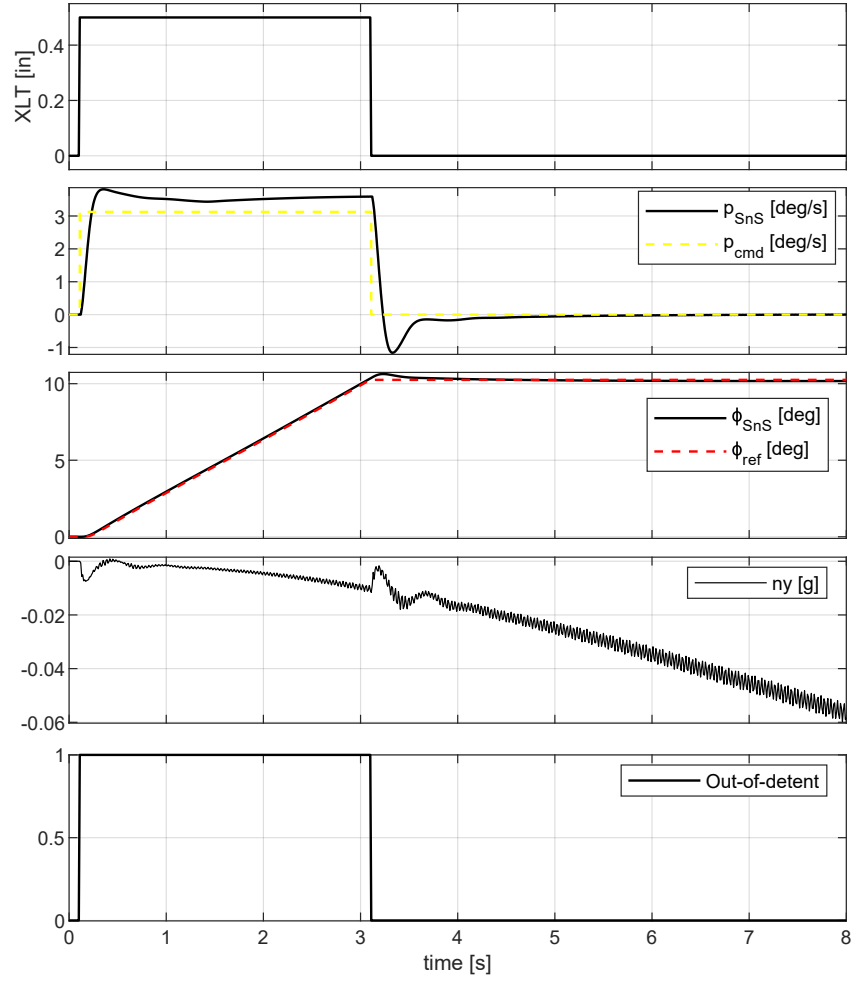


Figure 4.16: XV-15 model response to a lateral step input

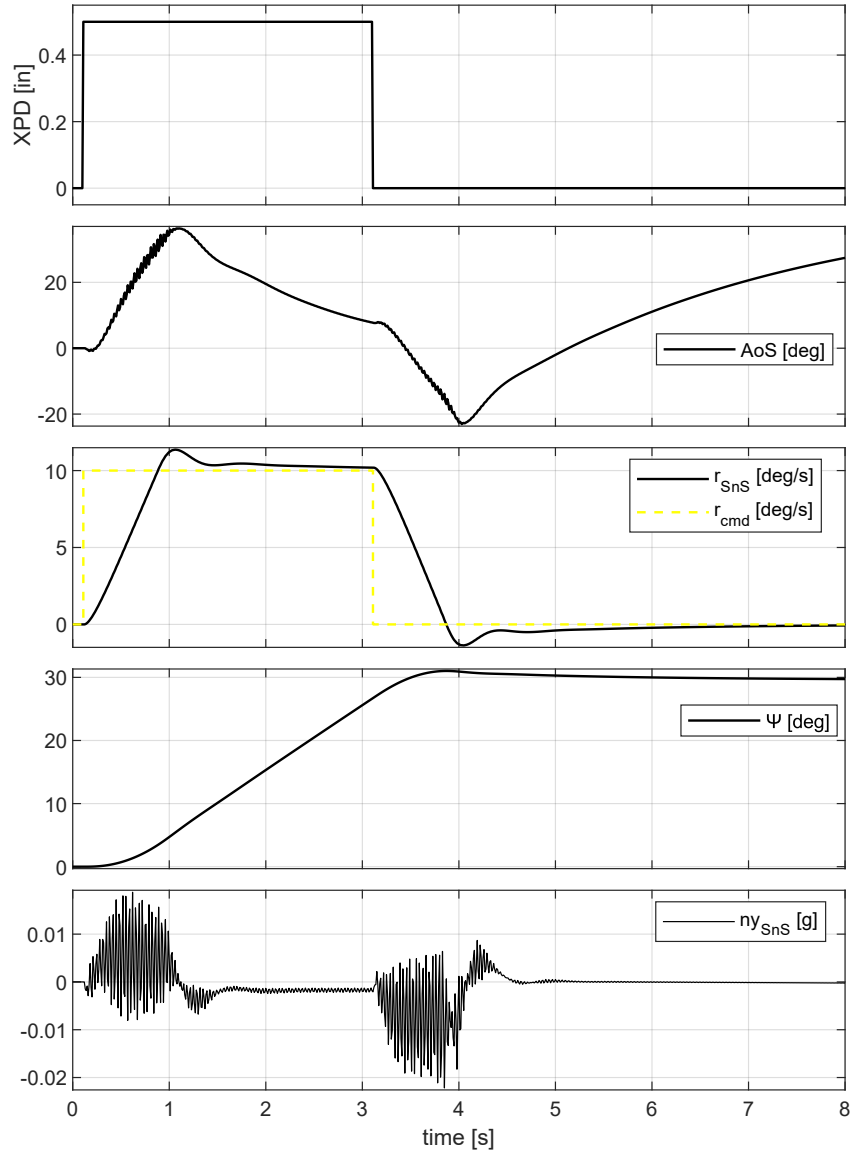


Figure 4.17: XV-15 model response to a pedal step input

Trimmed Airspeed 40 [kts]

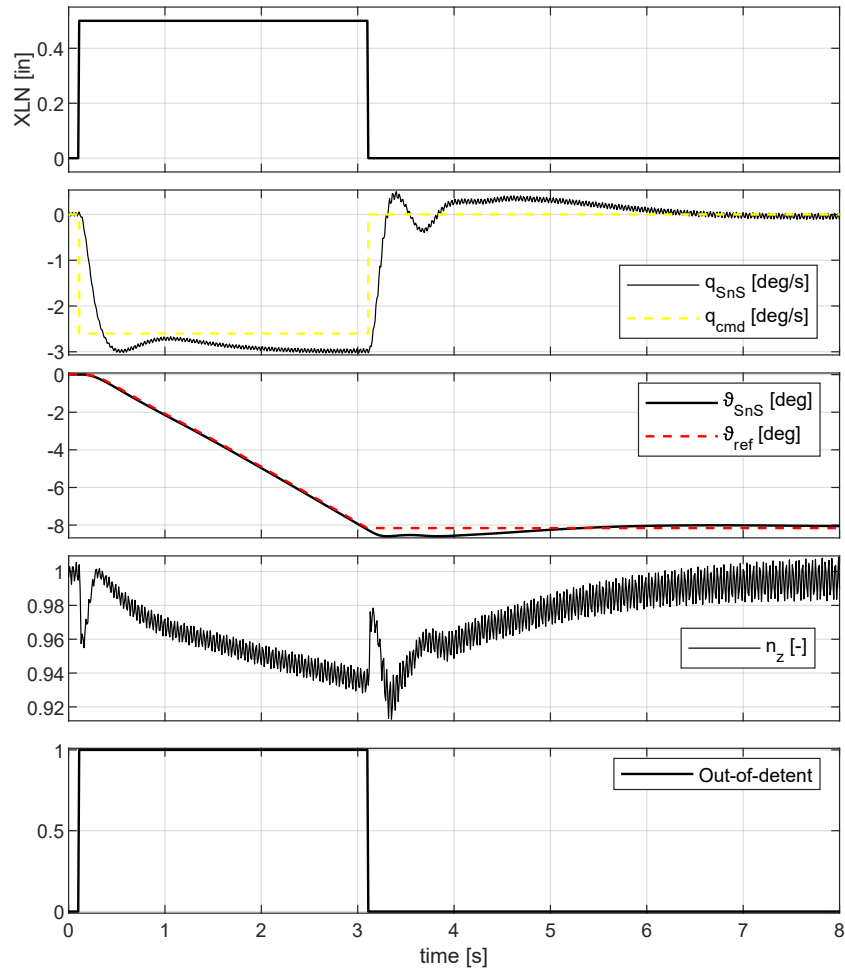


Figure 4.18: XV-15 model response to a longitudinal step input

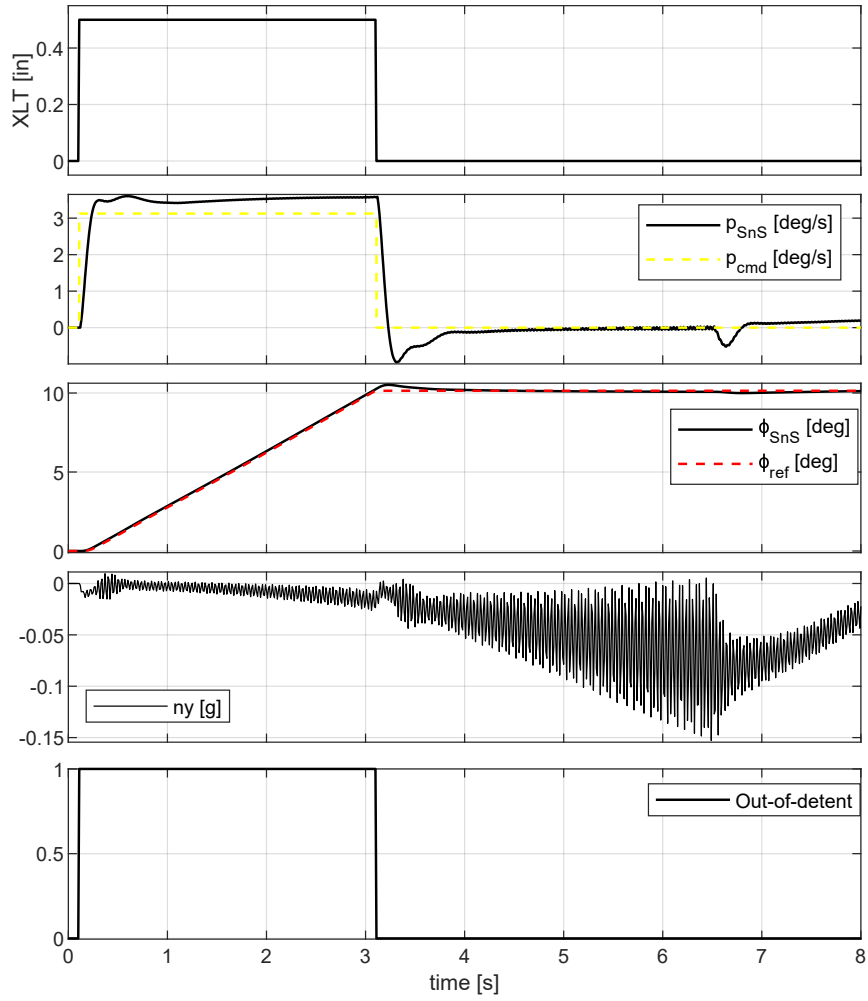


Figure 4.19: XV-15 model response to a lateral step input

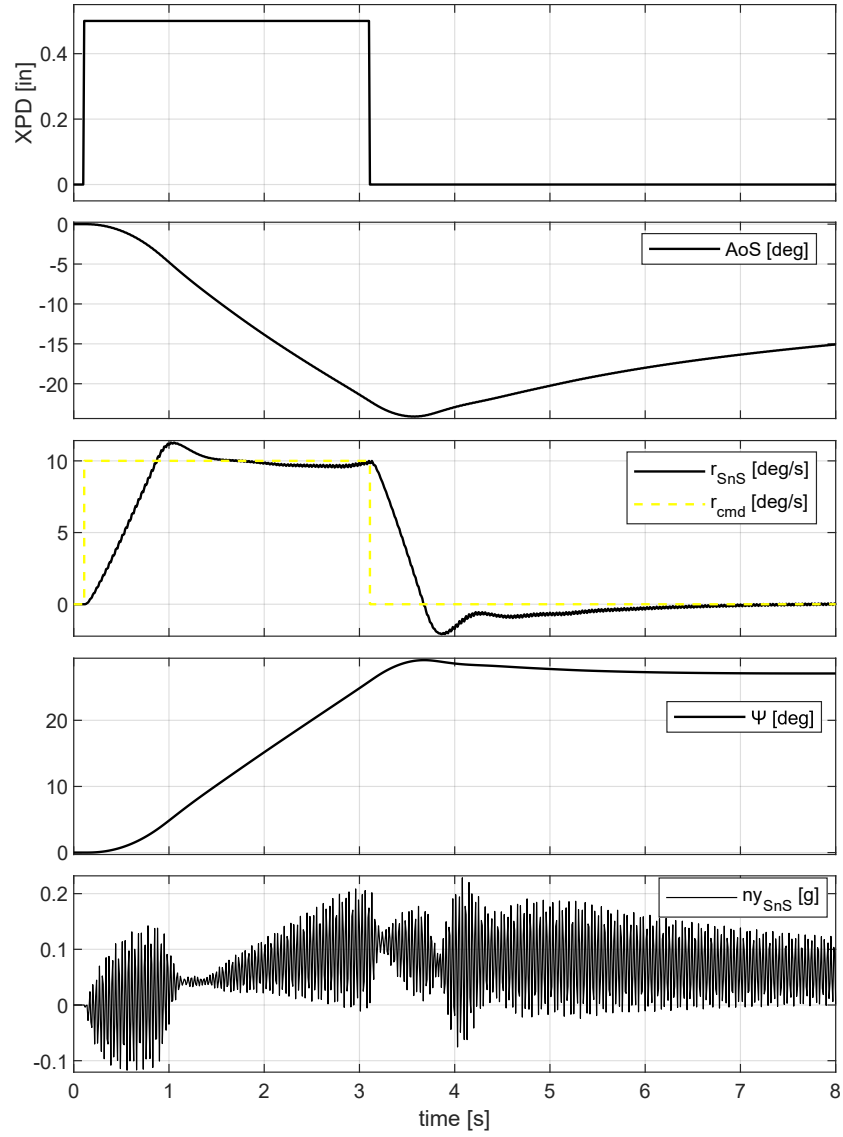


Figure 4.20: XV-15 model response to a pedal step input

4.2.2 Airplane mode

The following results relate to a nacelle angle of 0° . The angle of sideslip (AoS), as well as the out-of-detent logic and the heading (Ψ), is shown in the following figures.

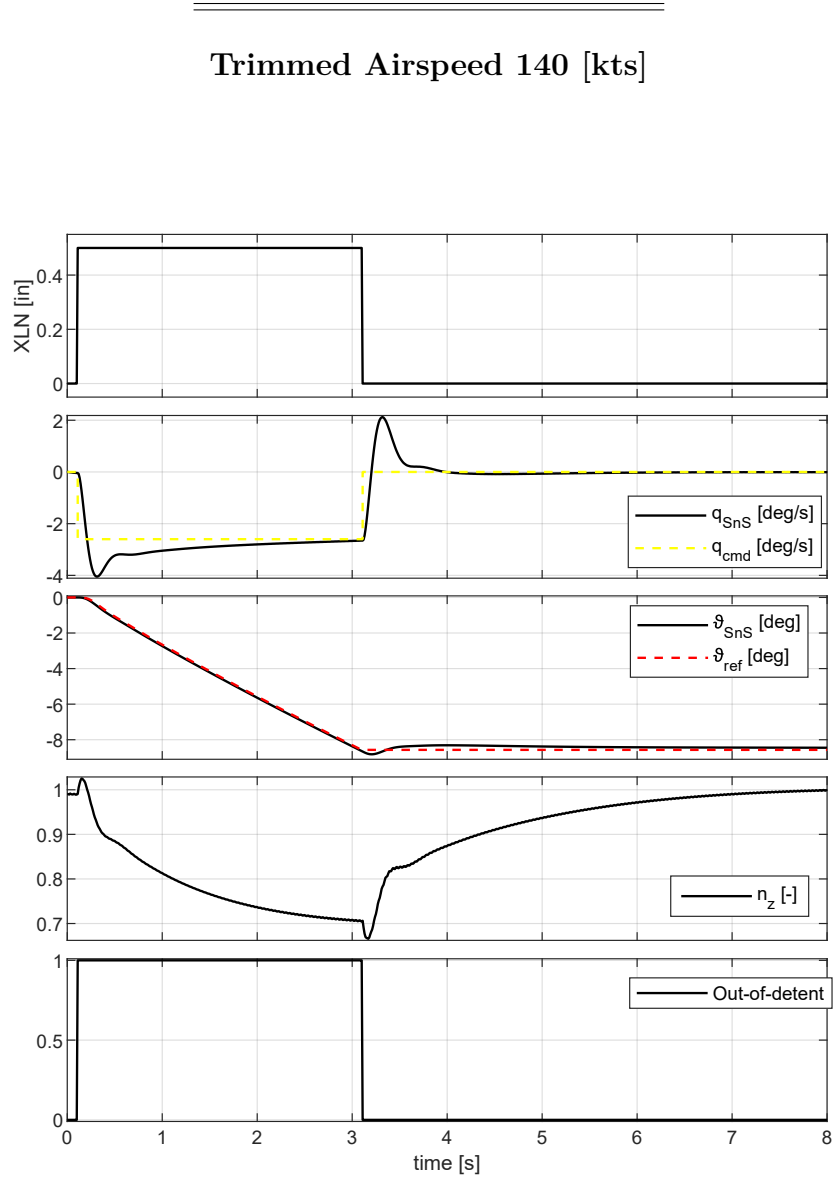


Figure 4.21: XV-15 model response to a longitudinal step input

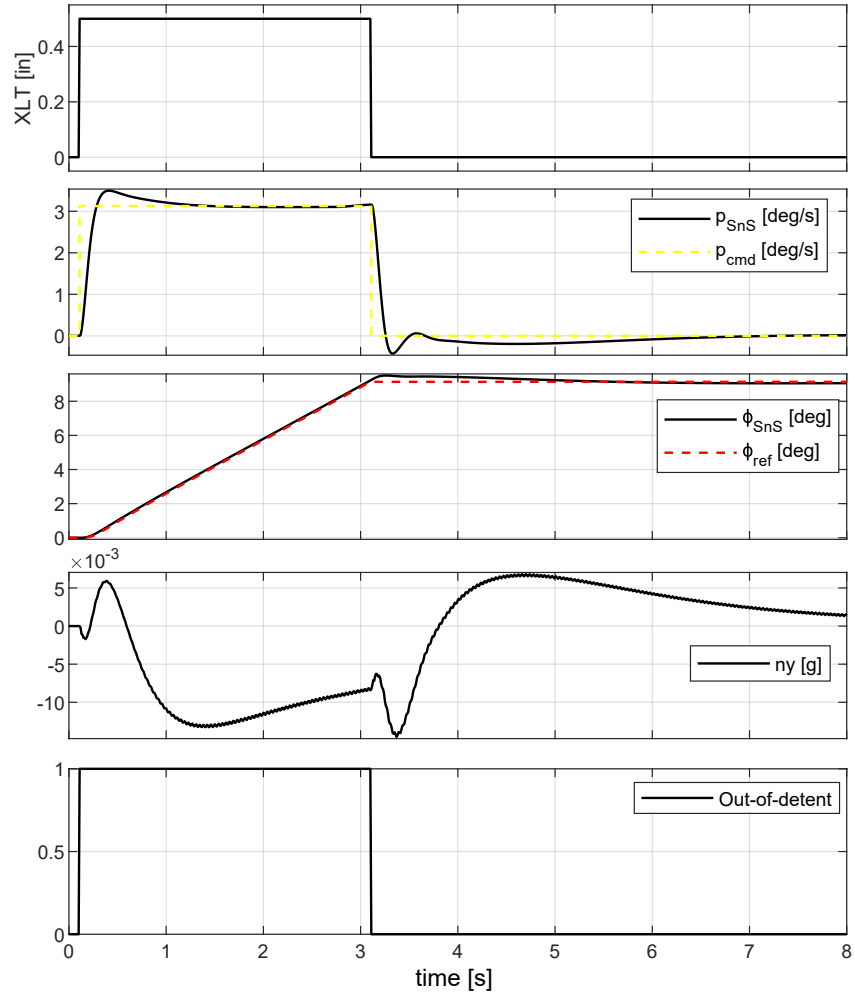


Figure 4.22: XV-15 model response to a lateral step input

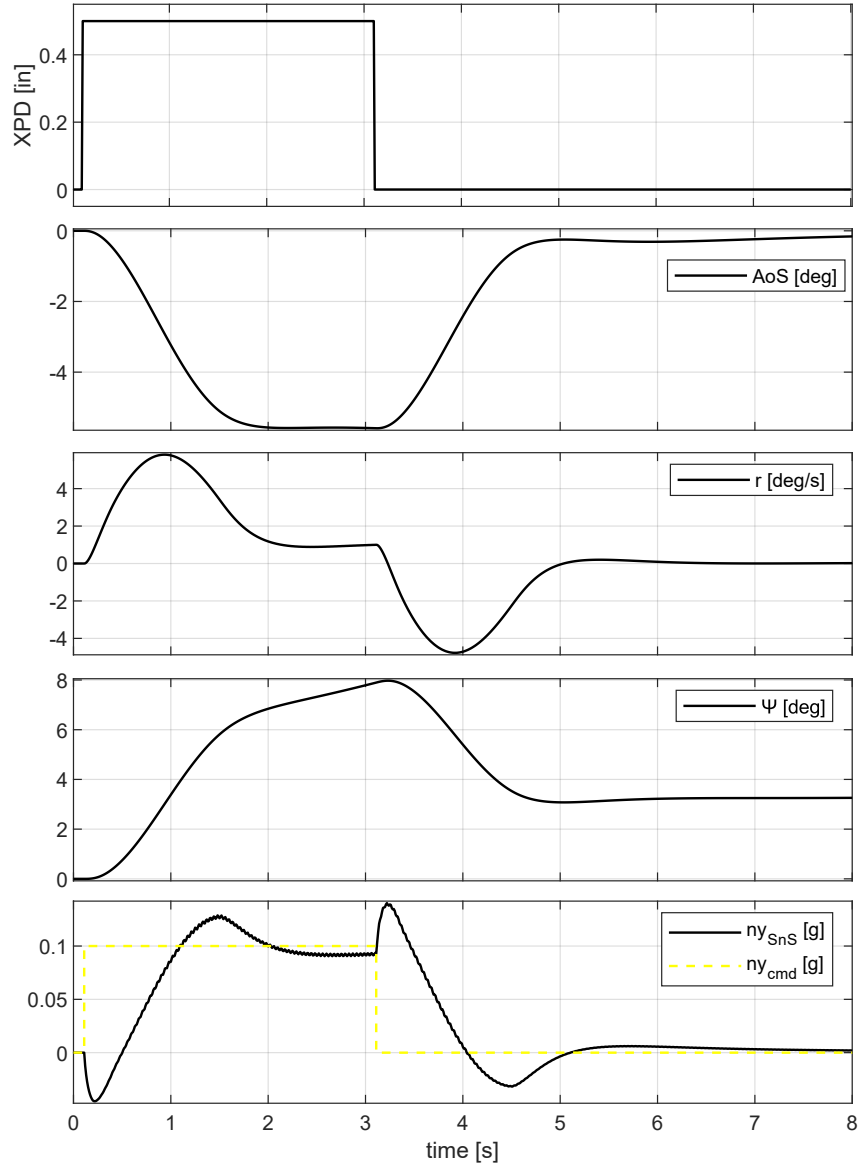


Figure 4.23: XV-15 model response to a pedal step input

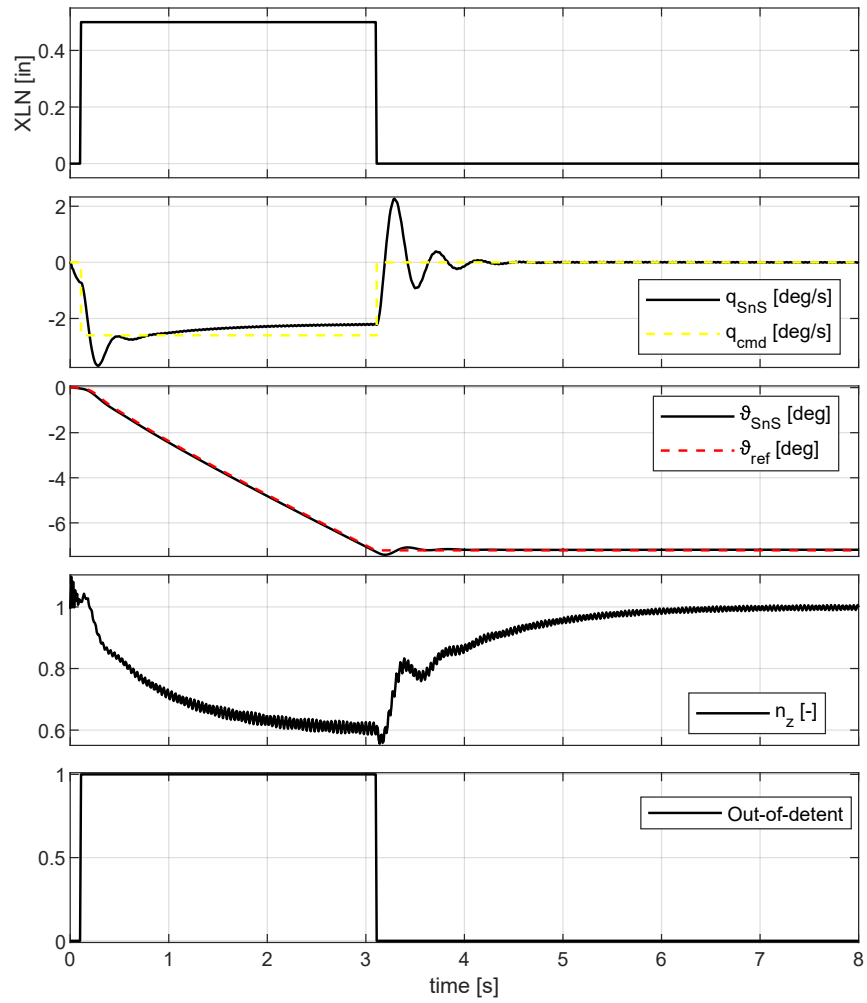
Trimmed Airspeed 200 [kts]


Figure 4.24: XV-15 model response to a longitudinal step input

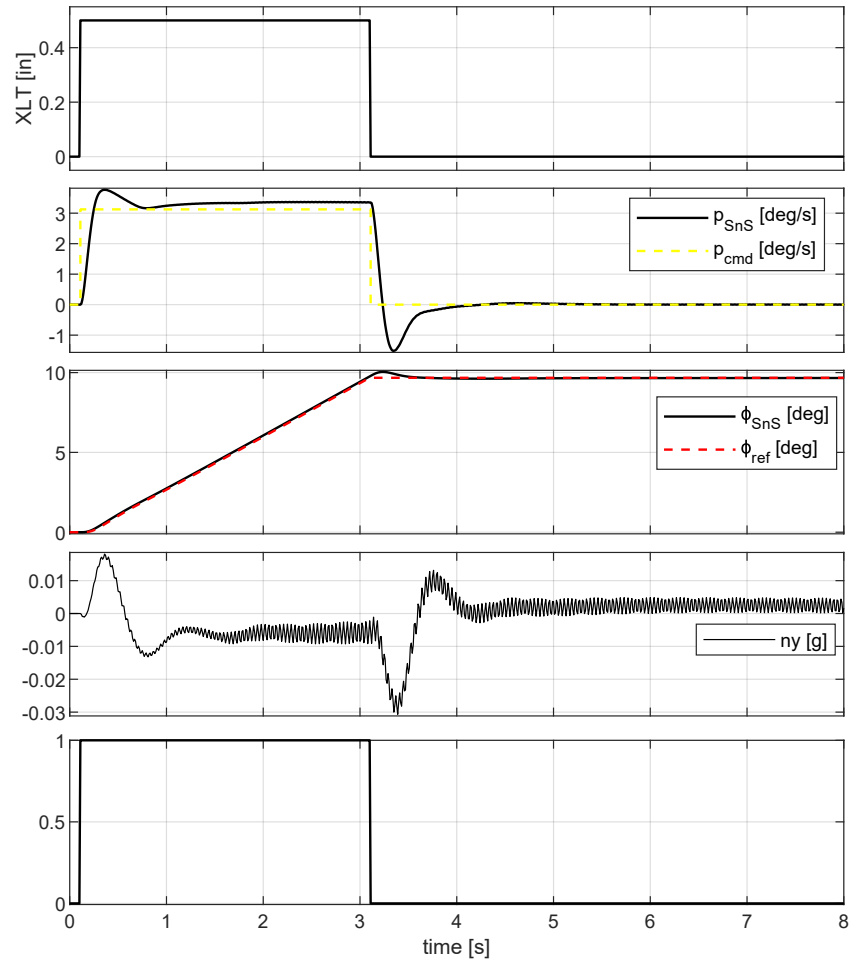


Figure 4.25: XV-15 model response to a lateral step input

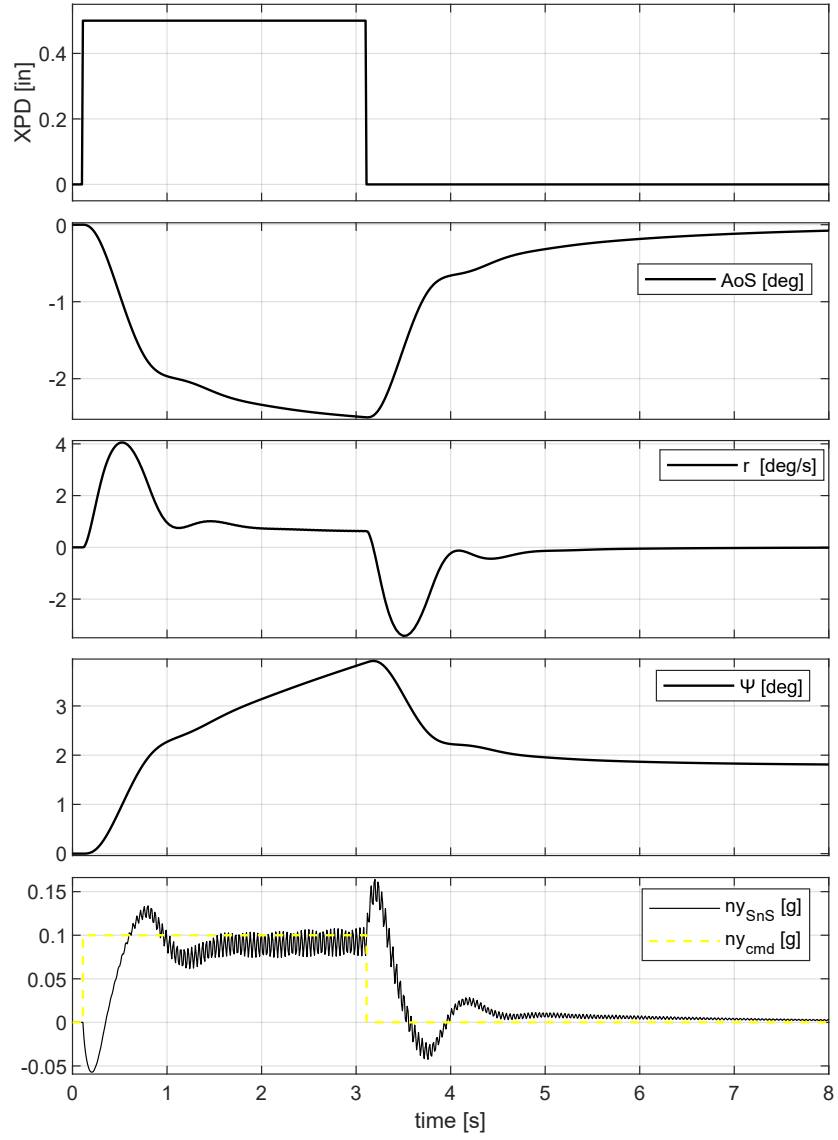


Figure 4.26: XV-15 model response to a pedal step input

4.2.3 CAS off test

A comparison between CAS on and off is considered in the following figures. Note that the dash lines are for the reference signals.

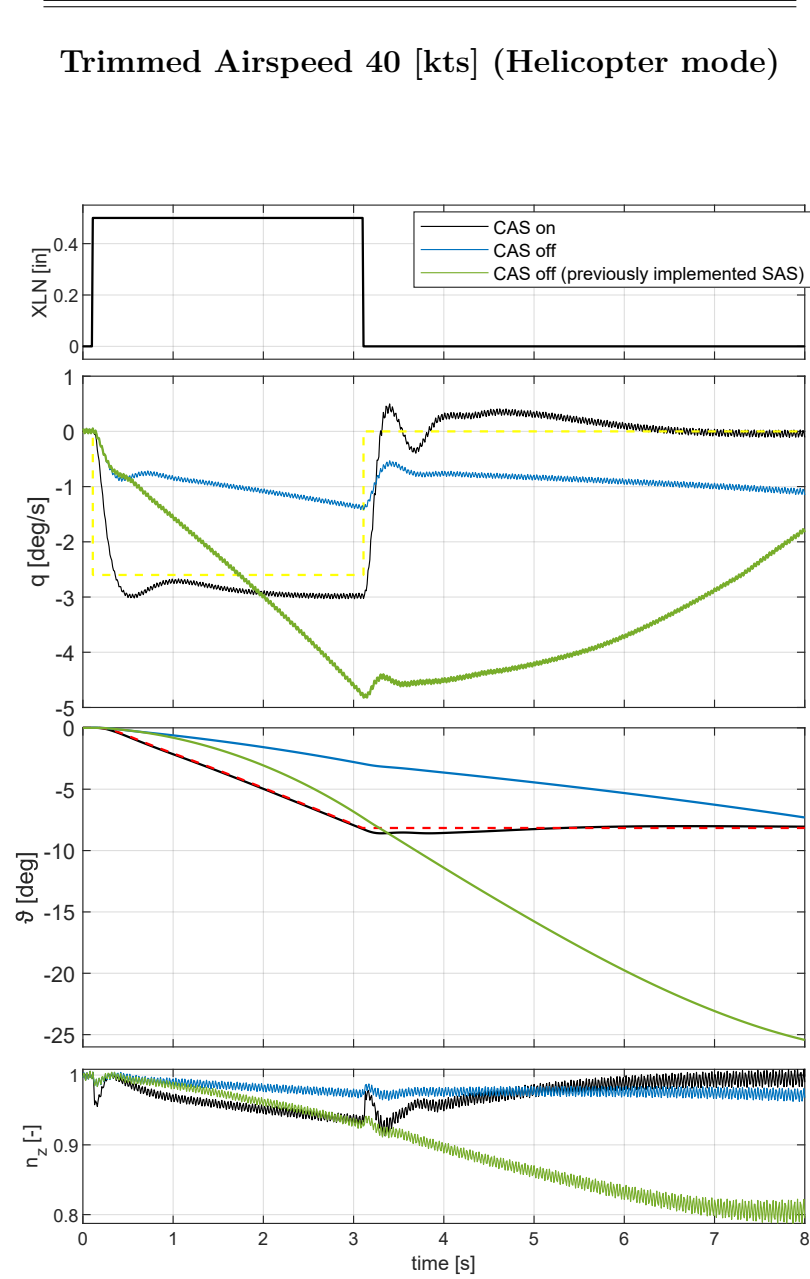


Figure 4.27: XV-15 model response to a longitudinal step input

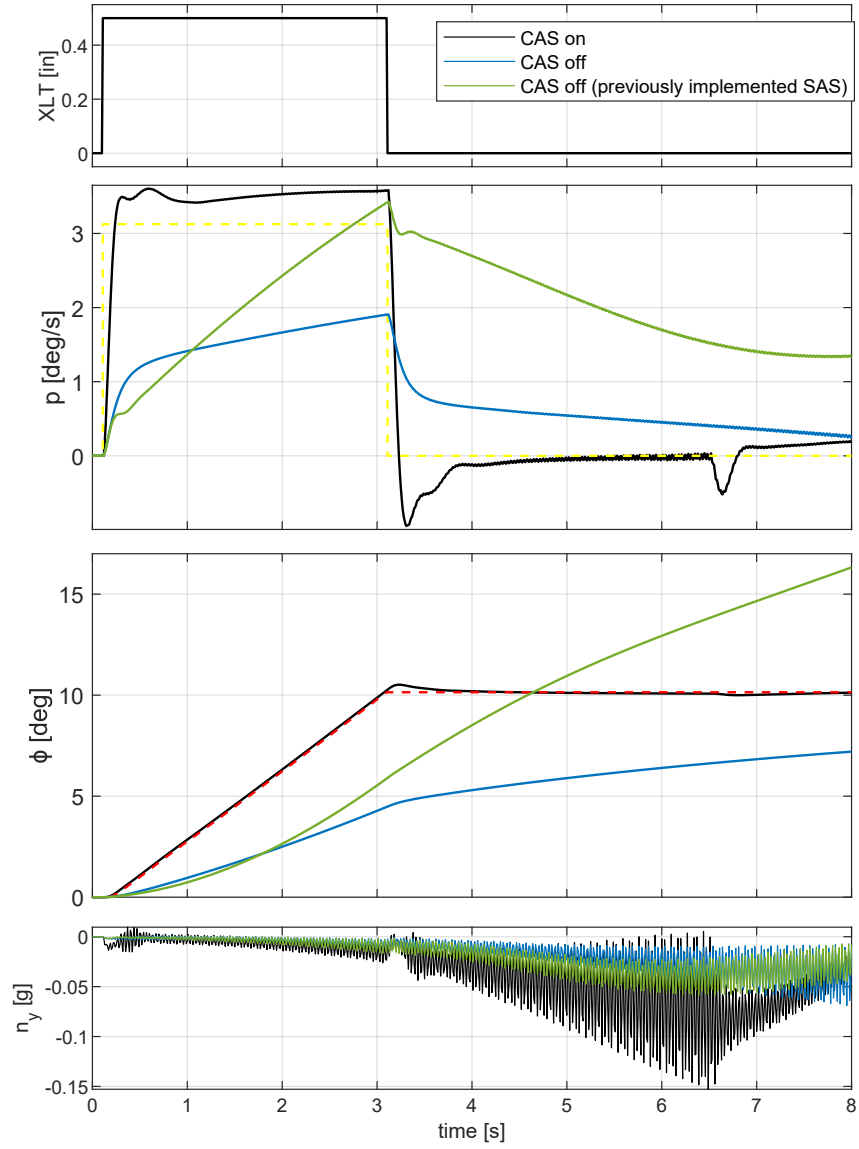


Figure 4.28: XV-15 model response to a lateral step input

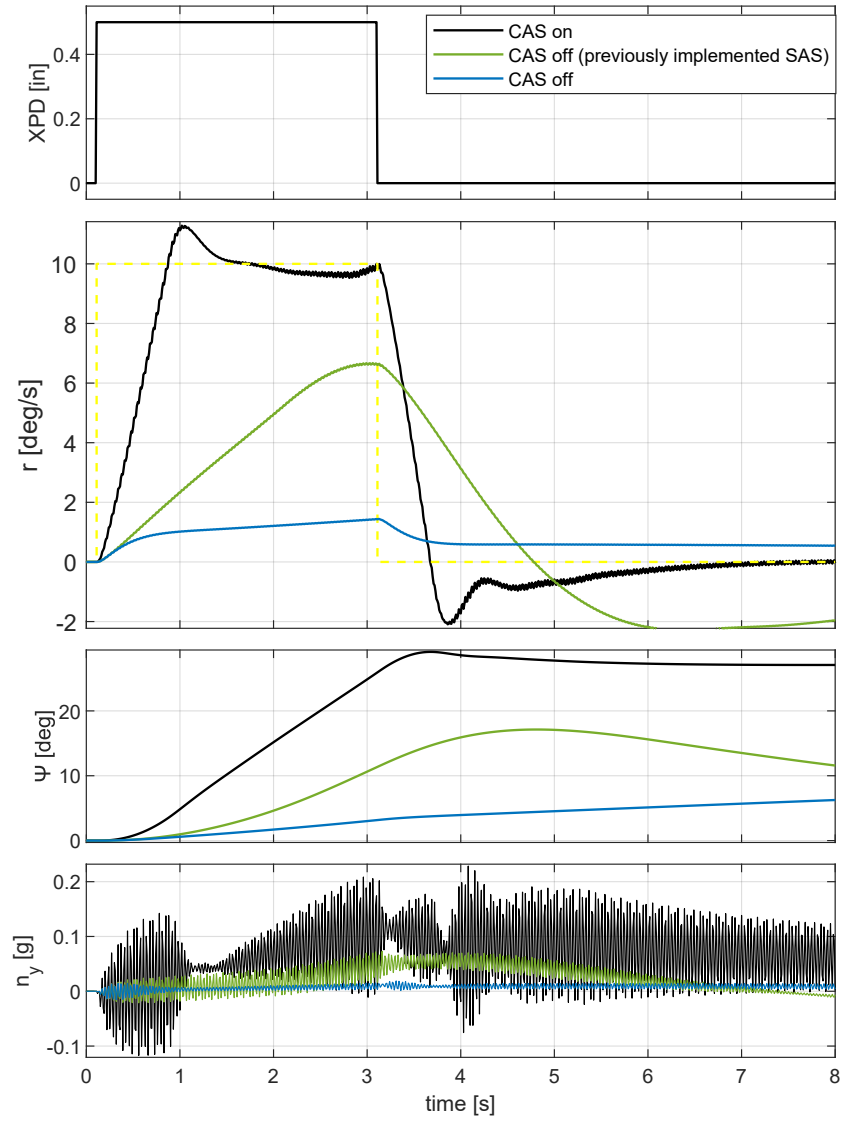


Figure 4.29: XV-15 model response to a pedal step input

Trimmed Airspeed 140 [kts] (Airplane mode)

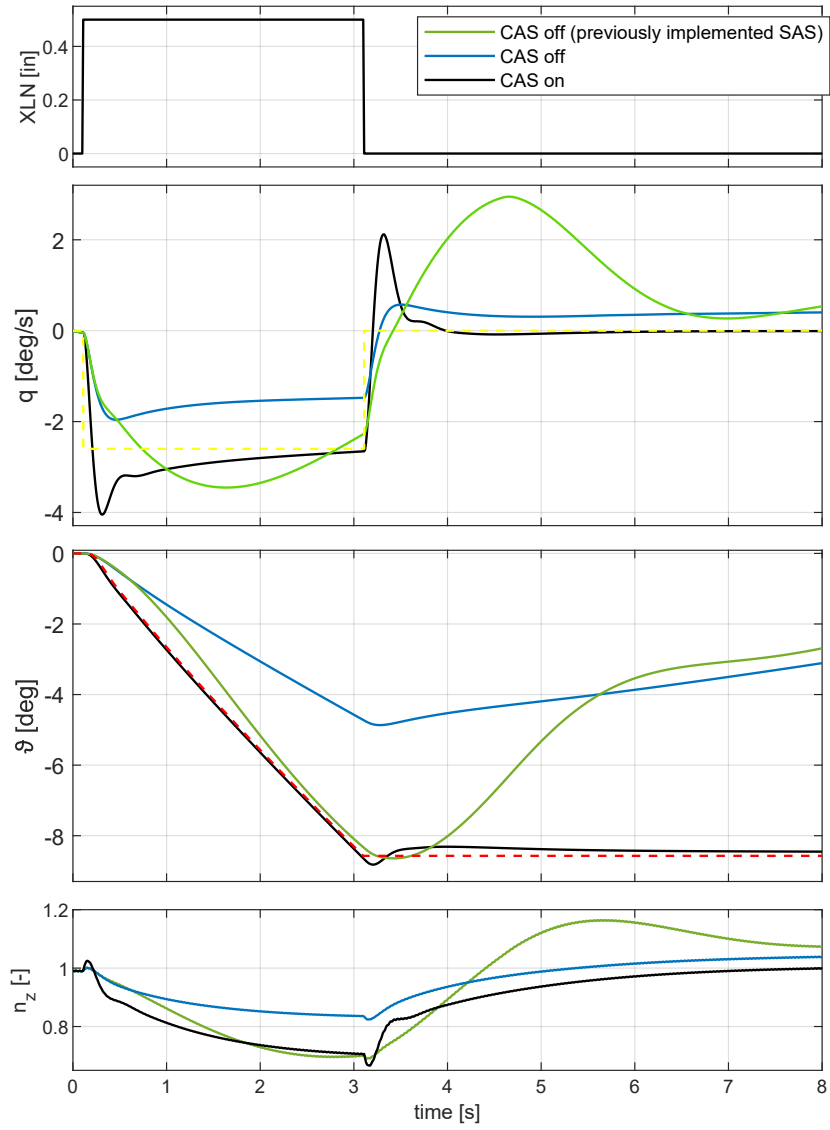


Figure 4.30: XV-15 model response to a longitudinal step input

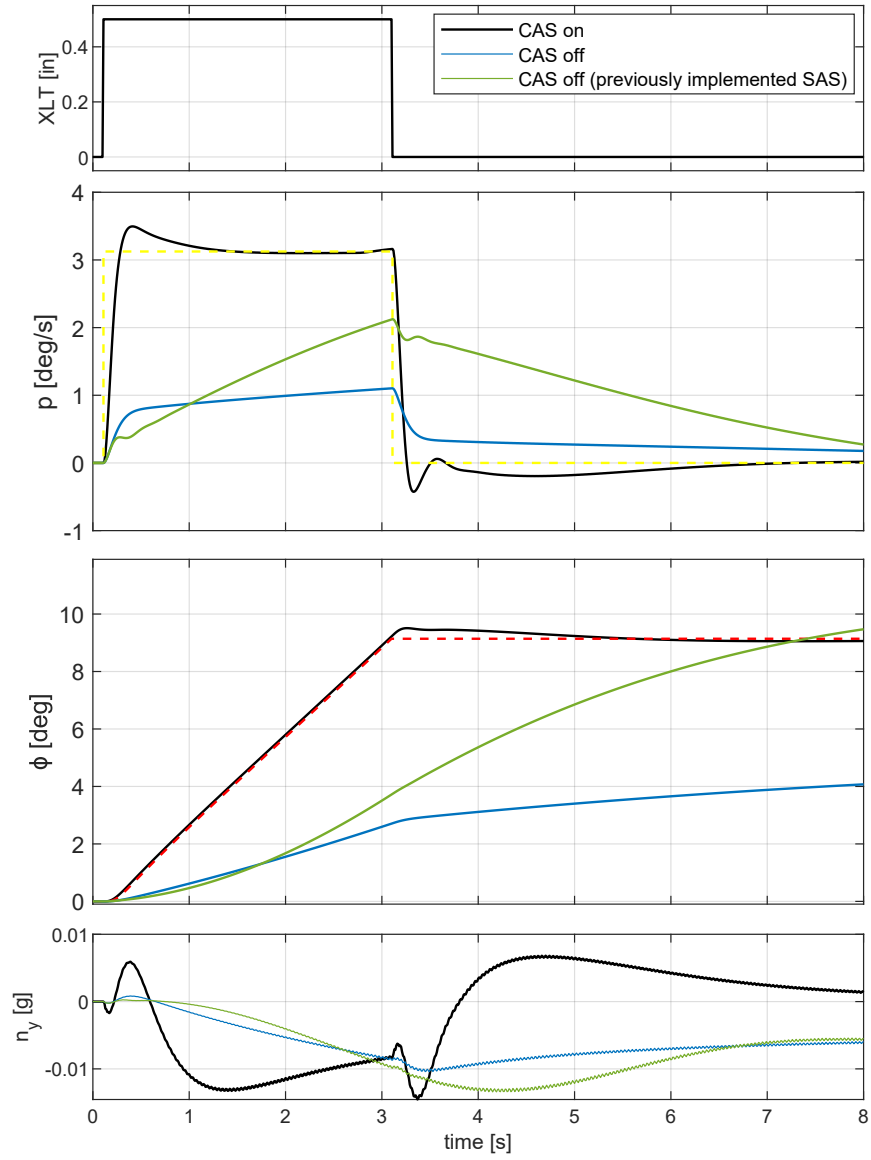


Figure 4.31: XV-15 model response to a lateral step input

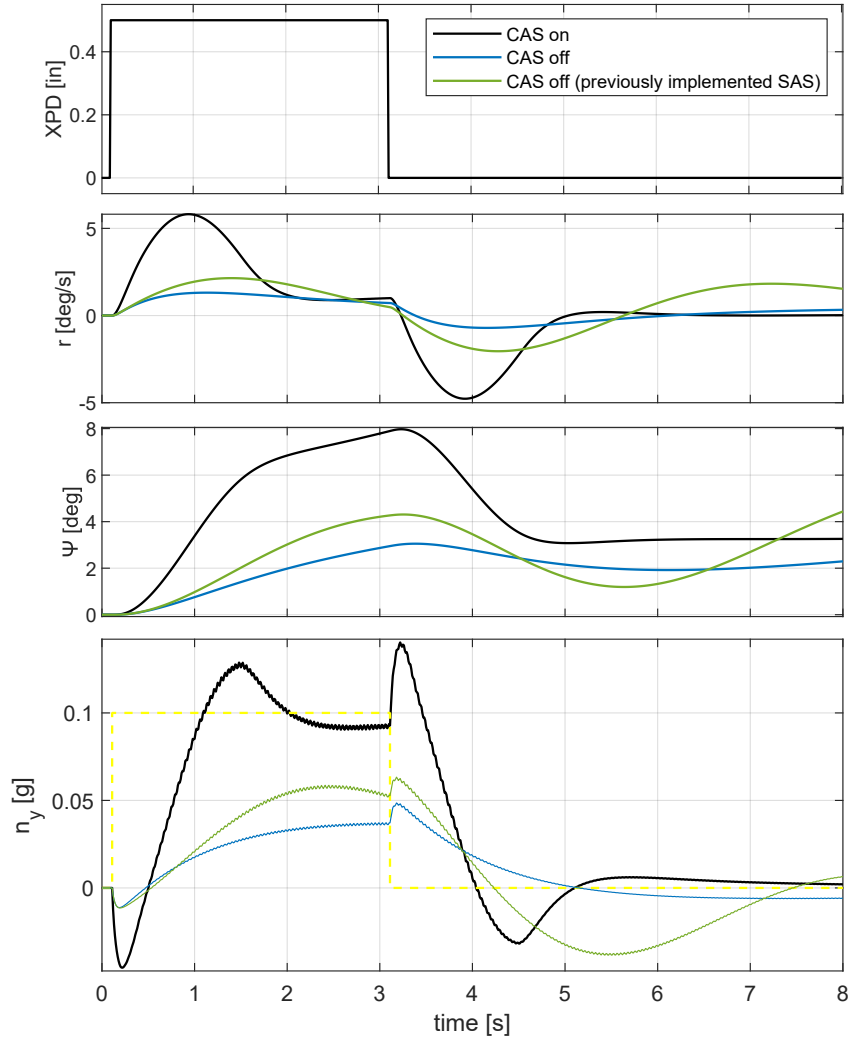


Figure 4.32: XV-15 model response to a pedal step input

4.2.4 Discussion

Control augmentation systems developed above gives adequate performance in terms of transient and steady state specifications. Some refinement on damping could reduce the peak overshoot, sometimes a bit large, as in the pitch rate response (e.g., $0kts$ and $200kts$). The model response to a lateral step input shows that the turn coordinator control system is not working, as expected, in helicopter mode, while the yaw rate control system tracks the commanded signal. The characteristics oscillations of helicopter behaviour are well depicted in vertical and lateral acceleration responses (n_z and n_y). An in-deep investigation would be required on the roll rate response at $40kts$, due to the signal shape at $\approx 6.5s$.

The sideslip is suppressed, in airplane mode, when a turn is performed. The model shows a non-zero minimum phase behaviour achieved in the lateral acceleration response (n_y) to a pedal input. Online simulations will prove if the pilot assesses it in an acceptable level.

Nevertheless, the gain scheduled CAS performs its job well compared to the results shown in 4.2.3. Although the CAS off simulations (SAS is set on) shows adequate enough performance in terms of transient and damping, the system cannot tracks the reference signal, both in helicopter and airplane mode. The model still exhibits a non-zero minimum phase behaviour achieved in the lateral acceleration response (n_y) to a pedal input. It means that this system way of behaving is not the result of the CAS implementation, but rather an intrinsic feature of the model itself.

Last, the CAS off simulations with the previously implemented SAS show a completely distorted shape response for each axis. Due to this considerations, the work carried out along this thesis, could provide an improvement of the flight handling quality according to a pilot point of view arising from an online simulation on the ReDSim (figure 4.33).

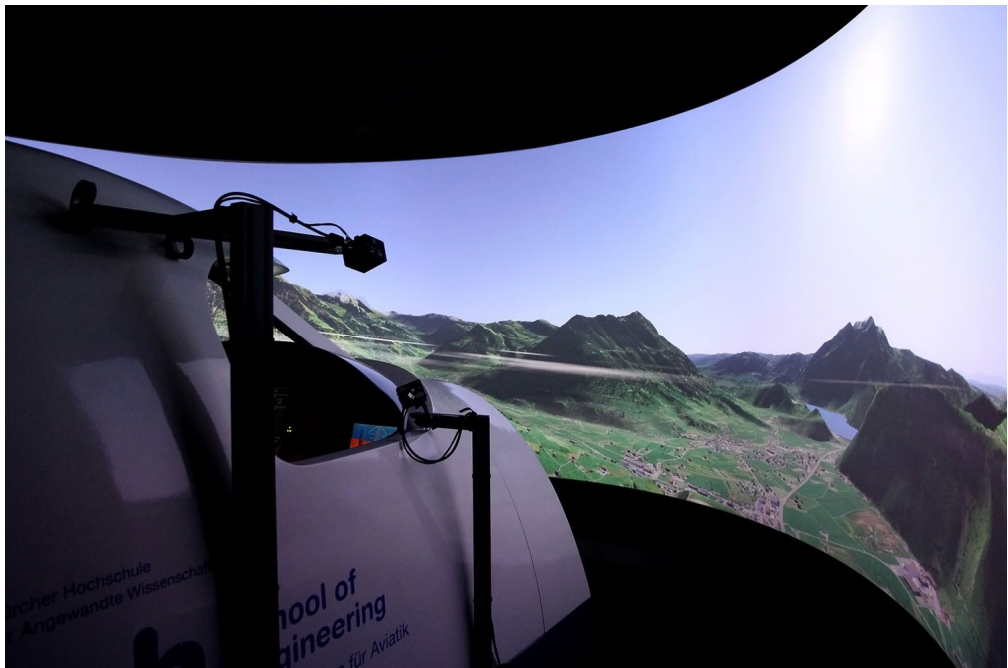


Figure 4.33: ReDSim (Courtesy of ZAV)

4.3 Pilot-in-the-loop Tests

As stated at the beginning of this chapter, model validation has also been performed by evaluating the piloting experience through a series of pilot-in-the-loop tests. To make the investigation as objective as possible, specific tasks have been defined, which could highlight the most significant features of the simulated aircraft/helicopter behaviour. The outcome of such tasks has been evaluated both by recording the simulation data, and by collecting the impressions of the pilot. These have been used to assess the handling qualities, with particular reference to the Cooper-Harper rating scale (figure 4.34).

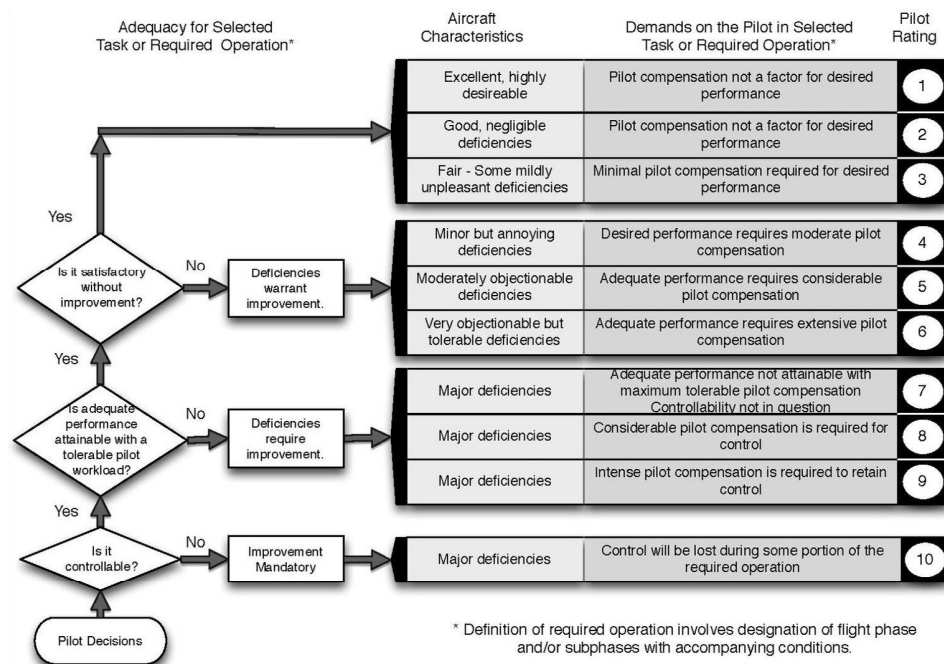


Figure 4.34: Cooper-Harper Handling Qualities Rating Scale

The following three maneuvers have been tested (on helicopter mode), with reference to the ADS-33E-PRF standard [4]:

- Hovering Turn
- Pirouette
- Vertical Maneuver

Task and test description, as well as objectives, are described in above mentioned document. Although the model data was recorded, only a single simulation was

performed. Thus, this simulation data covers each mentioned test, as well as XV-15 overall behaviour in airplane mode, making not possible to describe and analyse in-deep the maneuvers. Nevertheless, the impression related to the pilot has been that the current implemented system is finally controllable and has a more predictable behaviour throughout the XV-15 flight envelope², compared to the previous versions (several tests can be found in Reference [5]).

The previous rudimentary SAS was not able to mitigate the undesired behaviour, leading to relevant oscillations, so larger pilot workload. Pilots often experiences a suddenly variation in pitch, roll or yaw moment, such that any attempt to recovery the system was useless and the simulation had to be aborted.

The pilot rating, as well as suggestions to the above tested maneuvers, are shown as follows.

Maneuver performed	Hovering Turn
Test Pilot	Raphael Monstein
Pilot rating	3

Notes: Recommended to taking into account the lateral-longitudinal coupling.

Maneuver performed	Pirouette
Test Pilot	Raphael Monstein
Pilot rating	3

Notes: No need to compensate the lateral slide, while performing the turn.

²The transition maneuver performs satisfactorily too.

Maneuver performed	Vertical Maneuver
Test Pilot	Raphael Monstein
Pilot rating	2

Notes: No remarks.

The large controllability leads the XV-15 model to be rated as *Level 1*, according Cooper-Harper handling qualities rating. Although a satisfactory behaviour has been proved, some improvements could be taken into account (in future works), such as a feed-forward control, in order to minimize the coupling effects. The most relevant are described below.

- Coupling between forward speed and longitudinal axis.
As the vehicle increases its altitude, the forward speed decreases, demanding to increase the power applied to the engine proportionally to the error between the desired altitude and the current one.
- Coupling between lateral and longitudinal axis.
When performing a turn, the vehicle is prone to tilt the nose down, leading to loose altitude. This must be compensated by increasing the elevator from a value proportionally to the roll error.
- Coupling between lateral and directional axis.
This was already implemented through the turn coordinator control system. Indeed the pirouette maneuver benefits from it.

Chapter 5

FlightGear Simulation Environment

The CAS and the updated SAS, previously developed, were also implemented on a simulation model working with FlightGear, a free, open source multi-platform flight simulator. The simulator allows to reproduce the terrestrial environment including terrain, airports, cities, as well as the vehicle attitude and location (figure 5.1).



Figure 5.1: FlightGear screenshot

The simulation environment was developed by F. Veronese [6], as well as a peculiar *Pilot Interface Simulink block*, which connects the hardware (this consists of two commercial components: the flight stick and the rudder pedals) to the mathematical model, and the *FlightGear Interface Simulink block*, which takes the output data from the model and sends it to FlightGear. An *Export Simulink block* saves all the output data in MATLAB workspace.

The current work purpose concerns a switch implementation (on MATLAB Simulink simulation model) so that the user can set the CAS off, while the SAS is always on. In addition, a control logic was introduced for the CAS switch¹, on the flight stick, which alternates on/off signal by pressing the button illustrated in figure 5.2.



Figure 5.2: Flight stick

A simple task, consisting of take-off, vertical maneuver and transition from helicopter to airplane mode, was accomplished in order to check the CAS functionality and compare the resulting handling qualities. The longitudinal stick input, demanded for the flight mission fulfillment, is shown in figure 5.3.

¹Replacing the previous logic relating to SAS status.

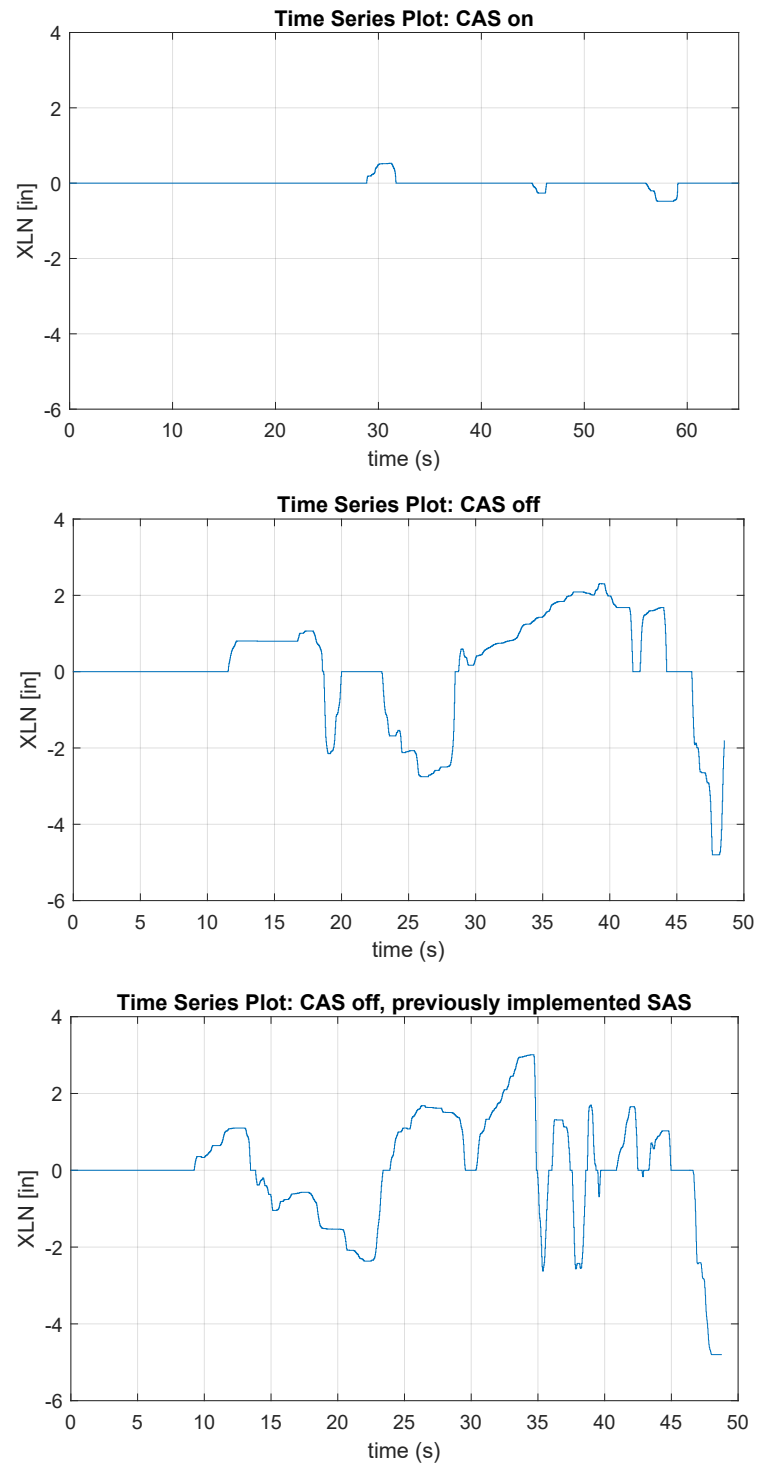


Figure 5.3: Longitudinal stick input - comparison

It's pretty clear how the implemented control augmentation system reduces dramatically the pilot effort, required to accomplish the mission, leading to a Cooper–Harper rating as *Level 1*. When the CAS is off, the SAS itself demands large and sustained pilot compensation, while the final rush during the transition could lead to abort the current simulation.

Although not perceptible from figure 5.3, the system with the previous implemented SAS shows worse performances. Furthermore, according to the user opinion, it is hard to keep a straight-and-level flight, without oscillations.

This satisfactory results finally enable performing a transition (used to be a challenge) without any trouble.

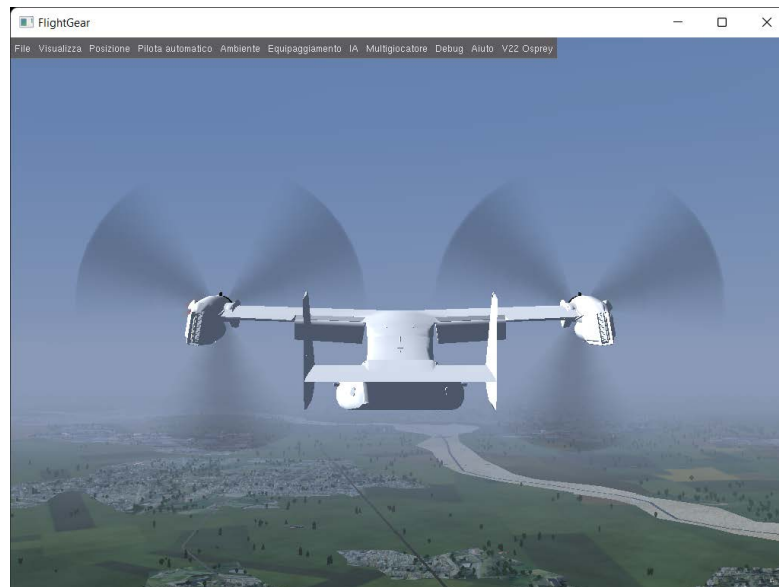


Figure 5.4: FlightGear screenshot

Chapter 6

Conclusions and Remarks

In this thesis, a control augmentation system for XV-15 tilt-rotor was designed using a sampled-data gain scheduling technique. The theory and framework related to sampled-data gain scheduled technique was introduced, as well as for nonlinear systems.

The main result of the work carried out consists of an impressive improvement of the tilt-rotor model, implemented in the ZAV ReDSim, due to the augmented controllability throughout the flight envelope, both in helicopter and airplane mode, shown in offline as well as online simulations.

Such results have been obtained through specific tasks, mostly on:

- an extensive review of the existing model, leading to a stability augmentation system re-design
- the control augmentation system architecture development together with the gain evaluations techniques (PID and LEAD-LAG compensator)
- the linear, sampled-data and nonlinear gain scheduled controller design. Through the implemented scheduling, a reasonable gain is used for each airspeed, providing a consistent system response along the whole XV-15 flight envelope

Optimum design requirements of all control system are achieved by perfect tuning of PID gains. As each of these have his own individual effects on performance specifications, it is possible that change in one variable affects the dynamic response and may gives undesired result. To avoid this, due consideration is given while tuning the gains, as considering that, apart from the performance and specifications to be meet, stability analysis is the most crucial aspect of any control

design. Control system can be tuned according to the stability constraints to get better performance. Stability analysis gives an idea about how far the system is from the critical point. This boundary is defined by Gain Margin and Phase Margin of each SISO system. The values of GM and PM can be obtained using different frequency domain analysis techniques such as Nyquist plot, Bode plots, etc.

So, it is important to remark that stability analysis should be pursued in future works, as it could not be performed during this work due to the limited available time. To the same extent, a refinement on the evaluated gains should be taken, according to design requirements (not defined in this work), as well as deal with the coupling effects, stated in 4.3.

Last, the lead-lag compensator could be used for achieving optimum design requirements. An in-deep investigation would be required on their implementation on the nonlinear model.

Appendix A

Simulink models

The nonlinear developed CAS is shown as Simulink model.

Figure A.1 is the Simulink block diagram of the longitudinal motion controller. Figure A.2 is the Simulink block diagram of the lateral motion controller. Figure A.3 is the Simulink block diagram of the directional motion controller.

These models match with the sampled-data ones. Note that the roll hold is implemented in helicopter mode as well in airplane mode too. In the directional controller, the output for the Relay block switches between two specified values. When the relay is on, it remains on until the input drops below the value of the Switch off point parameter. When the relay is off, it remains off until the input exceeds the value of the Switch on point parameter. For the present implementation, the Switch on point parameter is set to $42kts$, while the Switch off point parameter to $38kts$.

The Integrator block is provided with upper and lower limits, initial conditions and a state port input.

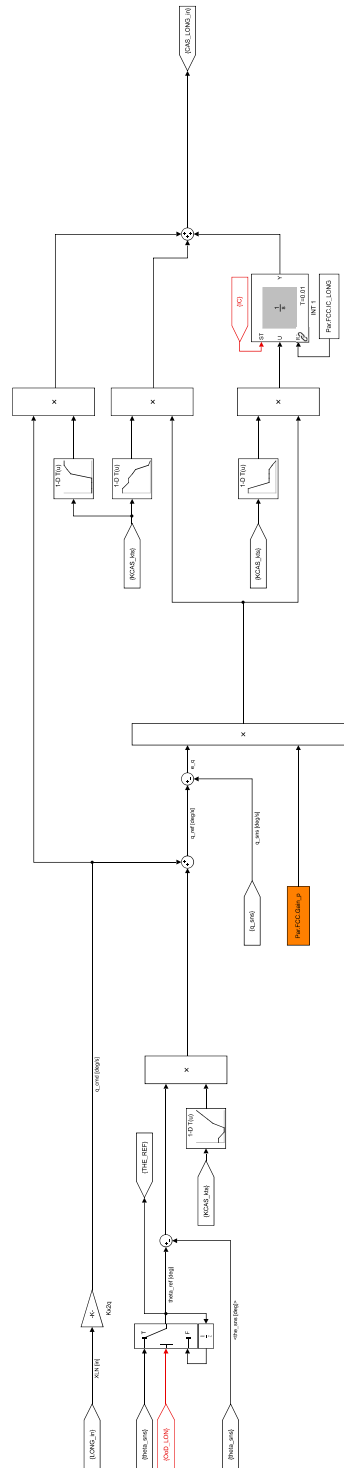


Figure A.1: Longitudinal motion controller

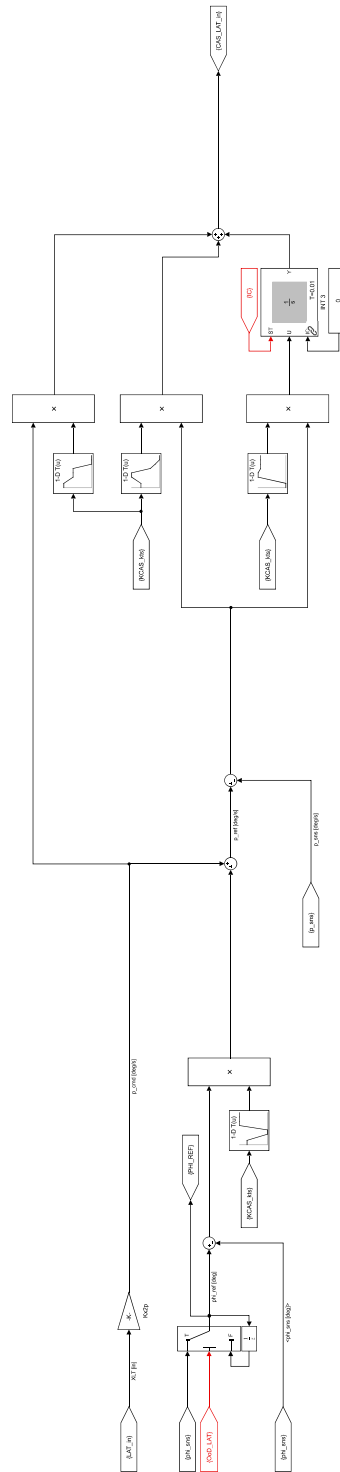


Figure A.2: Lateral motion controller

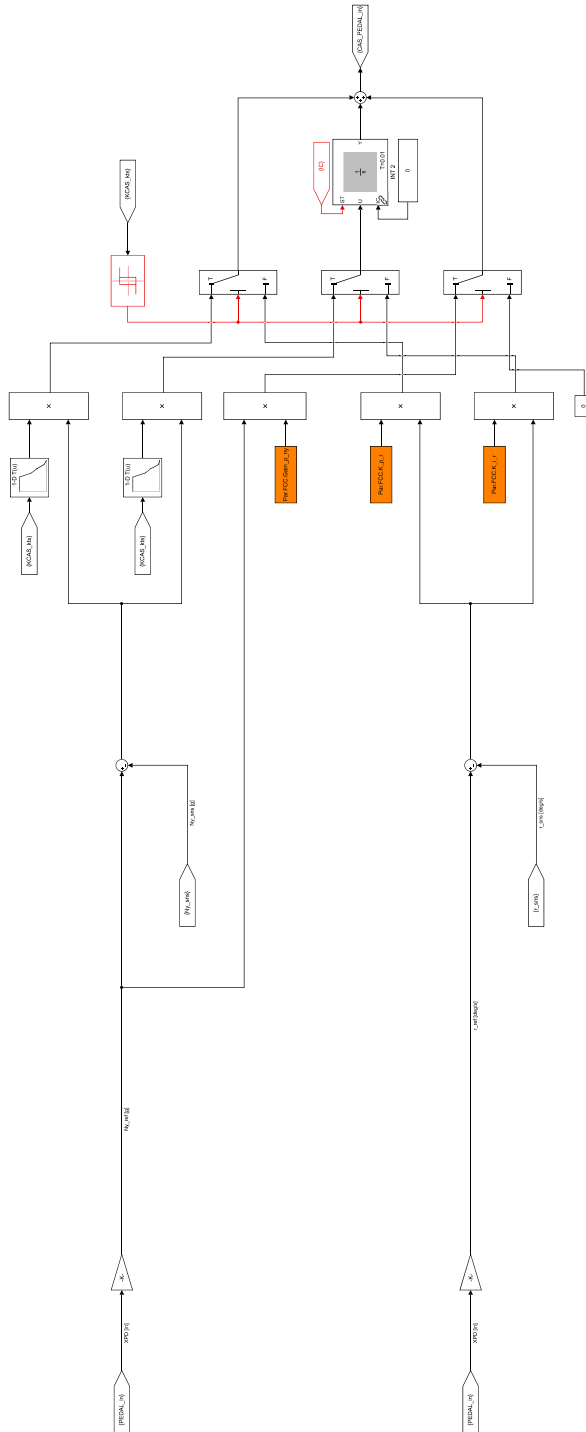


Figure A.3: Directional motion controller

Appendix B

Compensator

$$H = \frac{s + z}{s + p} \quad (\text{B.1})$$

Replacing $s = i\omega$:

$$\phi = \arctan \frac{\Im(s + z)}{\Re(s + z)} - \arctan \frac{\Im(s + p)}{\Re(s + p)} \quad (\text{B.2})$$

With real and imaginary part:

$$\Im(s + z) = \Im(s + p) = \omega \quad (\text{B.3})$$

$$\Re(s + z) = z \quad \Re(s + p) = p \quad (\text{B.4})$$

$$\Rightarrow \phi = \arctan \frac{\omega}{z} - \arctan \frac{\omega}{p} \quad (\text{B.5})$$

Differentiating:

$$\frac{d\phi}{d\omega} = \frac{z}{z^2 + \omega^2} - \frac{p}{p^2 + \omega^2} = 0 \quad (\text{B.6})$$

$$\Rightarrow \omega = \sqrt{pz} \quad (\text{B.7})$$

Then:

$$\phi_{max} = \arctan \frac{\sqrt{pz}}{z} - \arctan \frac{\sqrt{pz}}{p} \quad (\text{B.8})$$

$$\Rightarrow \phi_{max} = \arctan \sqrt{\frac{p}{z}} - \text{acotan} \sqrt{\frac{p}{z}} \quad (\text{B.9})$$

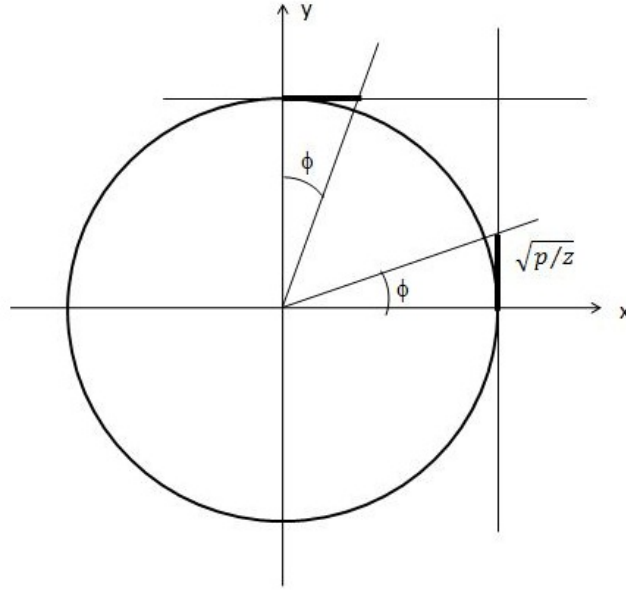


Figure B.1: Unit circle

From figure B.1:

$$\phi = \arctan \sqrt{\frac{p}{z}} \quad 90^\circ - \phi = \text{acotan} \sqrt{\frac{p}{z}} \quad (\text{B.10})$$

$$\arctan \sqrt{\frac{p}{z}} - \text{acotan} \sqrt{\frac{p}{z}} = \phi - 90^\circ + \phi = 2\phi - 90^\circ \quad (\text{B.11})$$

$$\phi_{max} = 2\phi - 90^\circ \quad (\text{B.12})$$

$$\sin \phi = \sin(2\phi - 90^\circ) = -\sin(90^\circ - 2\phi) = -\cos 2\phi = 1 - 2\cos^2 \phi \quad (\text{B.13})$$

$$\phi = \arctan \sqrt{\frac{p}{z}} = \arccos \frac{1}{\sqrt{1 + \frac{p}{z}}} \quad (\text{B.14})$$

$$\Rightarrow \sin \phi_{max} = 1 - 2\cos^2 \left(\arccos \frac{1}{\sqrt{1 + \frac{p}{z}}} \right) = 1 - 2 \left(\frac{1}{\sqrt{1 + \frac{p}{z}}} \right)^2 \quad (\text{B.15})$$

$$\frac{p}{z}(\sin \phi_{max} - 1) = -1 + \sin \phi_{max} \quad (\text{B.16})$$

$$\Rightarrow \frac{z}{p} = \frac{1 - \sin \phi_{max}}{1 + \sin \phi_{max}} \quad (\text{B.17})$$

References

- [1] S. W. Ferguson. *A Mathematical Model for Real Time Flight Simulation of a Generic Tilt-Rotor Aircraft*. NASA, 1988 (cit. on pp. 11, 42).
- [2] F. Barra. «Development of a tilt-rotor model for real-time flight simulation». In: *Politecnico di Torino (Journal)* (2018) (cit. on p. 11).
- [3] Dr. Robert C. Nelson. *Flight Stability and Automatic Control*. WCB/McGraw-Hil, 1998. ISBN: 0-07-046273-9 (cit. on p. 14).
- [4] Aviation Engineering Directorate. *ADS-33E-PRF - Handling Qualities Requirements for Military Rotorcraft*. Tech. rep. United States Army Aviation and Missile Command, 2000 (cit. on p. 123).
- [5] A. Abà. «XV-15 Rotor Mathematical Model». MA thesis. Politecnico di Torino, 2020 (cit. on p. 124).
- [6] F. Veronese. «Integration of a Tilt-Rotor Flight Simulation Platform». MA thesis. Politecnico di Torino, 2020 (cit. on p. 127).
- [7] Gene F. Franklin. *Digital Control of Dynamic System*. Ellis-Kagle, 1998. ISBN: 0-9791226-0-0.
- [8] Bernard Etkin. *Dynamics of Atmospheric Flight*. Dover Publications, 2000. ISBN: 0-486-44522-4.
- [9] Marcello Napolitano. *Aircraft Dynamics*. John Wtley Sons, 2012. ISBN: 978-0-470-62667-2.
- [10] Munther A. Hassouneh, Hsien-Chiarn Lee, and Eyad H. Abed. «Washout filters in feedback control: Benefits, limitations and extensions». In: *IEEE* (2004).
- [11] Vladimir Bobal, Roman Prokop, and Jiri Machacek. «Tuning of Digital PID Controllers based on Ziegler-Nichols method». In: *IFAC* (1997).
- [12] G. Sudha and S. N. Deepa. «Optimization for PID Control Parameters on Pitch Control of Aircraft Dynamics Based on Tuning Methods». In: *Applied Mathematics Information Sciences - An International Journal* (2016).

- [13] Mustafa Suphi Erden and Kemal Leblebicioğlu. «A Lateral Director Autopilot Design for Conflict Resolution Algorithms». In: *Proceedings of the First International Conference on Informatics in Control, Automation and Robotics* (2004).
- [14] Seth B. Anderson. «Historical Overview of V/STOL Aircraft Technology». In: *NASA journal* (1981).
- [15] Douglas A. Lawrence. «Analysis and design of gain scheduled sampled-data control systems». In: *Elsevier Science Ltd* (2000).
- [16] Isac Kaminer et al. «A Velocity Algorithm for the Implementation of Gain-scheduled Controllers». In: *Elsevier Science Ltd* (1995).
- [17] Ramesh Hun, Anshul Tiwari, and Nandan Kumar. «Design and Simulation of Autopilot Control System for Stratospheric Airship». In: *Elsevier Science Ltd* (2016).
- [18] Adriano Bittar and Neusa M. F. de Oliveira. «Central Processing Unit for an Autopilot: Description and Hardware-In-the-Loop Simulation». In: *Springer Science* (2012).
- [19] Ahmed Elsayed et al. «Design of Longitudinal Motion Controller of a Small Unmanned Aerial Vehicle». In: *International Journal of Intelligent Systems Technologies and Applications* (2015).
- [20] F. Barra, S. Godio, and G. Guglieri. «Implementation of a Comprehensive Mathematical Model for Tilt-Rotor Real-Time Flight Simulation». In: *Politecnico di Torino (Journal)* (2019).
- [21] A. Abà et al. «Mathematical Modelling of Gimballed Tilt-Rotors for Real-Time Flight Simulation». In: *mdpi journal* (2020).
- [22] Joël Bernhardsgrütter and Cyrill Bleuler. «VTOL Flight Control Concept Development of a Stability and Control Augmentation System for a Tilt-Rotor Aircraft». MA thesis. ZHAW - School of Engineering, 2020.
- [23] J.M. de Jong. «Model-based Flight Control for a VTOL Aircraft with Independently Tilting Rotors». MA thesis. Delft University of Technology, 2019.
- [24] S. Godio. «Multi-purpose Rotor Model for a Real-Time Flight Simulator». MA thesis. Politecnico di Torino, 2019.
- [25] Alexander Desilets. «Development of an Efficient Vertical Takeoff and Landing Aircraft». MA thesis. University of Rhode Island, 2019.
- [26] Chao Wang. «Aircraft Autopilot Design Using a Sampled-Data Gain Scheduling Technique». MA thesis. Ohio University, 1999.

- [27] S.Markman and B.Holder. *Bell 301 / XV-15*. 2000. URL: http://www.aviastar.org/helicopters_eng/bell_xv-15.php.
- [28] TechTarget Contributor. *Vertical Takeoff and Landing (VTOL) Aircraft*. 2019. URL: <https://www.techtarget.com/whatis/definition/vertical-takeoff-and-landing-VTOL-aircraft>.
- [29] European Union Aviation Safety Agency. *Vertical Take-off and Landing (VTOL)*. 2022. URL: <https://www.easa.europa.eu/light/topics/vertical-take-and-landing-vtol>.